Technische Universität München
Fakultät für Chemie
Bayerisches NMR Zentrum
Lehrstuhl für Biomolekulare NMR Spektroskopie

Characterization of the structure, dynamics, and immersion properties of the membrane-associating FATC domain of ataxia telangiectasia mutated by solution NMR spectroscopy and complementary methods

MUNIRAH SUFIYAH ABD RAHIM

Vollständiger Abdruck der von der Fakultät für Chemie Technischen Universität München zur Erlangerung des akademischen Grades eines

Doktors der Naturwissenschaften (Dr. rer. nat)

genehmigten Dissertation.

Vorsitzender: **Prof. Dr. Michael Sattler**

Prüfer der Dissertation:
1. **Priv.-Doz. Dr. Sonja A. Dames**
2. **Prof. Dr. Bernd Reif**

Die Dissertation wurde am 05.12.2018 bei der Technischen Universität München eingereicht und durch die Fakultät für Chemie am 10.01.2019 angenommen

Table of Contents

Abstract 3

Zusammenfassung 5

Acknowledgement 7

1. Introduction 9

1.1 Biological background 9
1.2 Nuclear magnetic resonance spectroscopy: a versatile tool 13
1.3 The principles of NMR spectroscopy 14

2. Methodology 24

2.1 Protein expression and purification 24
2.2 Preparation of membrane-mimetics 24
2.3 NMR sample preparation 25
2.4 NMR experiments and protein assignments 26
2.5 Structure calculation 26
2.6 NMR experiments with spin-labelled micelles 27

3. Summary of publications 28

3.1 Resonance assignments of micelle-immersed hATMfatc-gb1ent and hDNAPKfatc-gb1ent 28
3.2 The NMR structure, dynamics and immersion properties of micelles-associating hATMfatc 30

4. Mutagenesis studies of human DNA-PKcs FATC domain 32

Conclusion 38

References 40

Appendix 45

Publications 45

Abstract

Ataxia telangiectasia mutated (ATM) and DNA-dependent protein kinase catalytic subunit (DNA-PKcs) are important signal transducers in the DNA damage repair response. They are members of serine/threonine phosphatidylinositol-3 kinase-related kinases (PIKKs) family that control various biological processes in eukaryotic cells. The activity of PIKKs is determined by their specific location at different cellular compartments. Misregulation in these kinases is often associated with neurodegeneration and tumorigenesis. One common feature shared by all PIKKs members is that they have a similar domain organization: a HEAT repeats region, a kinase domain, a FAT domain and a FATC domain. The FATC domain has high sequence conservation in all organisms and is responsible for regulating the kinase activity in PIKKs. It has the ability to interact with various neutral membrane mimetics hence was proposed to play a significant role as membrane-anchoring unit in PIKK signalling complexes. This study focuses mainly on the characterization of the structure of micelles-associated FATC domain of human ATM (hATMfatc) by solution NMR spectroscopy. The structure information on hATMfatc derived from the NOEs distance restraints reveals a dynamic conformation of three stable helices with an RMSD of 4.47 Å. Further investigation on the immersion properties of hATMfatc in DPC micelles was carried out. For this, a series of ^{1}H-^{15}N HSQC spectra of hATMfatc was recorded in micelles containing spin label molecules and supplemented with molecular dynamics simulation data. The results showed that many residues in the FATC domain localize close to the polar head group region of micelles with none of the helices immersed deeply into the lipid bilayer's core. Besides, no significant tertiary contacts were detected between the helices.

Most of aromatic residues, especially tryptophans, are located close to the end region of FATC domain and are conserved in all PIKKs. Tryptophan is known to have a high affinity for membrane mimetics. Therefore, mutagenesis studies targeting these residues in the FATC domain of ATM and DNA-PKcs protein kinases were done by replacing them with alanine. By recording ^{1}H-^{15}N HSQC spectra of mutants in the absence and presence of selected neutral membrane mimetics including micelles, bicelles and small unilamellar vesicles (SUVs), the ability to interact with them was probed and the spectral changes were observed indicating the binding properties. The findings demonstrated that substituting only one tryptophan did not eliminate the interaction of hATMfatc with any

of the tested membrane mimetics. The interactions with micelles and bicelles can still be seen even after two conserved tryptophans were mutated. On the other hand, this double mutant lost its ability to bind to SUVs, whose features better mimic natural membranes, even at low concentration. In hDNAPKfatc, replacing only a single tryptophan was enough to impair the binding to SUVs.

In conclusion, the study presented detailed structural properties of micelle-associated hATMfatc including the protein dynamics, immersion depth in micelles, as well as the analysis of the role of specific amino acid residues in the FATC domain. The insight into the structure might lead to the understanding of the mechanism governing the PIKKs' kinase activity and their interaction with protein substrates.

Zusammenfassung

Ataxia-telangiectasia mutated (ATM) und die katalytische Untereinheit der DNA-abhängigen Proteinkinase (DNA-PKcs) sind zwei wichtige Signaltransduktoren in der Auslösung der Reparatur von DNA-Schäden. Sie sind Mitglieder der Ser/Thr-Phosphatidylinositol-3 Kinase-verwandten Kinasen (PIKKs), die verschiedene biologische Prozesse in eukaryotischen Zellen regulieren. Die Aktivität der PIKKs wird durch ihre Lokalisierung an verschiedenen Zellkompartimenten bestimmt, wobei Fehlregulationen häufig mit Neurodegeneration und Tumorentstehung einhergehen. Ein gemeinsames Merkmal aller PIKKs ist ihre ähnliche Domänenorganisation, bestehend aus der HEAT-Repeat, regia der Kinasedomäne, und den FAT- und FATC-Domänen. Die Sequenz der FATC-Domäne liegt in allen Organismen hochgradig konserviert vor und ist für die Regulation der Kinaseaktivität der PIKKs verantwortlich. Sie kann mit einer Vielfalt an neutralen Membranmimetika interagieren, weswegen ihr eine Rolle als Membrananker bei Wechselwirkungen mit Lipiden und anderen Proteinen zugeschrieben wurde. Diese Arbeit ist darauf konzentriert, die Struktur von micellenassoziiertem hATMfatc mittels Lösungs-NMR-Spektroskopie zu charakterisieren. Die Strukturen mizellengebundenen FATC-Domäne von humanen ATM (hATMfatc), die aus NOE-Distanzbeschränkungen gewonnen wurde, enthüllt eine dynamische Konformation von drei stabilen Helices mit einer mittleren quadratischen Abweichung von 4.47 Å. Weitere Untersuchungen der Eintaucheigenschaften von hATMfatc in DPC Micellen wurden ebenfalls durchgeführt. Hierbei wurde eine Reihe von ^{1}H-^{15}N HSQC-Spektren von hATMfatc in Micellen aufgenommen, die einen Spinlabel enthielten. Die Kombination dieser Spektren mit Daten aus Moleküldynamik-simulationen ergab, dass viele Reste der FATC-Domäne nahe den polaren Kopfgruppen liegen, während keine der Helices tief in den Lipidkern der Micellen eintaucht. Weiterhin konnten keine signifikanten Tertiärkontakte zwischen den Helices festgestellt werden.

Die meisten aromatischen Reste, speziell die Tryptophane, liegen nahe dem Ende der FATC-Domäne und sind in allen PIKKs evolutionär konserviert. Tryptophan ist bekannt dafür, eine hohe Affinität für Membranmimetika zu besitzen, weswegen Untersuchungen mittels Mutagenese durchgeführt wurden. Dazu wurden bestimmte genannten Tryptophanreste in den FATC-Domänen der Proteinkinasen ATM und DNA-PKcs,

sukzessive durch Alanine ersetzt. Anschließend wurden ^{1}H-^{15}N HSQC-Spektren der Mutanten mit und ohne ausgewählte neutrale Membranmimetika (Micellen, Bicellen und kleine unilamellare Vesikel (SUVs) aufgenommen und die spektralen Veränderungen als Indikator der Bindeeigenschaften beobachtet. Die Ergebnisse zeigen, dass der Ersatz eines einzelnen Tryptophanrests die Interaktion von hATMfatc mit den Membranmimetika nicht ausschaltet. Eine Interaktion mit Micellen und Bicellen ist selbst nach der Mutation zweier konservierter Trptophanreste noch erkennbar. Andererseits hat diese Doppelmutante ihre Fähigkeit zur Bindung an SUVs, deren Eigenschaften jene natürlicher Membranen selbst bei niedrigen Konzentrationen imitieren, verloren. Hingegen verliert eine Variante von hDNAPKfatc mit nur einem einzelnen mutierten Tryptophanrest bereits ihre Fähigkeit zur Bindung an SUVs.

Zusammengefasst präsentiert diese Arbeit detailliert die strukturellen Eigenschaften von micellenassoziiertem hATMfatc, einschließlich der Proteindynamik und der Immersionstiefe in Micellen. Außerdem wurde die Rolle einzelner Aminosäurereste in der FATC-Domäne untersucht. Dieser Einblick in die Struktur kann zum Verständnis des Mechanismus führen, der die Kinaseaktivität der PIKKs und ihre Interaktion mit Proteinsubstraten regelt.

Acknowledgement

I would like to dedicate this thesis to my parents, family and friends who have been supporting me silently from distance. And to those who are passionate about science, this might be my little contribution to the field.

The four-year stay in Germany will be one of the unforgettable experiences in my life. I am sincerely grateful for the opportunity given to sharpen my scientific skill and understandings in science and life in general. Therefore, I would like to express my appreciation to those who contributed directly or indirectly to my PhD journey.

First and foremost, I would like to express my deepest gratitude towards PD Dr. Sonja Alexandra Dames for giving me the opportunity to work in her group and guiding me throughout the course of study. Through her support, I have grown to be a better researcher.

I would also like to acknowledge Prof Michael Sattler for hosting our group (Dames group). With the opportunity, I can work with professional and experienced people in the field of protein NMR with an excellent biomolecular NMR facility.

Special thanks also goes to Prof. Reif for sharing with us his laboratory and equipment. I am also grateful for him, for inviting me to be part of his diverse group as well as for providing the financial support during my last stay.

A great appreciation goes to Deutscher Akademischer Austausch Dienst (DAAD) for the scholarship under the programme ‘the Grant for Young Scientists’ as well as their assistance in the administration stuff and related.

My endless appreciation is dedicated to my colleagues for their assistance at the beginning of my study. I thank Maristella for her assistance in the laboratory and I always enjoyed her delicious Italian delicacies. I thank Matthias, also for helping me in the laboratory and willingness to practice Deutsch. I would like to thank Teji and Zheng for keeping me company, sharing many interesting stories as well as for spending sweet and enjoyable time together. Besides that, I thank all my colleagues Arpita, Benita, Carina, Kai, Markus, Matthias B., Riddhiman and Saba, as well as our new group members Agnes, Natalia and others for the happy time together. I thank Nitin for tutoring me in the

NMR spectroscopy subject. I would also like to mention Asita, and Waltraud for their kindness and assistance in the administrative stuff.

I thank Sattlers', Hagns', Glasers', Shuetzs' and others for creating such a wonderful working environment since we moved to our new BNMRZ.

Being far away from my home country, I am grateful for my friends whom I knew during my stay in Germany. Thank you for the wonderful moments we have shared together and making my stay feels like 'at home'.

Lastly, I thank God for my parents and family for their unconditional love and support throughout my study. Especially to my parents whom their endless support and affection keep me going. I am grateful for my brothers and sisters for always being there and supportive through the thick and thin.

'It does not matter how slow you go as long as you do not stop'

-Confucius-

1. Introduction

1.1 Biological background

1.1.1 Phosphatidylinositol-3 kinase-related protein kinases (PIKKs)

Phosphatidylinositol-3 kinase-related protein kinases (PIKKs) is a group of protein kinases that control numerous cellular pathways particularly in eukaryotic cells by phosphorylating the target proteins at either serine or threonine residue. Six individual kinases have been identified in human, namely ataxia-telangiectasia mutated (ATM), DNA-dependent protein kinase catalytic subunit (DNA-PKcs), ataxia- and Rad3-related (ATR), mammalian/mechanistic target of rapamycin (mTOR), suppressor of morphogenesis in genitalia-1 (SMG-1) and transformation/transcription domain-associated protein (TRRAP).

The function of each PIKK has been widely reviewed. Mammalian/mechanistic TOR regulates the nutrient and energy supply for cellular growth and propagation [1, 2]. SMG-1 involves in controlling the nonsense-mediated mRNA decay (NMD) mechanism [3, 4]. ATM, DNA-PKcs and ATR play an eminent role in maintaining the genome stability through the mechanism of DNA repair [5-8]. TRRAP takes part in a multiprotein co-activator complex responsible in the histone acetyltransferase activity [9]. Despite possessing high sequence similarity with other PIKK members, TRRAP is not an active kinase due to the absence of the amino acids required for the activity [10].

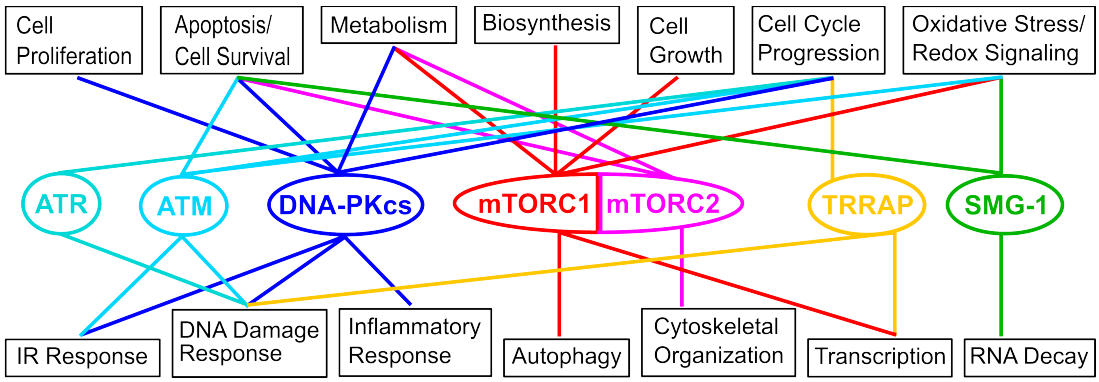

Figure 1.1: The correlation diagram summarizes the roles of the known human PIKKs at different cellular pathways [11].

1.1.2 PIKKs domain organization

PIKKs share a similar domain organization with the length of their amino acid sequence ranging from 2500-4500 residues (250-450 kDa). Each PIKK contains a region composed of alpha-helical HEAT repeats (huntingtin, elongation factor 3, regulatory subunit A of PP2A, TOR) [12], a FAT (FRAP-ATM-TRRAP) domain, a kinase domain and a FATC (FAT C-terminal) domain. The HEAT repeats region and the FAT domain are largely composed of helical repeats typically mediate protein-protein interactions [12-14]. The length of HEAT repeats region varies hence contributing to the PIKKs' structural diversity [15]. The structure of FAT domain was illustrated in the crystal structure of N-terminally truncated mTOR in complex with LST8 (lethal with SEC13 protein 8) [16]. The kinase domain residing close to the C-terminus of PIKKs shows a high sequence homology to phosphatidylinositol-3 kinases (PI3K) lipid kinases [17]. Furthermore, the PIKK regulatory domain (PRD) links the kinase and FATC domain in SMG-1 [17-19]. This region varies significantly in length and sequence composition between different PIKKs [17, 19]. The FATC domain is located at the extreme C-terminal of all PIKKs members. It encompasses only around 35 amino acid residues and is evolutionarily conserved suggesting its important in regulating the kinase function in PIKKs [20, 21]. The FATC domain mainly consists of aliphatic and aromatic residues such as tryptophan, contributing to the hydrophobic nature to this small domain. The FATC domains of ATM, DNA-PKcs, and ATR have been proposed to mediate protein-protein interactions [17, 21, 22]. A later study had suggested the function of FATC of PIKKs as conditional membrane anchor by investigating their interaction with various membrane mimetics using NMR spectroscopy [23].

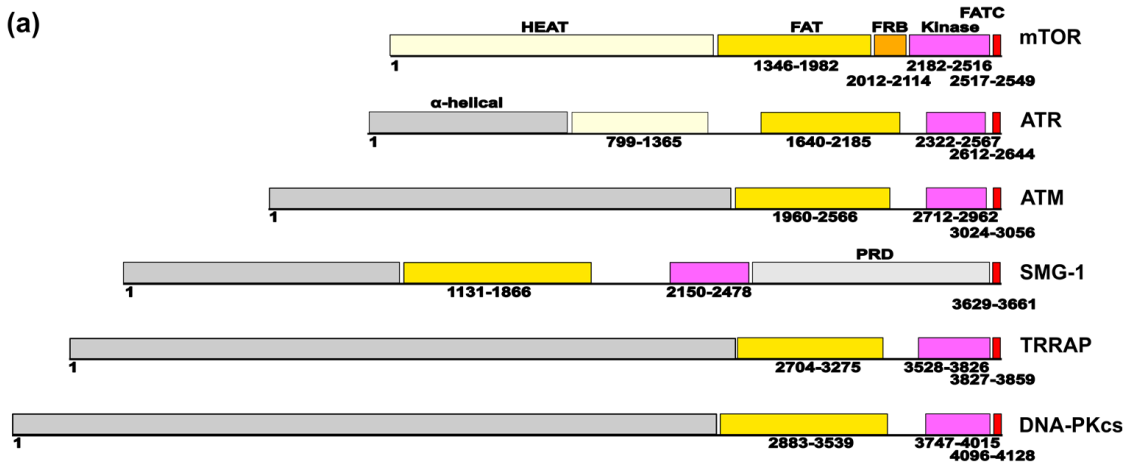

Figure 1.2: The general domain organization of PIKKs [11].

The FATC domain is indispensable for kinase function and apparently mutation would cause a detrimental effect to the PIKKs kinase activity [24]. For instance, the mutation of single residue at position L3733A in SMG-1 causes the loss of kinase activity [25]. In another case, replacing one conserved residue at a different position could affect the transcriptional properties and incorrect phenotypes in the FATC domain of yeast Tra1, leading to low cellular viability and growth defect [24]. Another interesting finding is that the FATC domains of certain PIKKs members are functionally equivalent due to their high degree of sequence conservation. This was observed in the ATM, whereby the FATC domain can be replaced by the one from ATR, TRRAP or DNA-PKcs without losing its kinase function. However, when the FATC domain of ATR or mTOR is substituted with the FATC domain of ATM, the loss of kinase activity was detected [21].

1.1.3 PIKKs localization

Signalling protein pathways involve a complex network of interacting protein substrates centred at a specific cellular membrane. In this respect, PIKKs govern a broad range of biological pathways and mechanisms in cells. The localization of these enzymes at specific cellular membrane compartments determines the efficiency of signalling outputs in response to particular stress factors [17, 18, 26]. In addition, the reliability of biochemical signalling process is improved through targeted membrane localization whereby the individual signalling branches are separated from each other [26, 27].

Localization of mTOR at different cellular membrane is closely related to the role it plays in controlling cellular growth. For example, the localization of TOR complexes at plasma membrane is required for the cells' survival [28]. Besides, active mTORC2 complex was found to bind physically to ribosomes and indirectly determine the growth capacity of a cell though ribosome content ensuring the TORC2 is active only in growing cell but not in cancer cells [29]. Another study indicated that a large fraction of mTOR is localized at the endoplasmic reticulum (ER) and Golgi body acting as the downstream effector [30, 31].

Eukaryotic cells maintain genome stability through the nonsense-mediated mRNA decay (NMD) mechanism in which the mRNA transcripts containing premature termination codons (PTCs) are degraded. This process is controlled by SMG-1 protein kinase and it can be found in the cytoplasm and nucleus [32, 33]. Recent study revealed the

localization of this kinase to the cytoplasmic stress granules upon exposure to the stress causing agents such as hydrogen peroxide and sodium arsenite [34].

TRRAP is an important transcription activation subunit in chromatin modification complexes. Despite being the true member of PIKKs family, TRRAP has no catalytic activity [35]. To date, there is no information found on the recruitment of TRRAP outside nucleus such as at the membrane compartments.

1.1.4 Ataxia-telangiectasia mutated (ATM) and DNA-dependent protein kinase catalytic subunit (DNA-PKcs)

ATM and DNA-PKcs respond to the presence of DNA double-strand breaks (DSBs) while ATR is activated in the presence of single-stranded DNA (ssDNA). DNA double-strand break is the most notorious form of DNA damage that might lead to cell death if not treated.

Consistent with the function in DNA damage recognition, ATM and its homologue DNA-PKcs were both detected in the nucleus. Upon exposure to the IR, ATM could be found at the cytoplasmic vesicle [36] or at the plasma membrane [37]. ATM is also an important signal transducer in the oxidative stress response linking the genome stability and carbon metabolism [36, 38, 39]. Similarly, the exposure to IR also triggers the localization of DNA-PKcs to detergent-insoluble glycolipid-enriched complexes (DIGs) or lipid rafts [40]. DNA-PKcs may further localize to mitochondria by interacting with protein kinase Cδ (PKCδ). It undergoes proteolytic cleavage followed by activation at the onset of apoptosis and is known to associate with DNA-PKcs [41]. Moreover, it has been suggested that during the oxidative stress response PKCδ is targeted to mitochondria [42].

In general, a better understanding of the regulation and activation network of PIKKs require further structural insights into the individual membrane-localizing interactions and their dependence on the membrane composition, for example regarding the presence of typical signalling lipids such as phosphatidic acid (PA) and phosphoinositol phosphate lipids (PIPs) or lipid oxidation products, apart from their detailed interaction and localization information. Recently, the role of protein localization for disease and therapy has been investigated. Since the localization is closely related to the physiological profile and function of protein, the disease-related subcellular mislocalization can be manipulated as a potential therapeutic approach [43].

1.2 Nuclear magnetic resonance spectroscopy: a versatile tool

Nuclear magnetic resonance (NMR) spectroscopy is a technique that detects the chemical environment of atomic nuclei in the presence of a high magnetic field at the same time the radio frequency electromagnetic radiation is projected perpendicular to the sample. In general, the technique can be used to investigate chemical, physical and biological properties of substance. At the present time, the application of NMR spectroscopy extends not only in chemical science but also in the structural biology.

NMR spectroscopy is necessary for a routine preliminary assessment especially in organic synthesis and natural products chemistry. Since NMR is sensitive to the chemical environment of nuclei, scientists are able to identify and characterize the structure of unknown organic molecules. Compared to other analytical techniques such as mass spectrometry (MS), NMR offers a fast, reliable and non-destructive analysis of samples.

On the other hand, proteins are present in the cellular environment as dynamic and complex system to assume their biological functions. At equilibrium, the conformation of protein is continuously exchanged in space and time ranging from nanometers to micrometers and femtoseconds to hours [44]. NMR spectroscopy provides advantage over other techniques in integrative structural biology. It allows us to investigate the behaviour of a protein in solution. Apart from determination of high-resolution biomolecular structures, NMR spectroscopy can be used to study the molecular interactions, protein folding-misfolding and dynamics in a native environment, in combination with the structural information from X-ray crystallography.

Current research has demonstrated that NMR spectroscopy can be applied for protein studies in living cells known as in-cell NMR. In in-cell NMR, a biological sample can be studied directly inside the cell. Rather than determination of protein structure *de novo*, in-cell NMR is more beneficial for investigating conformational changes in biomolecules. Therefore, changes in conformation caused by posttranslational modification or interaction with other molecules can be observed readily and accurately [45, 46].

NMR-based metabolomics is another interesting application and has been an important analytical tool to study metabolites in biological samples. NMR offers a quantitative and reliable identification of metabolites with high reproducibility despite its low sensitivity

compared to other analytical techniques. It can also be exploited to analyze the enzyme activity, metabolic fluxes as well as for identifying the metabolic pathways using isotope-labeled substrates [47].

Huge development and improvement in NMR techniques have been documented and this has broadened its application in various disciplines. This is not only limited to solution state NMR but also in solid-state NMR spectroscopy. Solid-state NMR has gained much attention recently due to the development of dynamics nuclear polarization (DNP) technique. The measurement of sample can be challenging due to its low sensitivity and the analysis of spectra can be difficult because of the spectral complexity. DNP enhances the sensitivity in the solid-state NMR experiments and subsequently, more information of the local structure and dynamics of the biomolecule can be extracted [48]. In general, sensitivity improvement has opened the doors for more possibilities to implement this method not only in the integrated structural biology approaches but also in inorganic and analytical chemistry [49].

1.3 The principles of NMR spectroscopy

1.3.1 Nuclear magnetic resonance spectroscopy

The basic of NMR spectroscopy lies on the magnetic properties of atomic nuclei. Every nucleus possesses a property known as spin which is represented by the nuclear spin angular momentum number, *I*. Only nuclei possessing non-zero spin angular momentum ($I \neq 0$) are considered to be 'NMR active'. In biomolecular NMR spectroscopy, the most widely detected nuclei are proton (^{1}H), carbon-13 (^{13}C) and nitrogen-15 (^{15}N). In principle, when the nucleus is exposed to the B_0 field, the nuclear spins are polarized. The nuclear spins are then subjected to the radio frequency (RF) pulse, B_1 perpendicular to the B_0 field resulting in the rotation of net macroscopic magnetization, M on x,y-plane. Under the influence of B_0, the transverse magnetization on the x,y-plane precesses at the resonance frequency called Larmor frequency, ν_0 producing electric current in the detection coil. The transverse magnetization decays with time as the system returns to the thermodynamics equilibrium state parallel to B_0. This process is known as free induction decay (FID) and will be recorded during the acquisition time. The NMR spectrum is obtained by performing a Fourier transformation (FT) on the FID data [50].

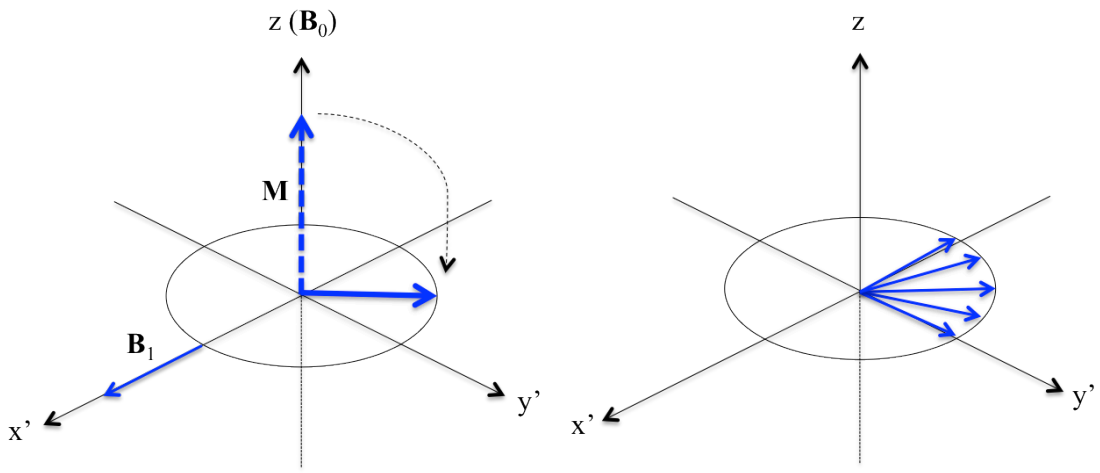

Figure 1.3: The diagram illustrates the effects of external magnetic field B_0. The B_1 field is projected from x'-axis producing a selected radio frequency pulse that turns M to the x,y-plane consequently rotates M about the plane. This state is called phase coherence. The magnetization is then decayed over time during the precession in the x,y-plane. The coordinate system of the rotating frame is denoted by x', y' and z'. (Adapted from reference [50])

In the absence of static magnetic field B_0, the population of atomic nuclei with spin $I = ½$ in a solution is randomly oriented and the nuclei have the same energy (degenerate). However, once the static magnetic field B_0 is applied, the degeneracy disappears, and the spins are splitted into different energy level as a result of the interaction of nuclear magnetic moment, μ with B_0. The spins reorient themselves into two energy states; namely the most favourable α-state (ground state) and the less favourable β-state (excited state), corresponding to the magnetic quantum number $m_1 = +1/2$ or $m_1 = -1/2$ respectively.

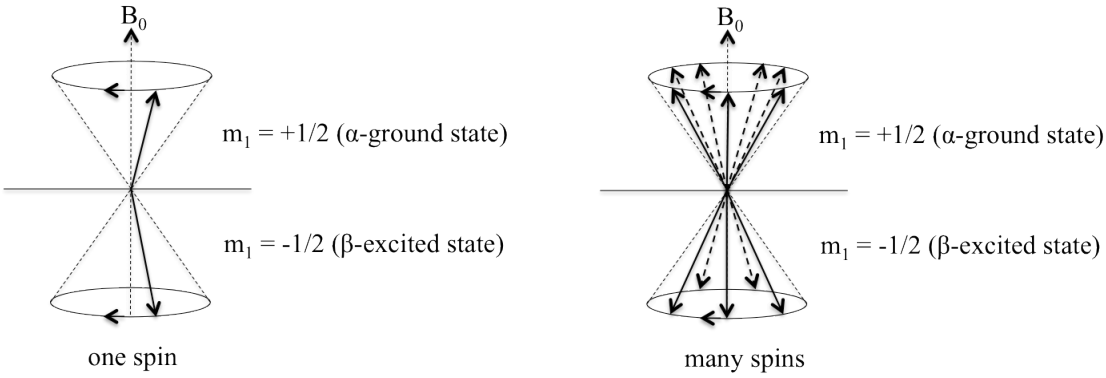

Figure 1.4: The relative spin orientations in B_0 field for one and many spin systems. A nuclear can be either in the 'spin-up' (α) or 'spin-down' (β) state. In an NMR sample, the spin population is slightly higher in the α-state compared to β-state, resulting in a macroscopic net magnetization.

In mathematical representation, the energy possessed by the spins along the positive z-axis based on the Cartesian coordinate system can be written as:

$$E = -\mu_z B_0$$

$$E = -m_1 \gamma \hbar B_0$$

in which γ is the gyromagnetic ratio of the nucleus and $\hbar$ is the Planck constant. Based on the above equations, the α-state and β-state will have energy, $E_{+1/2} = -1/2\gamma\hbar B_0$ and $E_{-1/2} = 1/2\gamma\hbar B_0$ respectively.

The energy difference between these two spin states is then,

$$\Delta E = \gamma \hbar B_0$$

The minuscule energy difference between these two states gives rise to the observable nuclear magnetization, M in the NMR spectrum. In the B_0 field, the nuclear spins with α-state and β-state are populated based on the Boltzmann distribution. The separation of energy between these spin states is proportional to the strength of the B_0 field, also known as nuclear Zeeman splitting or Zeeman effect. By definition, higher magnetic strength resulted in larger population difference between two spin states thus increasing the feasibility to measure the nuclear magnetization.

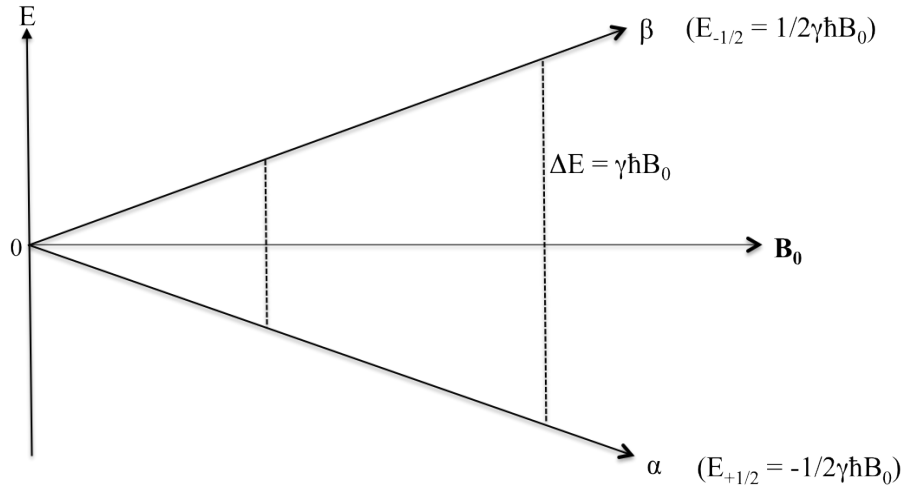

Figure 1.5: The energy separation between nuclear spin states in the absence of magnetic field to the increasing field strength B_0 (Nuclear Zeeman splitting), adapted from [51].

The NMR signals are relatively weak thus they require a proper instrumentation to be detected. The signals are often overshadowed by the noise generated by the electronics. These can be explained by the following signal to noise ratio (S/N) expression whereby the sensitivity of NMR spectroscopy is determined by certain parameters.

$$S/N \sim N\gamma_{ext}{\gamma_{det}}^{3/2}{B_0}^{3/2}NS^{1/2}T_2$$

in which S/N refers to the signal to noise ratio, N is the number of spins, γ_{exc} and γ_{det} are the gyromagnetic ratios of the excited and the detected spins, respectively, B_0 corresponds to the static magnetic field, NS attributes to the number of scans and T_2 is the contribution from the transverse relaxation (which is inversely proportional to the molecular weight of sample).

In this respect, many techniques have been developed over the decades to increase the signal's quality of NMR experiments. Based on the S/N proportionality, the quality of resonance signals can be improved by using high concentration of sample (corresponds to the number of spins, N). However, not all protein samples can be prepared at high concentration in solution without suffering from aggregation problem. Even though the use of detergents for example in membrane proteins could help in solubilisation, the unwanted signals might arise from the interaction of protein with detergent [52]. The sensitivity also relies on the magnetic susceptibility of the nuclei. In biomolecular NMR spectroscopy, proteins and nucleic acids are mainly composed of proton, carbon and nitrogen. For low natural abundant nuclei for instance ^{13}C and ^{15}N, the isotope labelling method overcomes this limitation. Besides, the strength of magnetic field will be also increased with the invention of high superconducting magnet. For low protein concentration, the signals can be improved by extending the length of the experiment, as the number of scans, NS increases. Besides, measuring samples at high temperature could narrow the peak resonance since the molecule tumble faster hence increasing the T_2 relaxation.

Table 1: The nuclear spin quantum number, *I*, the natural abundance of nuclei and the gyromagnetic ratio, γ of selected nucleus are listed in the following table (adapted from [53])				
Nucleus	Spin, *I*	Natural abundance (%)	γ $(T.s)^{-1}$ (10^7)	γ_{rel}
^{1}H	1/2	99.98	26.752	1.00
^{2}H	1	0.02	4.107	0.15
^{13}C	1/2	1.11	6.728	0.25
^{14}N	1	99.64	1.934	
^{15}N	1/2	0.36	-2.712	0.10
^{17}O	5/2	0.038	-3.628	
^{19}F	1/2	100.00	25.181	
^{23}Na	3/2	100.00	7.081	
^{31}P	1/2	100.00	10.841	0.41
^{113}Cd	1/2	12.22	-5.961	

The resonance signals in the NMR spectrum are termed chemical shift and used to identify specific nuclei in a molecule. It manifests the environment a nucleus experienced relative to the static magnetic field, B_0 as a function of frequency. Electron density around the nuclei reduces the applied magnetic field, B_0 experienced by the nucleus. As a result, the frequency required to achieve resonance is also reduced.

In practice, chemical shifts are measured relative to a reference resonance signal from a standard molecule for instance tetramethylsilane (TMS) or its derivative 4,4-dimethyl-4-silapentane-1-sulfonic acid (DSS) in part per million (ppm or δ):

$$\delta = \frac{\Omega - \Omega_{ref}}{B_0} \times 10^6 = (\sigma_{ref} - \sigma) \times 10^6$$

in which Ω and Ω_{ref} are the offset frequency of the signal of interest and reference signal while σ_{ref} and σ are the shielding constants of the reference molecule and sample respectively [53].

Magnetization transfer can happen between two spins that are close to each other, either through bond or though space. The first phenomenon is called scalar coupling or *J*-coupling and it arises when nuclear interaction is mediated by bonding electrons connected by 2-3 bonds apart. In an NMR spectrum, this spin-spin coupling produces line splitting of resonances known as multiplets. The difference between the splitting lines can be calculated and referred to coupling constant, *J*. In 1D ^{1}H NMR spectra of organic molecules, the magnitude of line splitting provides information on the number of neighbouring protons, which is useful for the structural characterization.

On the other hand, the magnetization can be transferred through space between nuclei in close proximity. This phenomenon is known as the nuclear Overhauser effect (NOE) and is governed by the dipolar relaxation process. The major factors contribute to the NOE are molecular tumbling and internuclear distance. For macromolecules, the transfer of magnetization rate between two protons is proportional to $1/r^6\ \tau_c$, in which r corresponds to the inter-proton distance and τ_c is the correlation time. The NOEs provide valuable information in determining the inter-proton distance close in space, in order to obtain the three-dimensional structure of biomolecules in solution. As a result, the relative orientation of atoms in a molecule can be obtained. The NOE can be manipulated to enhance the signal detection through proton nucleus especially for low gyromagnetic ratio, γ nuclei such as ^{13}C and ^{15}N, since the γ contributes to the sensitivity of NMR experiment.

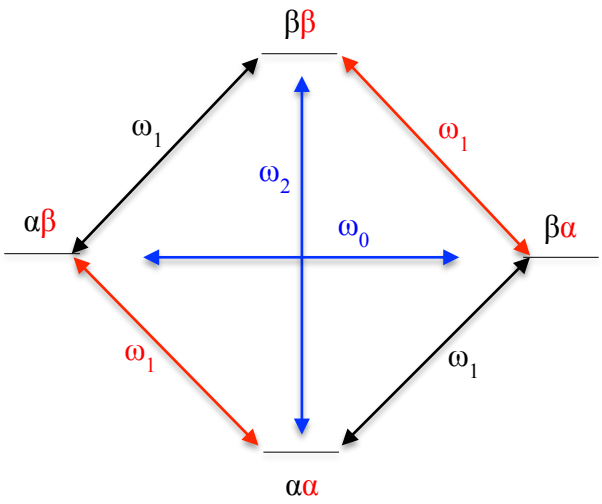

Figure 1.6: The nuclear Overhauser effect. The transition between energy level leading to zero (ω_0), single (ω_1) or double quantum (ω_2) where ω refers to the transition probability. α and β represent the spin- up and spin-down states respectively.

1.3.2 Relaxation

Relaxation is a process that drives the spins to their equilibrium state after they were subjected to a perturbation in the form of a radio frequency pulse (RF pulse). Two types of relaxation mechanisms in which the NMR signals decay over time were identified; the longitudinal relaxation (spin-lattice), T_1 and the transverse relaxation (spin-spin), T_2. T_1 is related to the loss of signal intensity while T_2 is responsible for the line broadening in NMR.

The spin-lattice relaxation, T_1 - The return of spins to its equilibrium state in the direction of magnetic field (z-axis) is also called the longitudinal relaxation. In an NMR sample tube, the spins are equally populated between two energy states and the total magnetic moment, $M_0 = 0$. Once it is placed under the magnetic field B_0, the spins establish an equilibrium state based on the Boltzmann distribution whereby the spins align themselves along the z-axis. As the RF pulse B_1 field is applied, the nuclei are excited to the higher energy states in which the population of the α-state is slightly higher than the β-state. After the RF perturbation, the nuclear magnetizations will return to their original states where the energy is transmitted to the lattice as a result of the transfer of nuclei from excited state to the ground state, giving rise to a measurable energy difference, ΔE.

The spin-spin relaxation, T_2 – the decay of magnetization perpendicular to the magnetic field, B_0 is known as the transverse relaxation. The 90° RF pulse rotates the macroscopic magnetization M from z-axis to the x,y-plane and the spins establish a phase coherence. Over time, the M component will lose its coherence and start to disperse, giving rise to the spin-spin relaxation. In general, T_2 relaxation is shorter than T_1. T_2 is correlated with the dynamic processes in the molecule of interest and it decreases proportionally with increasing molecular size. In other words, the bigger the molecule, the shorter the T_2 [50].

Paramagnetic Relaxation Enhancement (PRE) - Paramagnetic NMR is one of the indispensable tools to study the dynamic properties of biomolecules. Paramagnetic species refer to molecules or compounds with unpaired electrons, for example nitroxyl radicals or transition metal ions. The presence of paramagnetic species enhances the nuclear relaxation rate due to the dipolar interaction of nuclei with the electron spins. As a result, an observable effect on the nuclear magnetization up to 30 Å away from the paramagnetic centre can be detected. In contrary to the PRE, only the nuclear

magnetizations of interacting nuclei within 5 Å distance in space are accountable in NOE. This PRE effect allows us to study the interaction of protein with small molecules or other substrate as well as to map their specific binding sites [54].

1.3.3 Protein assignment strategy

Proteins are built from a unique sequence arrangement of amino acids residues that are linked together by peptide bonds. A network of peptide bonds constructs the backbone of protein. In the initial evaluation of the protein quality, it is common to record one-dimensional ^{1}H spectra, which provide useful information on protein folding and stability in solution. This is followed by acquiring the two-dimensional ^{1}H-^{15}N HSQC experiment on the protein construct in order to yield the information on the backbone amide correlation that serves as the starting point for the protein assignments. A well-folded protein has a distinct conformation hence producing unique signals for every residue. Besides, this allows us to plan whether a special labelling technique needs to be incorporated into the protein of interest in order to extract useful information from it. The first step in the protein assignment is to identify the individual amino acid followed by the sequential assignment of the protein backbone. These information were obtained from the combination of triple resonance experiments HNCA and CCONH. Next, the protein side chains were assigned based on the triple resonance experiments ^{13}C- and ^{15}N-NOESY, CCONH and HCCH-TOCSY. Additionally, the resonance signals of the respective δ- or γ-methyl groups of leucine and valine can also be distinguished stereospecifically by employing the method developed by Neri and co-workers. In this method, biosynthetically directed fractional ^{13}C labelling was implemented based on the idea that the biosynthesis pathway of valine and leucine is stereoselective [55]. Even though not all valine and leucine can be stereospecifically assigned due to overlapping signals, this assignment largely improves the local protein conformation in structure calculations [56].

1.3.4 Structure calculation

The main source of structural information in the protein structure determination are the distance restraints derived from the NOE assignments, correspond to the proton-proton distance belong to the residues close in space. The NOESY experiment measures the magnetization transfer rate between protons, which is proportional to $1/r^6$, whereby r is the distance between two protons. For this, the NOE distance restraints are usually divided into three categories based on the peak intensity, represented by strong, medium and weak signals; the upper bounds are 2.8 Å, 3.5 Å, 4.5 Å and 5.5 Å. The lower bound is set to 1.8 Å to account for the van der Waals radii.

$$J = \langle d_{ij}^{-6} \rangle f(\tau_c)$$

NOE distance restraints and hydrogen bond restraints define the distance of interacting nuclei in close proximity. While torsion angle restraints are important to further establish the local conformation of the protein. They can be described from the Karplus equation for the three-bond coupling constant, ^3J. Such information can be used to restrain the dihedral angles ϕ and ψ of the protein backbone and sometimes the side chain χ angles [57]. Hydrogen bond restraints can be additionally defined from the assessment of protein secondary structure either adopting α-helices or β-sheets conformation.

$$^3J(\theta) = A\cos^2\theta + B\cos\theta + C$$

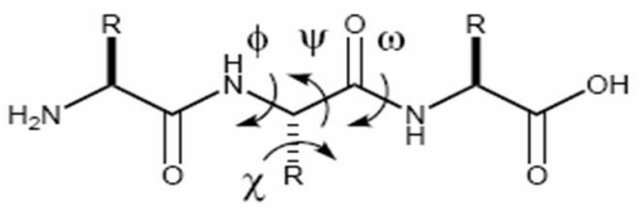

Figure 1.7: The picture displays the definition of protein dihedral angles ϕ (connects the amide N to the C_α), ψ (forms from the C_α to the carbonyl group) and χ (side chain angle) [57].

The three-dimensional structure of a protein derived from the NMR distance restraint data must obey defined geometrical constraints for instance bond angles, bond lengths and van der Waals forces. There are two methods commonly applied to calculate the protein structure namely the distance geometry (DG) and restrained molecular dynamics

(RMD). Distance geometry uses mathematical tool to generate protein structures that satisfy the internuclear distance obtained from NMR data. For protein structures, a major drawback of this method is the search for the local minima. This was later improved by applying restrained molecular dynamics which resulted in a better agreement between the calculated structure and the NMR data at the same time lowering the computed energy of the protein [58].

A combination of few computational methods is commonly used in protein structure calculation for example a hybrid of distance geometry-simulated annealing [59, 60]. The combined method not only improves the quality of structures but also reduce the calculation time with higher computational efficiency [61]. Generally, after the initial protein structure was built from the NOE distance restraints information, the protein ensemble is refined by implementing the simulated annealing calculation. The system is virtually heated to a high temperature followed by gradual cooling in order to search for a global minimum region by overcoming the energy barrier along the pathway [62]. Basically, an ensemble of 20-200 structures is calculated and 20 structures with the lowest energy were analyzed. The root mean square deviation (RMSD) reflects the conformational variation in the ensemble. Many software were developed for the qualitative assessment of the calculated structures for instance AQUA, PROCHECK [63] and CING [64].

2. Methodology

2.1 Protein expression and purification

The sequence coded for the C-terminal FAT (FATC) domain of human ATM (residue 3024-3056, UniProt ID 13315) and DNA-PKcs (residue 4096-4128, Uniprot ID P78527) protein kinases was cloned into GEV2 [65] as described earlier [23]. Both fusion proteins compose of GB1 (residues 1-56), a linker region composed of a thrombin (57-62) and an enterokinase (63-67) protease, and the subsequent C-terminal 33 residue of human ATM or DNA-PKcs (68-100) (denoted as hATMfatc-gb1ent and hDNAPKfatc-gb1ent respectively) were overexpressed in *Escherichia coli* BL21 at 37 ºC. Uniformly ^{15}N-, or $^{15}N,^{13}C$-labeled proteins were prepared in M9 minimal medium containing $^{15}NH_4Cl$ and/or ^{13}C-glucose as the sole nitrogen and carbon sources. The expression and the purification were accomplished by a heating step [66] followed by IgG affinity chromatography step as described previously [23, 67].

2.2 Preparation of membrane-mimetics

Dodecylphosphocholine (DPC), 1,2-diheptanoyl-*sn*-glycero-3-phosphocholine (DihepPC), 1,2-dimyristoyl-*sn*-glycero-3-phosphocholine (DMPC), 5-doxyl stearic acid (5-SASL), and 16-doxyl stearic acid (16-SASL) were purchased from Avanti Polar Lipids and/or Sigma-Aldrich. Deuterated DPC (d_{38}-DPC) was obtained from Cambridge Isotopes.

Membrane mimetic DPC micelles were prepared by pipetting a defined amount of DPC from a concentrated stock solution in chloroform (0.5 M) into a glass vial followed by drying under a stream of nitrogen gas. The resulting DPC film was then dissolved in NMR buffer containing the protein of interest. For NMR titration experiments samples containing >30 mM DPC samples were prepared in the same way, whereas those with DPC concentrations < 30 mM were prepared by diluting a 100 mM DPC stock in buffer with a protein stock and buffer. Note that a separate sample was prepared for each DPC concentration to avoid dilution effects and thus to keep the protein concentration constant. DihepPC micelles were prepared by diluting a 0.25 M stock solution in NMR buffer to 50 mM final concentration with the respective protein solution. The value of respective micelles above the critical micelle concentration (CMC) is 1.1 mM for DPC [68] and 1.4-1.8 mM for DihepPC [69, 70].

DMPC/DihepPC bicelles (q = 0.2, [DMPC] = 0.04 M, and [DihepPC] = 0.20 M, cL 15%) were prepared as follows. An appropriate amount of a 0.25 M stock of the long-chain phospholipid (DMPC) in chloroform was placed in a glass vial and the chloroform was blown away under a stream of nitrogen gas. In order to form bicelles, the right amount of the short-chain lipid (DihepPC) in NMR buffer was added into a vial and vortexed until a clear solution was obtained. Lastly, the protein solution was added to the concentrated bicelles solution.

Liposomes were prepared by drying an appropriate amount of DMPC in chloroform (0.25 M) under a stream of nitrogen gas. The resulting pellet was dissolved in NMR buffer obtaining a 100 mM solution. To dissolve the pellet, seven cycles of freezing-thawing were applied to it. This is done by alternately freezing the pellet in liquid nitrogen, then thawing it in a water bath at 40 °C while thoroughly vortexing between the cycle. To induce the formation of small unilamellar vesicles (SUVs) from large uni- and multilamellar vesicles, the DMPC suspension was incubated in an ultra-sonication bath for 30 minutes. A clear supernatant containing only SUVs was obtained after centrifuging the lipid mixture at about 15 krpm in a table-top centrifuge for 5 minutes. The resulting white precipitate at the bottom corresponds to large uni- and multilamellar vesicles. For the preparation of a protein sample in the presence of liposomes, only the clear supernatant containing small unilamellar vesicles was diluted 1:1 with protein solution. Thus, from the initial 100 mM stock solution the final sample would contain < 50 mM DMPC.

2.3 NMR sample preparation

For the NMR resonance assignment and structural characterization samples containing ~0.5 mM of uniformly labeled ^{15}N- or ^{15}N,^{13}C-(hATMfatc-gb1ent or hDNAPKfatc-gb1ent) in 50 mM Tris, 100 mM NaCl, 10 mM TCEP, 0.02% NaN_3 (95% H_2O/5% D_2O), pH 6.5, 150 mM d_{38}-DPC were used. We also prepared samples with 200 mM d_{38}-DPC (180 mM d_{38}-DPC and 20 mM DPC), but the spectral quality was overall lower (broad signals, more noises) than for samples with 150 mM DPC. The 10% ^{13}C-labeled of both protein samples were used for the stereospecific assignment of valine and leucine methyl groups contained 170 mM d_{38}-DPC micelles.

The mutant of hATMfatc-gb1ent and hDNAPKfatc-gb1ent samples contained about 0.15 mM ^{15}N-labeled protein in NMR buffer. All hDNAPKfatc-gb1ent mutants (W93A = W4121A, W96A = W4124A, and W93A/W96A = W4121A/W4124A) and the hATMfatc-gb1ent double mutant (F93/W96 = F3049A/W3052A) samples were suspended in buffer pH 6.5. While the single mutants (F93 = F3049A, W96 = W3052A) were measured at pH 7.4 in order to improve their solubility and stability.

The samples for NMR experiments acquired in the presence of spin-labeled micelles, protein samples containing about 0.1 mM protein and 50 mM undeuterated DPC were prepared. The concentration of 5- and 16-doxyl stearic acid (5-/16-SASL) was increased gradually by adding a small amount of spin labeled compound (from 1 mM to a maximum 4 mM) from a 0.25 M stock solution in chloroform.

2.4 NMR experiments and protein assignments

NMR spectra were recorded on Bruker Avance 500 MHz, 600 MHz, 750 MHz and 900 MHz spectrometers at a temperature of 298 K. The 500 MHz and 900 MHz spectrometers were equipped with cryogenic probes. Data were processed with NMRPipe [71] and analyzed using NMRView [72]. Assignments for the ^{13}C, ^{15}N, and ^{1}H nuclei of micelle-immersed hATMfatc fusion protein were based on 2D ^{1}H-^{15}N and various ^{1}H-^{13}C HSQC spectra, partially without decoupling, 3D HNCA [73] HNCACB [74], CCONH-TOCSY [75, 76], HCCH-TOCSY [77], HNHA, HNHB and ^{15}N- and ^{13}C-edited NOESY [78] spectra as described [67]. The NOESY mixing times were 90 ms for the ^{15}N-edited NOESY, 100 ms for the aromatic and aliphatic ^{13}C-edited NOESY experiments. Information about backbone dynamics was derived from the analysis of ^{15}N relaxation data, including T_1 (spin-lattice longitudinal relaxation rate), T_2 (spin-spin transverse relaxation rate), and (^{1}H)-^{15}N NOE.

2.5 Structure calculation

The structure calculation was performed with XPLOR-NIH [79] using molecular dynamics in torsion angle and Cartesian coordinate space. Distance restraints were generated in NMRView [72] and classified according to NOE-cross peak intensities. Upper bounds were 2.8 Å, 3.5 Å, 4.5 Å and 5.5 Å. The lower bound was always 1.8 Å to account for the van der Waals radii. For all NOE restraints, r^{-6} sum averaging was used.

Backbone dihedral angle restraints for ϕ and ψ as well as hydrogen bond restraints for helical regions were derived based on the determined $^{13}C^{\alpha}$ chemical shifts, observed helix typical NOE restraints and the initial structure calculations.

2.6 NMR experiments with spin-labelled micelles

The immersion depth properties of hATMfatc in DPC micelles were derived by recording ^{1}H-^{15}N HSQC and 1D ^{1}H-NMR spectra of samples containing increasing amounts of paramagnetic 5- or 16-doxyl stearic acid (5- and 16-SASL). The resulting paramagnetic relaxation enhancement (PRE) effects were derived based on the observed changes in signal intensity. In addition, the average chemical shift changes of the backbone amide nitrogen and proton $[(\Delta\delta(N,H)_{av}]$ were calculated based on the formula $[(\Delta\delta_{HN})^2 + (\Delta\delta_N/5)^2]^{1/2}$. The interaction of mutant proteins with membrane mimetics was monitored by recording 1D ^{1}H and 2D ^{1}H-^{15}N HSQC spectra.

3. Summary of publications

This thesis is submitted as a publication-based dissertation. The first article has been published in the journal of Biomolecular NMR Assignment while the second article has been submitted to the Journal of Biological Chemistry.

3.1 Resonance assignments of micelle-immersed hATMfatc-gb1ent and hDNAPKfatc-gb1ent

Title: ^{1}H, ^{15}N, and ^{13}C chemical shift assignments of the micelle immersed FAT C-terminal (FATC) domain of the human protein kinases ataxia-telangiectasia mutated (ATM) and DNA-dependent protein kinase catalytic subunit (DNA-PKcs) fused to the B1 domain of streptococcal protein G (GB1).

The FATC domain is located at the extreme C-terminal of PIKK protein kinases and regulates kinase activity in PIKKs. Extended information on the protein structure allows us to understand the function and regulation of PIKK in general. Furthermore, the structure characterization of protein membrane bound state may provide useful information related to their proper cellular localization at different membranes. The article presents the NMR assignments for micelles-immersed state of FATC domain belong to the two PIKK homologues; human ATM and DNA-PKcs. Both compose of 100 amino acid residues; 1-56 correspond to the GB1 tag, followed by linkers LVPRGS (thrombin) and DDDDK (enterokinase) or IEGR (factor Xa) and FATC domain from residue 68-100.

For resonance assignment purposes, a high concentration of protein is needed. While the cleavage of the tag significantly reduces the yield and compromises the protein stability in solution, fusing with GB1 tag has proven to help in improving the yield, stability and solubility of protein in buffer. Most importantly, the tag has a negligible interaction with membrane mimetics hence does not disturb the interaction of FATC with membrane mimetics [80]. In addition, the FATC domain can tumble independently in solution due to the presence of relatively long linker. Therefore, in this study we utilized the GB1-tagged fusion proteins in all NMR experiments.

The resonance signals of the ^{1}H and ^{15}N nuclei of 96 residues (except for 3 prolines and one terminal methionine) were assigned. The assignments also include the side chain -NH_2 groups belong to glutamine and asparagine as well as the side chain -NHε group of

tryptophans. However only the signal from tryptophans in the GB1 tag could be distinguished due to overlapping signal. The aliphatic side chain chemical shifts were obtained from 3D CCONH and HCCH-TOCSY data in combination with 3D HNHB and ^{15}N- and ^{13}C-edited NOESY experiments. Additionally, the δ-methyl leucine and γ-methyl valine were stereo-specifically assigned based on ^{1}H-^{13}C HSQC spectra of 10% ^{13}C-labeled protein. Some of the aromatic side chain chemical shifts could also be assigned even though the signals were relatively weak compared to those from the GB1 tag.

The NMR chemical shift assignments for the micelle-immersed ATM and DNA-PKcs FATC domains were deposited in the BMRB database under the accession number 27167 and 27168 respectively.

3.2 The NMR structure, dynamics and immersion properties of micelles-associating hATMfatc

Title: Structural characterization of the membrane-associating FATC domain of ataxia telangiectasia mutated by NMR and MD simulations (submission in progress)

In this study, we have performed various multidimensional heteronuclear NMR experiments to determine the three-dimensional structure of human ATM FATC domain (hATMfatc) in DPC micelles. The NMR distance restraints are the basis for the structure calculation. The immersion properties of the hATMfatc were investigated by performing molecular dynamics simulations as well as recording NMR spectra of protein in the presence of spin-labelled compounds in DPC micelles. The insight into the atomic structure of micelle-associated hATMfatc is gained, leading to a better understanding of the mechanisms governing the regulation of PIKKs.

Distance restraints were generated from the NOE data and used for the structure calculation with XPLOR-NIH program [79]. The results revealed that micelle-associating hATMfatc consists of three helices connected by flexible linkers. Unlike yeast TOR FATC domain whose structure adopts a well-defined helix [81], hATMfatc is relatively dynamic and only adopts a more ordered structure upon interaction with membrane mimetics. The whole hATMfatc structure shows a high RMSD value of 4.47Å due the presence of flexible linkers. From the N-terminal of hATMfatc domain, the three helices are denoted as α1, α2 and α3 with RMSD values of 0.37 Å, 0.22 Å and 0.27 Å respectively. On average, α1 encompasses residues G73/3029-A83/3039, α2 residues K87/3043-R91/3047 and finally α3 residues G95/3051-W99-3055. 85.5% of the residues in the structure ensemble occupy the most favoured region of the Ramachandran plot.

The analysis of micelle-associated hATMfatc backbone dynamics based on ^{1}H-^{15}N-NOE, ^{15}N-T_1 and -T_2 data and MD simulation pointed out that the flexible linkers contribute largely to the dynamic properties of the protein compared to local conformational changes. Therefore, performing MD simulation on the micelle-associating hATMfatc structures is tricky due the broad-range structural conformations of the protein ensembles. In this case, the first three best structures from the group of 20 NMR structures with the lowest energy were selected for the simulations. The results demonstrated that all helices localize near the polar head group region of DPC micelles and not deeply into the

aliphatic core. Experimentally, we performed ^{1}H-^{15}N HSQC titration experiments on micelle-associating hATMfatc domain containing paramagnetic 5- or 16-doxyl stearic acids (5-/16-SASL) to estimate the immersion properties. Residues residing close to the micelle polar head group are expected to show strong PRE effects. On the other hand, the chemical shifts from GB1 tag do not change significantly and does not show strong PRE effects supporting the fact that the GB1 tag does not interact with the membrane mimetics as reported previously [23, 80].

The amino acid sequence of the FATC domain is highly conserved in all PIKKs. Aromatic residues such as tryptophan and phenylalanine are known to bind strongly to the membrane mimetics [82-84]. In this study, either tryptophan or phenylalanine at position F93/3049, W96/3052 or both F93/3049-W96/3052 were replaced by alanine and the effect of mutation on the binding properties to membrane mimetics was investigated. For this, the 2D ^{1}H-^{15}N HSQC spectra of hATMfatc in the presence of various membrane mimetics; DPC and DihepPC micelles, bicelles as well as SUVs were recorded. Strong spectral changes in micelles, bicelles and SUVs were observed for both single mutants, indicating that they interact with all tested membrane mimetics. On the other hand, double mutant F93/3049A-W96/3052A could no longer interact with SUVs even though the interaction with micelles and bicelles could still be observed.

It is also worth noting that the presented structure is similar to the cryo-electron microscopy (cryo-EM) structure which composes of two α-helices and a C-terminal helix or turn-like structure [85].

4. Mutagenesis studies of human DNA-PKcs FATC domain

DNA-PKcs is another homologue from the PIKK family, responsible in DNA damage repair through non-homologous end joining (NHEJ) mechanism [86, 87]. The following results are not published, however will provide additional information on the role of aromatic residues in the FATC domain for membrane interactions.

4.1 Results

We have performed a study to investigate the effect of specific mutation in the FATC domain of human DNA-PKcs (hDNAPKfatc) on the interaction with selected neutral membrane mimetics by NMR spectroscopy. In order to monitor if the mutants either interact or not with membrane mimetics, a series of ^{1}H-^{15}N HSQC experiments were acquired on the mutant proteins in the absence and presence of each membrane mimetic. The membrane mimetics used in this study were DPC and DihepPC micelles, DMPC/DihepPC bicelles and DMPC SUVs. In this study, tryptophans either at position 93/4121 or 96/4124 or at both positions at the same time were substituted with alanine by site-directed mutagenesis. All mutant proteins were expressed as fusion proteins containing a GB1 tag, thrombin and factor Xa recognition sites as linkers (residues 1-66) followed by 33-residue long FATC domain (67-99).

Based on the NMR spectra recorded on the single mutants (W93/4121A and W96/4124) as well as double mutant (Fig 4.1, 4.2 and 4.3), residues corresponding to the FATC region showed some noticeable chemical shift changes upon binding to DPC and dihepPC membrane micelles, as well as DMPC/dihepPC bicelles except for W93/4121A which showed very weak interaction to DihepPC micelles. On the other hand, the NMR spectra in the presence of SUVs indicated no or very small chemical shift changes, suggesting that all mutants do not or only very weakly interact with SUVs.

We also investigated the chemical shift changes of both single mutant proteins with increasing concentration of DPC (Fig 4.2A, 4.3A). Gradually increasing the chemical shift changes can be seen for peaks belonging to the FATC domain. However, in double mutant (Fig 4.1A), the chemical shift changes can only be observed at 5 mM DPC compared to the single mutants at 2.5 mM. This indicates that the double mutant has a lower affinity for DPC micelles than the single mutants.

4.2 Discussion

The amino acid sequence of the FATC domain of all PIKKs is evolutionarily conserved in eukaryotic cells, ranging from yeast to human. In fact, some PIKKs members still retained their function even after the FATC domain was exchanged with the one from other PIKK members [21]. Mutations in this domain are associated with cancer and other diseases [20, 24, 88]. One interesting property of the FATC domain of PIKKs is the ability to interact with specific membrane [23]. The study explained the general role of FATC domain as a membrane anchor with special preference for membrane mimetics based on their surface charges and lipid composition or membrane curvature. The preference for particular membrane curvature could also be the result of specific sequence conservation feature in the FATC domain [23]. Aromatic residues such as tryptophan and phenylalanine are hydrophobic in nature and are known for their high affinity for membrane lipids [83, 89]. In this study, the role of specific amino acids particularly tryptophan was investigated by performing mutagenesis study on FATC domain of DNA-PKcs (hDNAPKfatc). The data indicates that replacement of one or both tryptophans by alanine hampers the interaction with SUVs and reduces that of the double mutant with DPC micelles.

Previous study demonstrated that the wild type hDNAPKfatc interacts with DPC micelles and DMPC/DihepPC bicelles but not with DMPC SUVs. Further titration experiment on hDNAPKfatc with DPC micelles resulted in strong chemical shift changes at the region C4106-D4113 as well as at the C-terminal half of FATC domain whose regions rich in tryptophan residues (W4121-M4128) [23].

In comparison, mutagenesis studies on the FATC domain of yeast target of rapamycin (y1fatc) were done in great detail whereby up to seven residues in FATC were mutated [90]. The study showed that replacing even up to seven residues did not abrogate the binding to micelles and bicelles. However, no significant interaction was observed in SUVs when specific single aromatic residues were replaced for example residues Y4263 and W2466.

Table 2: Summary of the NMR-monitored interaction analysis of mutant hDNAPKfatc-gb1xa proteins in the presence of selected neutral membrane mimetics

Mutation	DPC micelles (50 mM)	DihepPC micelles (50 mM)	DMPC/dihepPC bicelles	DMPC SUVs (<50 mM DMPC)
W93/4121A	+	(+)	+	(+)
W96/4124A	+	+	+	-
W93/W96-4121A/4124A	+	+	+	-

+ = significant spectral changes indicating interaction with membrane mimetics
(+) = small spectral changes indicating very weak interaction with membrane mimetics
- = no significant spectral changes, hence no interaction with membrane mimetics

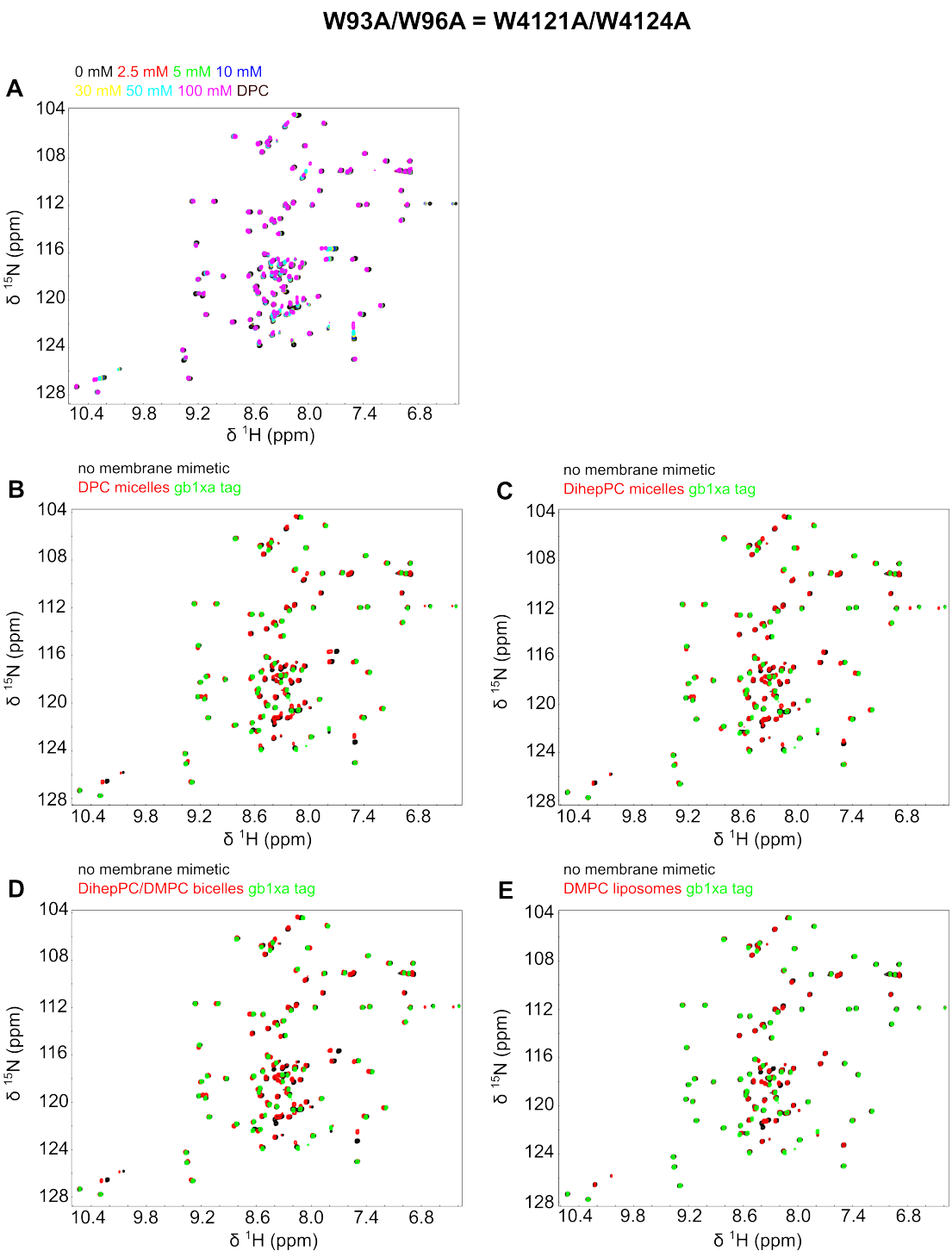

Figure 4.1: Results of the NMR-monitored study of mutant hDNAPKfatc (W93/W96-4121A/4124A) in the presence of neutral membrane mimetics. **(A)** The superposition of ^{1}H-^{15}N-HSQC spectra in the presence of stepwise increasing concentrations of DPC. **(B-E)** – illustrate superposition of the ^{1}H-^{15}N HSQC spectra of the respective mutant in the absence and presence of 50 mM DPC micelles **(B)**, 50 mM DihepPC micelles **(C)**, DMPC/DihepPC bicelles (q = 0.2, [DMPC] = 0.04 M, and [DihepPC] = 0.20 M, cL 15%, **(D)**) and DMPC liposomes (< 50 mM DMPC, **(E)**). The spectrum of the free form is coloured in black and the spectrum in the presence of membrane mimetic is shaded in red. In order to differentiate the signals of the FATC part, the spectrum of the GB1 tag followed by a thrombin and factor Xa site (= gb1xa) is added on top in green.

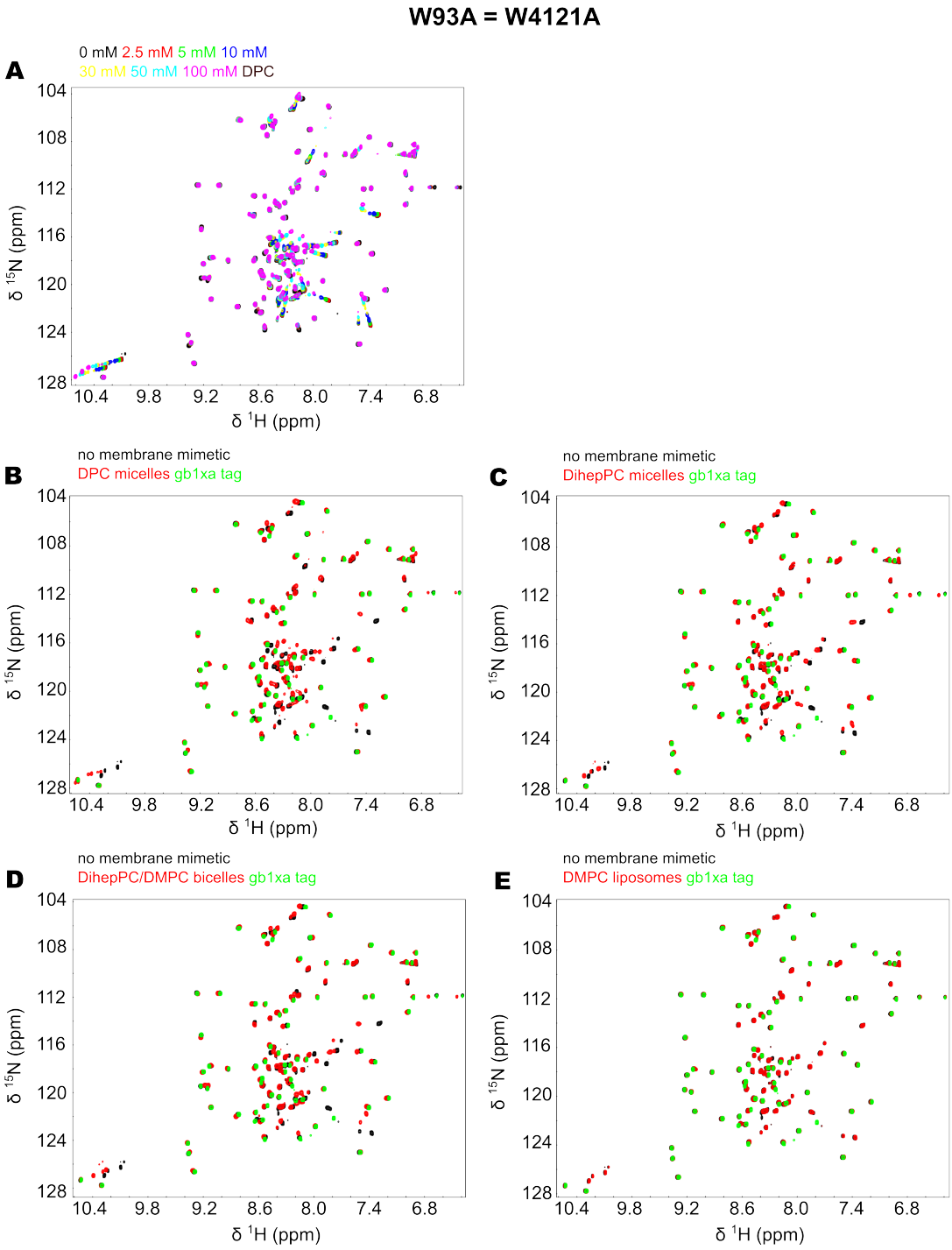

Figure 4.2: Results of the NMR-monitored study of mutant hDNAPKfatc (W93/4121A) in the presence of neutral membrane mimetics. **(A)** The superposition of ^{1}H-^{15}N-HSQC spectra in the presence of stepwise increasing concentrations of DPC. **(B-E)** – illustrate superposition of the ^{1}H-^{15}N HSQC spectra of the respective in the absence and presence of 50 mM DPC micelles **(B)**, 50 mM DihepPC micelles **(C)**, DMPC/DihepPC bicelles (q = 0.2, [DMPC] = 0.04 M, and [DihepPC] = 0.20 M, cL 15%, **(D)**) and DMPC liposomes (< 50 mM DMPC, **(E)**). The spectrum of the free form is coloured in black and the spectrum in the presence of membrane mimetic is shaded in red. In order to differentiate the signals of the FATC part, the spectrum of the GB1 tag followed by a thrombin and factor Xa site (= gb1xa) is added on top in green.

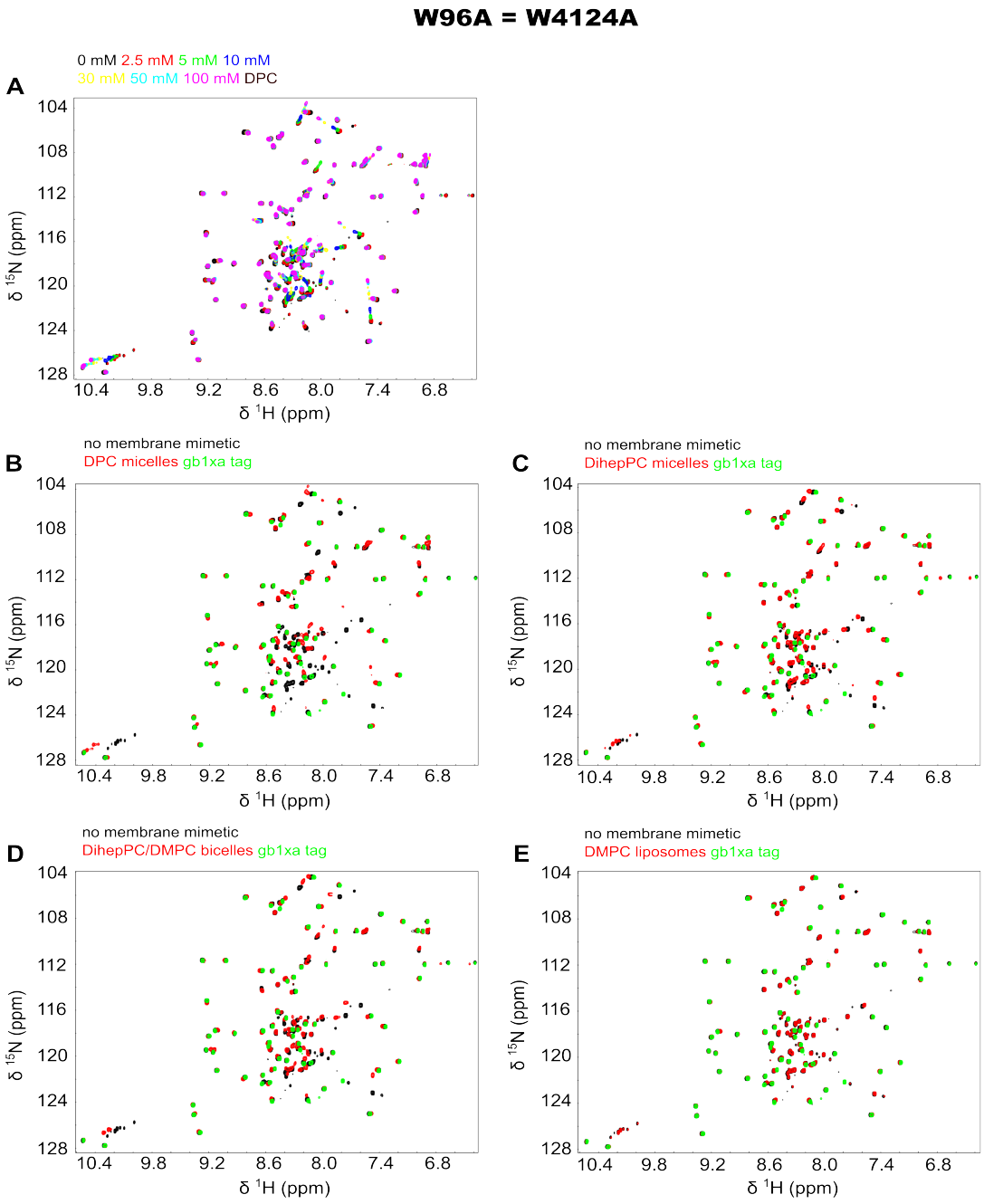

Figure 4.3: Results of the NMR-monitored study of mutant hDNAPKfatc (W96/4124A) in the presence of neutral membrane mimetics. **(A)** The superposition of ^{1}H-^{15}N-HSQC spectra in the presence of stepwise increasing concentrations of DPC. **(B-E)** – illustrate the superposition of the ^{1}H-^{15}N HSQC spectra of the respective mutant in the absence and presence of 50 mM DPC micelles **(B)**, 50 mM DihepPC micelles **(C)**, DMPC/DihepPC bicelles (q = 0.2, [DMPC] = 0.04 M, and [DihepPC] = 0.20 M, cL 15%, **(D)**) and DMPC liposomes (< 50 mM DMPC, **(E)**). The spectrum of the free form is coloured in black and the spectrum in the presence of membrane mimetic is shaded in red. In order to differentiate the signals of the FATC part, the spectrum of the GB1 tag followed by a thrombin and factor Xa site (= gb1xa) is added on top in green.

Conclusion

The structure of hATMfatc associated with DPC micelles was elucidated at the atomic level by solution NMR spectroscopy and structure calculation techniques. While the investigation of the dynamic and immersion properties of this protein in micelles was achieved by performing molecular dynamics simulation in combination with ^{15}N-relaxation data and NMR-based studies on the interaction of respective FATC domain with micelles containing spin-labelled molecules. Thus, the study not only provides a structural insight of hATMfatc in micelle-bound form, but also about the relative orientation and immersion in the micelle environment. These data complements the previous one on the tendency of FATC domain to interact with membrane mimetics that differ on their shape and lipids composition. The observed dynamic structure constituting of these short but rather flexibly linked helices may enable the interaction with specific membrane-localization binding partners in the cellular environment.

The FATC domain of PIKKs is relatively hydrophobic in nature because of the presence of many aliphatic and aromatic amino acid residues. Aromatic residues in particular tryptophans are known to show a high affinity for membrane mimetics [82-84]. Therefore, additional qualitative studies on the effect of mutation to the binding property of the FATC of human ATM and DNA-PKcs have been analysed by monitoring the interaction of specific mutants with different neutral membrane mimetics. Compared to the single mutants, the double mutant of hDNAPKfatc (W93/W96-4121A/4124A), showed a reduce affinity for DihepPC micelles. On the other hand, replacement of two aromatic residues in hATMfatc (F93/W96-3049A/3052A) was needed to abrogate the interaction with SUVs while substituting single tryptophan at W96/4124A in the hDNAPKfatc was enough to eliminate the ability to interact with SUVs. Meanwhile, both single mutants (F93/3049A or W96/3052A) were able to interact with all tested membrane mimetics. Besides, information on mutants' backbone dynamics in comparison to their wild type was also gained from these investigations. In general, the FATC domains of both ATM and DNA-PKcs are unstructured in their membrane-free forms and became more structured upon binding with membrane mimetics [23].

In general, the detailed structural information on FATC domain of human ATM might pave the route to a better understanding of the function and localization of membrane-

bound protein, besides opening the possibility to study mutants that have lost the binding ability to SUVs in *in-vivo* study. Since the sequence of FATC domain in PIKKs is well conserved, the atomic resolution structure of human ATM FATC could complement the current structural information obtained from either X-Ray crystallography or cryo-electron microscopy technique.

References

1. Laplante, M. and D.M. Sabatini, *mTOR signaling at a glance.* J Cell Sci, 2009. **122**(Pt 20): p. 3589-94.
2. Laplante, M. and D.M. Sabatini, *mTOR signaling in growth control and disease.* Cell, 2012. **149**(2): p. 274-93.
3. Yamashita, A., et al., *Human SMG-1, a novel phosphatidylinositol 3-kinase-related protein kinase, associates with components of the mRNA surveillance complex and is involved in the regulation of nonsense-mediated mRNA decay.* Genes & Development, 2001. **15**(17): p. 2215-2228.
4. Yamashita, A., I. Kashima, and S. Ohno, *The role of SMG-1 in nonsense-mediated mRNA decay.* Biochim Biophys Acta, 2005. **1754**(1-2): p. 305-15.
5. Abraham, R.T., *Cell cycle checkpoint signaling through the ATM and ATR kinases.* Genes Dev, 2001. **15**(17): p. 2177-96.
6. Bakkenist, C.J. and M.B. Kastan, *DNA damage activates ATM through intermolecular autophosphorylation and dimer dissociation.* Nature, 2003. **421**(6922): p. 499-506.
7. Falck, J., J. Coates, and S.P. Jackson, *Conserved modes of recruitment of ATM, ATR and DNA-PKcs to sites of DNA damage.* Nature, 2005. **434**(7033): p. 605-11.
8. Serrano, M.A., et al., *DNA-PK, ATM and ATR collaboratively regulate p53-RPA interaction to facilitate homologous recombination DNA repair.* Oncogene, 2012.
9. Ard, P.G., et al., *Transcriptional regulation of the mdm2 oncogene by p53 requires TRRAP acetyltransferase complexes.* Mol Cell Biol, 2002. **22**(16): p. 5650-61.
10. Grant, P.A., et al., *The ATM-Related Cofactor Tra1 Is a Component of the Purified SAGA Complex.* Molecular Cell, 1998. **2**(6): p. 863-867.
11. De Cicco, M., M.S. Abd Rahim, and S.A. Dames, *Regulation of the Target of Rapamycin and Other Phosphatidylinositol 3-Kinase-Related Kinases by Membrane Targeting.* Membranes (Basel), 2015. **5**(4): p. 553-75.
12. Groves, M.R. and D. Barford, *Topological characteristics of helical repeat proteins.* Curr Opin Struct Biol, 1999. **9**(3): p. 383-9.
13. Knutson, B.A., *Insights into the domain and repeat architecture of target of rapamycin.* J Struct Biol, 2010. **170**(2): p. 354-63.
14. Bosotti, R., A. Isacchi, and E.L. Sonnhammer, *FAT: a novel domain in PIK-related kinases.* Trends Biochem Sci, 2000. **25**(5): p. 225-7.
15. Imseng, S., C.H.S. Aylett, and T. Maier, *Architecture and activation of phosphatidylinositol 3-kinase related kinases.* Current Opinion in Structural Biology, 2018. **49**: p. 177-189.
16. Yang, H., et al., *mTOR kinase structure, mechanism and regulation.* Nature, 2013. **497**(7448): p. 217-23.
17. Lempiainen, H. and T.D. Halazonetis, *Emerging common themes in regulation of PIKKs and PI3Ks.* EMBO J, 2009. **28**(20): p. 3067-73.
18. Lovejoy, C.A. and D. Cortez, *Common mechanisms of PIKK regulation.* DNA Repair (Amst), 2009. **8**(9): p. 1004-8.
19. Mordes, D.A., et al., *TopBP1 activates ATR through ATRIP and a PIKK regulatory domain.* Genes Dev, 2008. **22**(11): p. 1478-89.
20. Sun, Y., et al., *A role for the Tip60 histone acetyltransferase in the acetylation and activation of ATM.* Proc Natl Acad Sci U S A, 2005. **102**(37): p. 13182-7.

21. Jiang, X., et al., *The FATC domains of PIKK proteins are functionally equivalent and participate in the Tip60-dependent activation of DNA-PKcs and ATM.* J Biol Chem, 2006. **281**(23): p. 15741-6.
22. Sun, Y., et al., *DNA damage-induced acetylation of lysine 3016 of ATM activates ATM kinase activity.* Mol Cell Biol, 2007. **27**(24): p. 8502-9.
23. Sommer, L.A.M., M. Schaad, and S.A. Dames, *NMR- and Circular Dichroism-monitored Lipid Binding Studies Suggest a General Role for the FATC Domain as Membrane Anchor of Phosphatidylinositol 3-Kinase-related Kinases (PIKK).* Journal of Biological Chemistry, 2013. **288**(27): p. 20046-20063.
24. Hoke, S.M., et al., *Mutational analysis of the C-terminal FATC domain of Saccharomyces cerevisiae Tra1.* Curr Genet, 2010. **56**(5): p. 447-65.
25. Morita, T., et al., *Distant N- and C-terminal domains are required for intrinsic kinase activity of SMG-1, a critical component of nonsense-mediated mRNA decay.* J Biol Chem, 2007. **282**(11): p. 7799-808.
26. Mugler, A., F. Tostevin, and P.R. ten Wolde, *Spatial partitioning improves the reliability of biochemical signaling.* Proceedings of the National Academy of Sciences, 2013. **110**(15): p. 5927.
27. Mugler, A., et al., *Membrane Clustering and the Role of Rebinding in Biochemical Signaling.* Biophys J, 2012. **102**(5): p. 1069-78.
28. Berchtold, D. and T.C. Walther, *TORC2 plasma membrane localization is essential for cell viability and restricted to a distinct domain.* Mol Biol Cell, 2009. **20**(5): p. 1565-75.
29. Zinzalla, V., et al., *Activation of mTORC2 by association with the ribosome.* Cell, 2011. **144**(5): p. 757-68.
30. Drenan, R.M., et al., *FKBP12-rapamycin-associated protein or mammalian target of rapamycin (FRAP/mTOR) localization in the endoplasmic reticulum and the Golgi apparatus.* J Biol Chem, 2004. **279**(1): p. 772-8.
31. Liu, X. and X.F. Zheng, *Endoplasmic reticulum and Golgi localization sequences for mammalian target of rapamycin.* Mol Biol Cell, 2007. **18**(3): p. 1073-82.
32. Ohnishi, T., et al., *Phosphorylation of hUPF1 Induces Formation of mRNA Surveillance Complexes Containing hSMG-5 and hSMG-7.* Molecular Cell, 2003. **12**(5): p. 1187-1200.
33. Brumbaugh, K.M., et al., *The mRNA Surveillance Protein hSMG-1 Functions in Genotoxic Stress Response Pathways in Mammalian Cells.* Molecular Cell, 2004. **14**(5): p. 585-598.
34. Brown, J.A., et al., *A novel role for hSMG-1 in stress granule formation.* Mol Cell Biol, 2011. **31**(22): p. 4417-29.
35. McMahon, S.B., M.A. Wood, and M.D. Cole, *The essential cofactor TRRAP recruits the histone acetyltransferase hGCN5 to c-Myc.* Mol Cell Biol, 2000. **20**(2): p. 556-62.
36. Watters, D., et al., *Cellular localisation of the ataxia-telangiectasia (ATM) gene product and discrimination between mutated and normal forms.* Oncogene, 1997. **14**(16): p. 1911-21.
37. Yan, J., K.K. Khanna, and M.F. Lavin, *Defective radiation signal transduction in ataxia-telangiectasia cells.* Int J Radiat Biol, 2000. **76**(8): p. 1025-35.
38. Kruger, A. and M. Ralser, *ATM is a redox sensor linking genome stability and carbon metabolism.* Sci Signal, 2011. **4**(167): p. pe17.
39. Ditch, S. and T.T. Paull, *The ATM protein kinase and cellular redox signaling: beyond the DNA damage response.* Trends Biochem Sci, 2012. **37**(1): p. 15-22.

40. Lucero, H., D. Gae, and G.E. Taccioli, *Novel localization of the DNA-PK complex in lipid rafts: a putative role in the signal transduction pathway of the ionizing radiation response.* J Biol Chem, 2003. **278**(24): p. 22136-43.
41. Bharti, A., et al., *Inactivation of DNA-dependent protein kinase by protein kinase Cdelta: implications for apoptosis.* Mol Cell Biol, 1998. **18**(11): p. 6719-28.
42. Majumder, P.K., et al., *Targeting of protein kinase C delta to mitochondria in the oxidative stress response.* Cell Growth Differ, 2001. **12**(9): p. 465-70.
43. Hung, M.C. and W. Link, *Protein localization in disease and therapy.* J Cell Sci, 2011. **124**(Pt 20): p. 3381-92.
44. Kleckner, I.R. and M.P. Foster, *An introduction to NMR-based approaches for measuring protein dynamics.* Biochim Biophys Acta, 2011. **1814**(8): p. 942-68.
45. Serber, Z. and V. Dötsch, *In-Cell NMR Spectroscopy.* Biochemistry, 2001. **40**(48): p. 14317-14323.
46. Luchinat, E. and L. Banci, *A Unique Tool for Cellular Structural Biology: In-cell NMR.* Journal of Biological Chemistry, 2016. **291**(8): p. 3776-3784.
47. Nagana Gowda, G.A. and D. Raftery, *Recent Advances in NMR-Based Metabolomics.* Analytical Chemistry, 2017. **89**(1): p. 490-510.
48. Lilly Thankamony, A.S., et al., *Dynamic nuclear polarization for sensitivity enhancement in modern solid-state NMR.* Progress in Nuclear Magnetic Resonance Spectroscopy, 2017. **102-103**: p. 120-195.
49. Plainchont, B., et al., *Dynamic Nuclear Polarization Opens New Perspectives for NMR Spectroscopy in Analytical Chemistry.* Anal Chem, 2018. **90**(6): p. 3639-3650.
50. Wuerthrich, K., *NMR of Proteins and Nucleic Acids*. 1986: John Wiley & Sons.
51. Guenther, H., *NMR Spectroscopy Basic Principles, Concepts, and Applications in Chemistry*. 2013: Wiley-VCH.
52. Zoonens, M., et al., *Dangerous Liaisons between Detergents and Membrane Proteins. The Case of Mitochondrial Uncoupling Protein 2.* Journal of the American Chemical Society, 2013. **135**(40): p. 15174-15182.
53. Cavanagh, J., *Protein NMR spectoscopy : principle and practice*. 1996, San Diego: Academic Press.
54. Clore, G.M. and J. Iwahara, *Theory, Practice, and Applications of Paramagnetic Relaxation Enhancement for the Characterization of Transient Low-Population States of Biological Macromolecules and Their Complexes.* Chemical Reviews, 2009. **109**(9): p. 4108-4139.
55. Neri, D., et al., *Stereospecific nuclear magnetic resonance assignments of the methyl groups of valine and leucine in the DNA-binding domain of the 434 repressor by biosynthetically directed fractional carbon-13 labeling.* Biochemistry, 1989. **28**(19): p. 7510-7516.
56. Driscoll, P.C., A.M. Gronenborn, and G.M. Clore, *The influence of stereospecific assignments on the determination of three-dimensional structures of proteins by nuclear magnetic resonance spectroscopy: Application to the sea anemone protein BDS-I.* FEBS Letters, 1989. **243**(2): p. 223-233.
57. Eberstadt, M., et al., *Scalar Coupling Constants—Their Analysis and Their Application for the Elucidation of Structures.* Angewandte Chemie International Edition in English, 1995. **34**(16): p. 1671-1695.
58. Clore, G.M., et al., *Three-dimensional structure of phoratoxin in solution: combined use of nuclear magnetic resonance, distance geometry, and restrained molecular dynamics.* Biochemistry, 1987. **26**(6): p. 1732-1745.

59. Nilges, M., et al., *Refinement of the solution structure of the DNA hexamer 5'd(GCATGC)2: combined use of nuclear magnetic resonance and restrained molecular dynamics.* Biochemistry, 1987. **26**(12): p. 3718-3733.
60. Nilges, M., et al., *Refinement of the solution structure of the DNA decamer 5'd(CTGGATCCAG)2: combined use of nuclear magnetic resonance and restrained molecular dynamics.* Biochemistry, 1987. **26**(12): p. 3734-3744.
61. Bax, A., *Two-Dimensional NMR and Protein Structure.* Annual Review of Biochemistry, 1989. **58**(1): p. 223-256.
62. Nilges, M., G.M. Clore, and A.M. Gronenborn, *Determination of three-dimensional structures of proteins from interproton distance data by hybrid distance geometry-dynamical simulated annealing calculations.* FEBS Letters, 1988. **229**(2): p. 317-324.
63. Laskowski, R.A., et al., *AQUA and PROCHECK-NMR: Programs for checking the quality of protein structures solved by NMR.* Journal of Biomolecular NMR, 1996. **8**(4): p. 477-486.
64. Doreleijers, J.F., et al., *NRG-CING: integrated validation reports of remediated experimental biomolecular NMR data and coordinates in wwPDB.* Nucleic acids research, 2012. **40**(Database issue): p. D519-D524.
65. Huth, J.R., et al., *Design of an expression system for detecting folded protein domains and mapping macromolecular interactions by NMR.* Protein Sci, 1997. **6**(11): p. 2359-64.
66. Koenig, B.W., M. Rogowski, and J.M. Louis, *A rapid method to attain isotope labeled small soluble peptides for NMR studies.* J Biomol NMR, 2003. **26**(3): p. 193-202.
67. Abd Rahim, M.S., et al., *1H, 15N, and 13C chemical shift assignments of the micelle immersed FAT C-terminal (FATC) domains of the human protein kinases ataxia-telangiectasia mutated (ATM) and DNA-dependent protein kinase catalytic subunit (DNA-PKcs) fused to the B1 domain of streptococcal protein G (GB1).* Biomolecular NMR Assignments, 2018.
68. Stafford, R.E., T. Fanni, and E.A. Dennis, *Interfacial properties and critical micelle concentration of lysophospholipids.* Biochemistry, 1989. **28**(12): p. 5113-20.
69. Tausk, R.J., et al., *Physical chemical studies of short-chain lecithin homologues. I. Influence of the chain length of the fatty acid ester and of electrolytes on the critical micelle concentration.* Biophys Chem, 1974. **1**(3): p. 175-83.
70. Weschayanwiwat, P., J. Scamehorn, and P. Reilly, *Surfactant properties of low molecular weight phospholipids.* Journal of Surfactants and Detergents, 2005. **8**(1): p. 65-72.
71. Delaglio, F., et al., *NMRPipe: a multidimensional spectral processing system based on UNIX pipes.* J Biomol NMR, 1995. **6**(3): p. 277-93.
72. Johnson, B.A., *Using NMRView to visualize and analyze the NMR spectra of macromolecules.* Methods Mol Biol, 2004. **278**: p. 313-52.
73. Kay, L.E., et al., *Three-dimensional triple-resonance NMR spectroscopy of isotopically enriched proteins.* Journal of Magnetic Resonance (1969), 1990. **89**(3): p. 496-514.
74. Wittekind, M. and L. Mueller, *HNCACB, a High-Sensitivity 3D NMR Experiment to Correlate Amide-Proton and Nitrogen Resonances with the Alpha- and Beta-Carbon Resonances in Proteins.* Journal of Magnetic Resonance, Series B, 1993. **101**(2): p. 201-205.
75. Grzesiek, S., J. Anglister, and A. Bax, *Correlation of Backbone Amide and Aliphatic Side-Chain Resonances in 13C/15N-Enriched Proteins by Isotropic Mixing of 13C Magnetization.* Journal of Magnetic Resonance, Series B, 1993. **101**(1): p. 114-119.

76. Montelione, G.T., et al., *An efficient triple resonance experiment using carbon-13 isotropic mixing for determining sequence-specific resonance assignments of isotopically-enriched proteins.* Journal of the American Chemical Society, 1992. **114**(27): p. 10974-10975.
77. Olejniczak, E.T., R.X. Xu, and S.W. Fesik, *A 4D HCCH-TOCSY experiment for assigning the side chain1H and13C resonances of proteins.* Journal of Biomolecular NMR, 1992. **2**(6): p. 655-659.
78. Marion, D., et al., *Overcoming the overlap problem in the assignment of proton NMR spectra of larger proteins by use of three-dimensional heteronuclear proton-nitrogen-15 Hartmann-Hahn-multiple quantum coherence and nuclear Overhauser-multiple quantum coherence spectroscopy: application to interleukin 1.beta.* Biochemistry, 1989. **28**(15): p. 6150-6156.
79. Schwieters, C.D., et al., *The Xplor-NIH NMR molecular structure determination package.* J Magn Reson, 2003. **160**(1): p. 65-73.
80. Sommer, L.A.M., M.A. Meier, and S.A. Dames, *A fast and simple method for probing the interaction of peptides and proteins with lipids and membrane-mimetics using GB1 fusion proteins and NMR spectroscopy.* Protein Sci, 2012. **21**(10): p. 1566-70.
81. Dames, S.A., *Structural basis for the association of the redox-sensitive target of rapamycin FATC domain with membrane-mimetic micelles.* J Biol Chem, 2010. **285**(10): p. 7766-75.
82. Liu, W. and M. Caffrey, *Interactions of tryptophan, tryptophan peptides, and tryptophan alkyl esters at curved membrane interfaces.* Biochemistry, 2006. **45**(39): p. 11713-26.
83. Sun, H., et al., *The preference of tryptophan for membrane interfaces: insights from N-methylation of tryptophans in gramicidin channels.* J Biol Chem, 2008. **283**(32): p. 22233-43.
84. Sommer, L.A.M. and S.A. Dames, *Characterization of residue-dependent differences in the peripheral membrane association of the FATC domain of the kinase 'target of rapamycin' by NMR and CD spectroscopy.* FEBS Letters, 2014. **588**(9): p. 1755-1766.
85. Baretic, D., et al., *Structures of closed and open conformations of dimeric human ATM.* Sci Adv, 2017. **3**(5): p. e1700933.
86. Dobbs, T.A., J.A. Tainer, and S.P. Lees-Miller, *A structural model for regulation of NHEJ by DNA-PKcs autophosphorylation.* DNA Repair (Amst), 2010. **9**(12): p. 1307-14.
87. Gapud, E.J. and B.P. Sleckman, *Unique and redundant functions of ATM and DNA-PKcs during V(D)J recombination.* Cell Cycle, 2011. **10**(12): p. 1928-35.
88. Takahashi, T., et al., *Carboxyl-terminal region conserved among phosphoinositide-kinase-related kinases is indispensable for mTOR function in vivo and in vitro.* Genes Cells, 2000. **5**(9): p. 765-75.
89. de Jesus, A.J. and T.W. Allen, *The role of tryptophan side chains in membrane protein anchoring and hydrophobic mismatch.* Biochimica et Biophysica Acta (BBA) - Biomembranes, 2013. **1828**(2): p. 864-876.
90. Sommer, L.A.M., et al., *Characterization of the Immersion Properties of the Peripheral Membrane Anchor of the FATC Domain of the Kinase "Target of Rapamycin" by NMR, Oriented CD Spectroscopy, and MD Simulations.* The Journal of Physical Chemistry B, 2014. **118**(18): p. 4817-4831.

Appendix

Publications

1. **Title**: ^{1}H, ^{15}N and ^{13}C chemical shift assignments of micelles immersed FATC-terminal domain of the human protein kinases ataxia telangiectasia mutated (ATM) and DNA-dependent protein kinase catalytic subunit (DNA-PKcs) fused to the B1 domain of *streptococcal* protein G (GB1)

Authors: Munirah S. Abd Rahim, Lisa A. M. Sommer, Anja Wacker, Martin Schaad and Sonja A. Dames

Journal: Biomolecular NMR Assignments

Volume: 12 (1)

Pages: 149-154

Year: 2018

DOI: 10.1007/s12104-018-9798-3

2. **Title**: Structural characterization of the membrane-associating FATC domain of ataxia telangiectasia mutated by NMR and MD simulations

Authors: Munirah S. Abd Rahim, Yevhen K. Cherniavskyi, D. Peter Tieleman, Sonja A. Dames

Journal is submitted to: Journal of Biological Chemistry

Biomolecular NMR Assignments
https://doi.org/10.1007/s12104-018-9798-3

ARTICLE

^{1}H, ^{15}N, and ^{13}C chemical shift assignments of the micelle immersed FAT C-terminal (FATC) domains of the human protein kinases ataxia-telangiectasia mutated (ATM) and DNA-dependent protein kinase catalytic subunit (DNA-PKcs) fused to the B1 domain of *streptococcal* protein G (GB1)

Munirah S. Abd Rahim[1] · Lisa A. M. Sommer[1,2] · Anja Wacker[1,3] · Martin Schaad[4] · Sonja A. Dames[1,5]

Received: 13 October 2017 / Accepted: 1 January 2018

Abstract
FAT C-terminal (FATC) is a circa 33 residue-long domain. It controls the kinase functionality in phosphatidylinositol-3 kinase-related kinases (PIKKs). Recent NMR- and CD-monitored interaction studies indicated that the FATC domains of all PIKKs can interact with membrane mimetics albeit with different preferences for membrane properties such as surface charge and curvature. Thus they may generally act as membrane anchoring unit. Here, we present the ^{1}H, ^{15}N, and ^{13}C chemical shift assignments of the DPC micelle immersed FATC domains of the human PIKKs ataxia-telangiectasia mutated (ATM, residues 3024–3056) and DNA protein kinase catalytic subunit (DNA-PKcs, residues 4096–4128), both fused to the 56 residue long B1 domain of *Streptococcal* protein G (GB1). Each fusion protein is 100 amino acids long and contains in the linking region between the GB1 tag and the FATC region a thrombin (LVPRGS) and an enterokinase (DDDDK) protease site. The assignments pave the route for the detailed structural characterization of the membrane mimetic bound states, which will help to better understand the role of the proper cellular localization at membranes for the function and regulation of PIKKs. The chemical shift assignment of the GB1 tag is useful for NMR spectroscopists developing new experiments or using GB1 otherwise for case studies in the field of in-cell NMR spectroscopy or protein folding. Moreover it is often used as purification tag. Earlier we showed already that GB1 does not interact with membrane mimetics and thus does not disturb the NMR monitoring of membrane mimetic interactions of attached proteins.

Keywords Ataxia telangiectasia mutated (ATM) · DNA-dependent kinase catalytic subunit (DNA-PKcs) · FATC · Phosphatidylinositol-3 kinase-related kinases (PIKKs) · B1 domain of *Streptococcal* protein G (GB1) · Chemical shift assignment

✉ Sonja A. Dames
sonja.dames@tum.de

1 Department of Chemistry, Biomolecular NMR Spectroscopy, Technische Universität München, Lichtenbergstr. 4, 85747 Garching, Germany

2 Present Address: Roche Diagnostics GmbH, Centralised and Point of Care Solutions, Nonnenwald 2, 82377 Penzberg, Germany

3 Present Address: Division of Radiopharmaceutical Chemistry, German Cancer Research Center (DKFZ), Im Neuenheimer Feld 280, 69120 Heidelberg, Germany

4 Quintiles AG, Hochstrasse 50, 4053 Basel, Switzerland

5 Institute of Structural Biology, Helmholtz Zentrum München, Ingolstädter Landstr. 1, 85764 Neuherberg, Germany

Biological context

Ataxia-telangiectasia mutated (ATM) and DNA-dependent protein kinase catalytic subunit (DNA-PKcs) are members of the family of phosphatidylinositol-3 kinase-related kinases (PIKKs), which phosphorylate serine/threonine residues of various substrates (Lempiäinen and Halazonetis 2009). PIKKs govern numerous cellular pathways regulating cell growth and metabolism and generally the response to different types of cellular stress thereby controlling processes such as the DNA damage response, mRNA decay, transcription and other (Lempiäinen and Halazonetis 2009; Lovejoy and Cortez 2009; Morita et al. 2007; Wullschleger et al. 2006). ATM and DNA-PKcs are long known to regulate the DNA

Published online: 18 January 2018

damage response (Shiloh 2003). More recently it has been shown that they are further involved in the control of metabolic processes and the oxidative stress response (Chen et al. 2012; Kong et al. 2011; Kruger and Ralser 2011; Shiloh and Ziv 2013). They are large multidomain proteins consisting of circa 2500–4500 amino acids residues and share a similar domain organization (De Cicco et al. 2015; Lempiäinen and Halazonetis 2009; Lovejoy and Cortez 2009). All contain besides the catalytic kinase domain (KD), the FAT and the FAT C-terminal (FATC) domains. In addition, they harbor other domains that are as the FAT domain often composed of helical repeat units that typically mediate protein–protein interactions (Bosotti et al. 2000; Perry and Kleckner 2003). Mutagenesis studies indicated that the short but highly evolutionary conserved FATC domain plays an important role for the control of the PIKK kinase functionality (Hoke et al. 2010; Jiang et al. 2006; Mordes et al. 2008; Morita et al. 2007). Based on NMR- and CD-monitored interaction studies with different membrane mimetics, the FATC domains of all PIKKs can interact with membrane mimetics albeit showing differences regarding the preferences for specific membrane properties such as surface charge and curvature and the lipid packing density (Dames 2010; Sommer and Dames 2014; Sommer et al. 2013, 2014). This suggested that the FATC domains of PIKKs act further as one component of a network of protein–lipid and protein–protein interactions mediating the observed localization at different cellular membrane regions (De Cicco et al. 2015; Sommer et al. 2013). Whereas the FATC domain of yeast TOR1 can be cleaved off the GB1 purification tag (Dames et al. 2005), the respective yields for the FATC domains of ATM and DNA-PKcs were only low. Thus the GB1 tagged fusion proteins had been used for NMR monitored interaction studies with membrane mimetic micelles, bicelles, and liposomes of the small unilamellar vesicle (SUV) type (Sommer et al. 2013). It has been shown before that the presence of the GB1 tag does not disturb the monitoring of membrane mimetic interactions of fused target proteins (Sommer et al. 2012). The GB1 tag is not only known to improve the protein expression level, solubility and folding efficiency (Cheng and Patel 2004; Huth et al. 1997), but allows for small and easy to refold target proteins to employ a heat purification approach (Koenig et al. 2003).

In order to better understand the role of PIKK membrane localization for the specific signaling output, a detailed characterization of their interactions with membrane mimetics and how they influence their structures and dynamics would be beneficial. Here, we present the assignment of the resonances of the GB1 tagged FATC domains of human ATM and human DNA-PKcs immersed in membrane mimetic micelles composed of dodecylphosphocholine (DPC). The assignment of the resonances provides the basis for the structural and dynamic characterization of the membrane mimetic immersed states by multidimensional, heteronuclear NMR spectroscopy. The GB1 tag does not interact with membrane mimetics (Sommer et al. 2012). Thus the additionally provided assignments of the GB1 part correspond to the free, buffer dissolved state. These are useful for scientists using GB1 tagged proteins (Huth et al. 1997) for membrane mimetic (Sommer et al. 2012) and other interaction studies and to characterize the effect of the GB1 tag on the solubility and stability of the fused target protein (Huang et al. 2010). GB1 is further used as test protein for newly developed NMR methods (Clore et al. 1998; Frueh et al. 2005) and in-cell NMR experiments (Luchinat and Banci 2016; Selenko et al. 2006), the characterization of specific NMR phenomena (Walsh et al. 2010), and protein folding studies (Byeon et al. 2004; Ding et al. 2004).

Methods and experimental

Plasmid cloning, expression and purification

Residues 3024–3056 of human ATM (Uniprot-ID Q13315) and residues 4096–4128 of human DNA-PKcs (Uniprot-ID P78527) corresponding to the highly conserved FATC domains were cloned into the expression vector pGEV2 (Huth et al. 1997) and overexpressed in *Escherichia coli* strain BL21 (DE3) as described previously (Sommer et al. 2013). The expressed 100-residue long fusion proteins (Fig. 1) comprise the B1 domain of *Streptococcal* protein G (GB1 tag), a linker region with a thrombin (LVPRGS) and an enterokinase (DDDDK) protease recognition site and either the 33-residue long FATC domain of human ATM (=hATMfatc-gb1ent) or that of human DNA-PKcs (=hDNAPKfatc-gb1ent). Cells were grown in M9 minimal media containing $^{15}NH_4Cl$ and/or ^{13}C-glucose as the sole nitrogen and carbon sources for the fully isotope labeled samples or 10% ^{13}C- and 90% ^{12}C-glucose for the sample used for the stereo-specific assignment of valine and leucine methyl groups (Neri et al. 1989) at 37 °C until the optical density at 600 nm (OD_{600}) reached a value of 0.7–0.9 and then induced with 1 mM IPTG for 3 h. Cells were harvested by centrifugation for 30 min at 6000*xg* at 4 °C. The supernatant was discarded. Cells were lysed and the GB1 tagged protein extracted and initially purified based on a published heating procedure (Koenig et al. 2003). For this the cell pellet was resuspended in 15 ml 50 mM Tris, 100 mM NaCl, 2 mM EDTA and 2 mM benzamidine, pH 7.6 per 0.5 l culture and incubated for 5 min at 80 °C in a water bath, followed by 10 min incubation on ice. Most of the *E. coli* proteins precipitate at this temperature leaving rather pure GB1 tagged fusion protein in the soluble fraction if the attached target protein is a peptide (Koenig et al. 2003) or a rather small protein. The fusion proteins hATMfatc-gb1ent

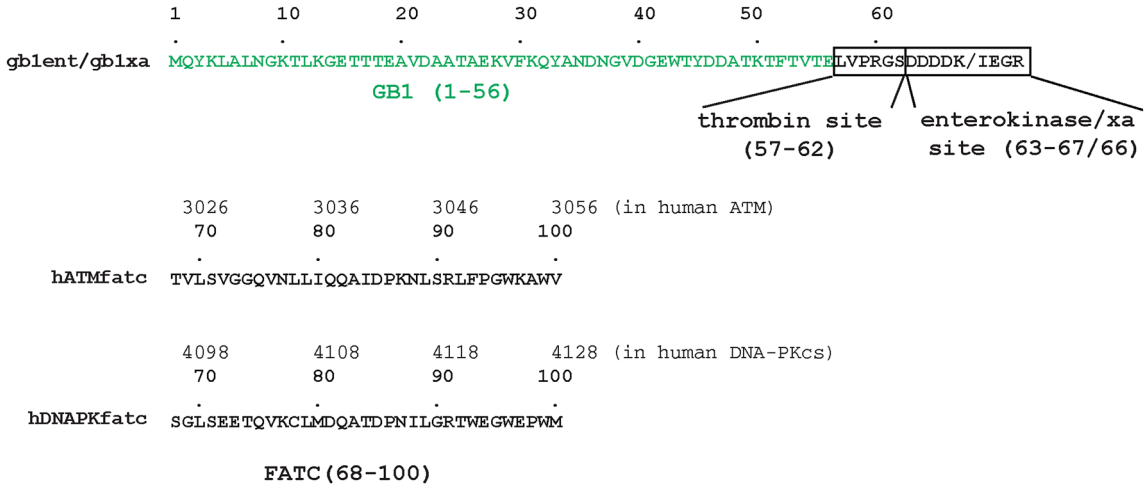

Fig. 1 Amino acid sequences of the fusion proteins hATMfatc-gb1ent and hDNAPKfatc-gb1ent consisting of GB1 [as expressed from pGEV2 (Huth et al. 1997)] followed by a thrombin and an enterokinase site (=gb1ent) and the coding sequence for either the human ATM FATC (hATMfatc, Uniprot-ID Q13315) or the human DNA-PKcs FATC (hDNAPKfatc, Uniprot-ID P78527) domain as well as that of GB1 followed by a thrombin and a factor Xa instead of a enterokinase site (=gb1xa)

and hDNAPKfatc-gb1ent were further purified using IgG Sepharose affinity chromatography following the protocol from the manufacturer (GE Healthcare). Fractions containing based on SDS-PAGE analysis pure fusion protein were pooled, concentrated, washed 3–6 times with 50 mM Tris, 100 mM NaCl, pH 6.5 and finally concentrated using a centrifugal filter device (Amicon Ultra, Millipore Merck, MWCO 3000). The so purified GB1 tagged proteins were directly used for the NMR measurements in the presence of membrane mimetic DPC micelles because the GB1 tag does not disturb the detection of the NMR signals arising from the FATC parts (Sommer et al. 2012).

Preparation of membrane mimetics and NMR samples

Deuterated DPC (d_{38}-DPC) was purchased from Cambridge Isotopes. Protein samples in the presence of DPC were prepared as follows and as described previously (Sommer et al. 2013). A defined amount of DPC from a concentrated stock in chloroform (usually 0.5 M) was placed in a glass vial and dried under a stream of nitrogen gas. The dried DPC film was then dissolved by a protein sample. The samples used to record NMR data for the chemical shift assignment and the structure determination contained circa 0.4 mM protein in 50 mM Tris, 100 mM NaCl, 150 mM d_{38}-DPC, 0.02% NaN_3, pH 6.5 (95%/5% H_2O/D_2O).

NMR spectroscopy

The NMR data for hATMfatc-gb1ent were acquired at 298 K on Bruker Avance 500, 600, and 900 MHz spectrometers, the 500 and 900 MHz ones equipped with cryogenic probes and that for hDNAPKfatc-gb1ent at 298 K on Bruker Avance 500 and 750 MHz spectrometers, the 500 MHz one equipped with a cryogenic probe. Assignments for ^{13}C, ^{15}N, and ^{1}H nuclei were based on two-dimensional ^{1}H-^{15}N- and ^{1}H-^{13}C-HSQC spectra [for the 10% ^{13}C-labeled sample used for the stereo-specific assignments of valine and leucine methyl groups without decoupling (Neri et al. 1989)], three-dimensional HNCA (Grzesiek and Bax 1992), HNCACB, HCCH-TOCSY (Bax et al. 1990; Olejniczak et al. 1992), CCONH-TOCSY (Grzesiek et al. 1993; Lyons and Montelione 1993; Montelione et al. 1992), HNHA (Vuister and Bax 1993, 1994), HNHB (Archer et al. 1991), and ^{15}N- and ^{13}C-edited NOESY spectra. Data were processed with NMRPipe (Delaglio et al. 1995) and analyzed using NMRView (Johnson 2004).

Assignments and data deposition

Figure 1 depicts the amino acid sequences of the each 100-residue long hATMfatc-gb1ent and hDNAPKfatc-gb1ent fusion proteins as well as that of GB1 followed by a thrombin and a factor Xa protease recognition site (=gb1xa). Figures 2 and 3 show superpositions of the ^{1}H–^{15}N HSQC spectra of hATMfatc-gb1ent and hDNAPKfatc-gb1ent in the presence of DPC micelles (150 mM d38-DPC) and of gb1xa in buffer. Due to the interaction of the FATC domains with the circa 20 kDa micelles their signals were generally broader and thus appeared less intense than those of the GB1 tag that does not interact with membrane mimetic micelles (Sommer et al. 2012).

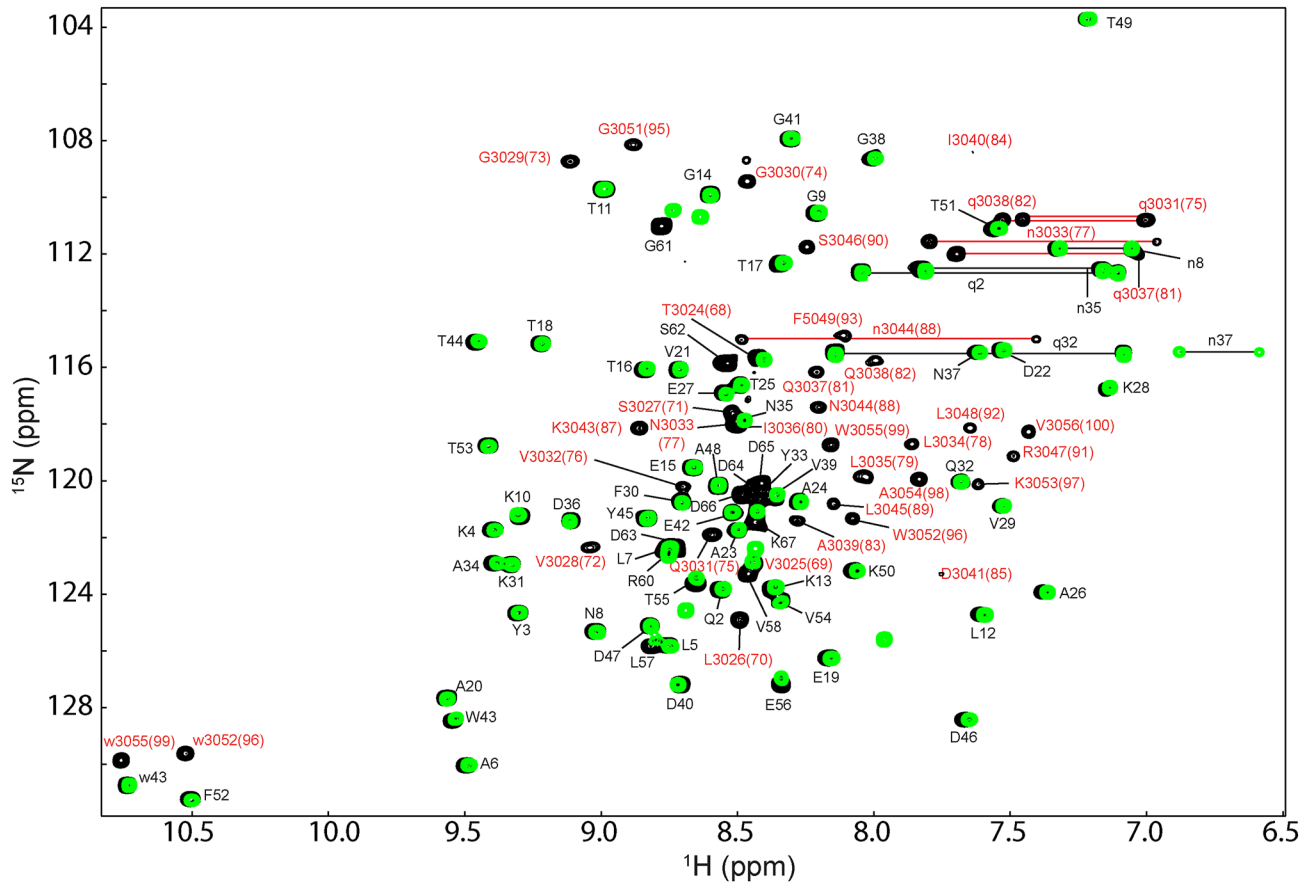

Fig. 2 Superposition of the ^{1}H–^{15}N HSQC spectra of micelle immersed hATMfatc-gb1ent (black) and gb1xa in micelle-free buffer (green). The sequence-specific assignments are indicated by the one-letter amino acid code (capital letters for backbone and small letters for side chain signals) and the sequence position in the 100-residue long hATMfatc-gb1ent fusionprotein (for the FATC part—numbers in brackets). For the FATC domain also the sequence position in full-length human ATM (Uniprot ID Q13315) is provided

The backbone ^{1}H and ^{15}N nuclei were assigned for 96% of the residues (both: 100–3 prolines and the N-terminal methionine) and the backbone ^{13}Cα for all residues. Figures 2 and 3 show further the assignment of the side chain –NH_2 signals of glutamines and asparagines. Whereas the side chain –NH signals of tryptophans could be assigned for the GB1 part and the FATC domain of ATM, this was not possible for the three tryptophans of the FATC domain of DNA-PKcs due to partial signal overlap and only weak signals in the NOESY data.

The aliphatic ^{1}H and ^{13}C side chain resonances of both FATC domains and those of the GB1 tag were successfully assigned based on 2D ^{1}H–^{13}C constant time HSQC, 3D CCONH and HCCH-TOCSY data in combination with 3D HNHB, and ^{15}N- and ^{13}C-edited NOESY data. In addition, stereospecific assignments for the leucine δ-methyl and valine γ-methyl groups of the GB1 part and of the FATC of human ATM, except for V3025 (69), could be obtained using a 10% ^{13}C-labeled sample (Neri et al. 1989). Despite overall weak signal intensity in the 2D aromatic ^{1}H–^{13}C HSQC and 3D ^{13}C-edited aromatic NOESY data, the aromatic ^{1}H and ^{13}C nuclei of the phenylalanine and the two tryptophans of the ATM FATC domain could be assigned.

The chemical shift assignments of the each 100-residue long fusion proteins hATMfatc-gb1ent and hDNAPKfatc-gb1ent in the presence of DPC micelles have been deposited at the BioMagResBank under the BMRB accession numbers 27167 and 27168, respectively. Note the assignments for the GB1 tag correspond to the free, buffer

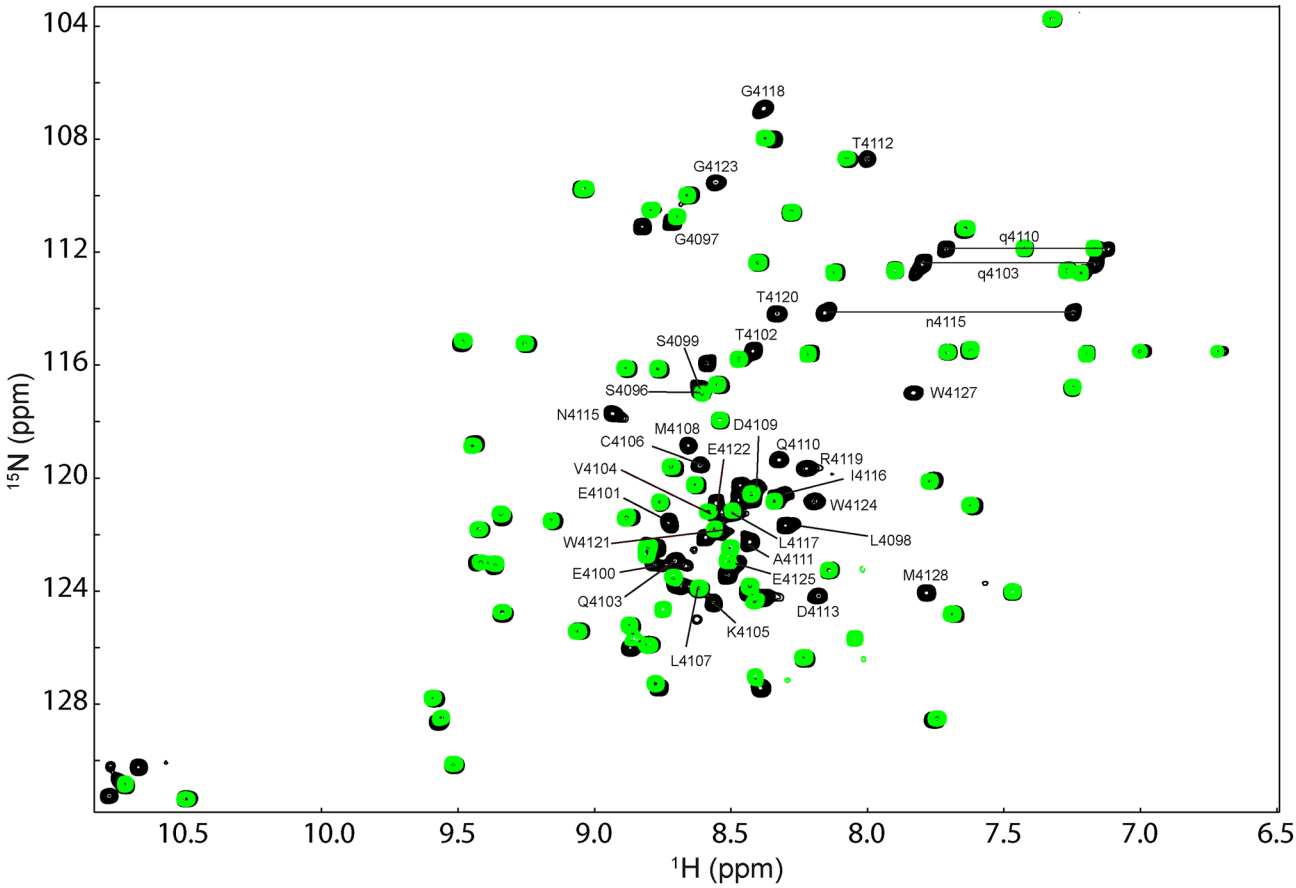

Fig. 3 Superposition of the ^{1}H–^{15}N HSQC spectra of micelle immersed hDNAPKfatc-gb1ent (black) and gb1xa in micelle-free buffer (green). The sequence-specific assignments are indicated by the one-letter amino acid code (capital letters for backbone and small letters for side chain signals) and the sequence position in full-length human DNA-PKcs (Uniprot ID P78527)

dissolved state since it does not interact with membrane mimetics (Sommer et al. 2012).

Acknowledgements This work was supported by a grant from the German Research Foundation to S.A.D. (DA1183/3-1 and -2). S.A.D acknowledges further financial support from the Technische Universität München diversity and talent management office (Laura Bassi award) and the Helmholtz portfolio theme 'metabolic dysfunction and common disease' of the Helmholtz Zentrum München. M.S.A.R. is supported by a Ph. D. fellowship from the German academic exchange service (DAAD). Prof. Dr. Michael Sattler and Prof. Dr. Bernd Reif from the Technische Universität München (TUM) and the Helmholtz Zentrum München we thank very much for hosting our group and for sharing their facilities with us.

References

Archer SJ, Ikura M, Torchia DA, Bax A (1991) An alternative 3D NMR technique for correlating backbone 15N with side chain Hβ resonances in larger proteins. J Magn Reson (1969) 95:636–641. https://doi.org/10.1016/0022-2364(91)90182-S

Bax A, Clore GM, Gronenborn AM (1990) ^{1}H–^{1}H correlation via isotropic mixing of ^{13}C magnetization, a new three-dimensional approach for assigning ^{1}H and ^{13}C spectra of ^{13}C-enriched proteins. J Magn Reson 88:425–431. https://doi.org/10.1016/0022-2364(90)90202-K

Bosotti R, Isacchi A, Sonnhammer EL (2000) FAT: a novel domain in PIK-related kinases. Trends Biochem Sci 25:225–227

Byeon IJ, Louis JM, Gronenborn AM (2004) A captured folding intermediate involved in dimerization and domain-swapping of GB1. J Mol Biol 340:615–625. https://doi.org/10.1016/j.jmb.2004.04.069

Chen BP, Li M, Asaithamby A (2012) New insights into the roles of ATM and DNA-PKcs in the cellular response to oxidative stress. Cancer Lett 327:103–110. https://doi.org/10.1016/j.canlet.2011.12.004

Cheng Y, Patel DJ (2004) An efficient system for small protein expression and refolding. Biochem Biophys Res Commun 317:401–405. https://doi.org/10.1016/j.bbrc.2004.03.068

Clore GM, Gronenborn AM, Bax A (1998) A robust method for determining the magnitude of the fully asymmetric alignment tensor of oriented macromolecules in the absence of structural information. J Magn Reson (San Diego, CA: 1997) 133:216–221. https://doi.org/10.1006/jmre.1998.1419

Dames SA (2010) Structural basis for the association of the redox-sensitive target of rapamycin FATC domain with membrane-mimetic micelles. J Biol Chem 285:7766–7775. https://doi.org/10.1074/jbc.M109.058404

Dames SA, Mulet JM, Rathgeb-Szabo K, Hall MN, Grzesiek S (2005) The solution structure of the FATC domain of the protein kinase

target of rapamycin suggests a role for redox-dependent structural and cellular stability. J Biol Chem 280:20558–20564. https://doi.org/10.1074/jbc.M501116200

De Cicco M, Rahim MS, Dames SA (2015) Regulation of the target of rapamycin and other phosphatidylinositol-3 kinase-related kinases by membrane targeting. Membranes 5:553–575. https://doi.org/10.3390/membranes5040553

Delaglio F, Grzesiek S, Vuister GW, Zhu G, Pfeifer J, Bax A (1995) NMRPipe: a multidimensional spectral processing system based on UNIX pipes. J Biomol NMR 6:277–293

Ding K, Louis JM, Gronenborn AM (2004) Insights into conformation and dynamics of protein GB1 during folding and unfolding by NMR. J Mol Biol 335:1299–1307

Frueh DP, Arthanari H, Wagner G (2005) Unambiguous assignment of NMR protein backbone signals with a time-shared triple-resonance experiment. J Biomol NMR 33:187–196. https://doi.org/10.1007/s10858-005-3204-z

Grzesiek S, Bax A (1992) Improved 3D triple-resonance NMR techniques applied to a 31 kDa protein. J Magn Reson (1969) 96:432–440. https://doi.org/10.1016/0022-2364(92)90099-S

Grzesiek S, Anglister J, Bax A (1993) Correlation of backbone amide and aliphatic side-chain resonances in 13C/15N-enriched proteins by isotropic mixing of 13C magnetization. J Magn Reson Ser B 101:114–119. https://doi.org/10.1006/jmrb.1993.1019

Hoke SM et al (2010) Mutational analysis of the C-terminal FATC domain of saccharomyces cerevisiae Tra1. Curr Genet 56:447–465

Huang A, de Jong RN, Folkers GE, Boelens R (2010) NMR characterization of foldedness for the production of E3 RING domains. J Struct Biol 172:120–127. https://doi.org/10.1016/j.jsb.2010.07.014

Huth JR, Bewley CA, Clore GM, Gronenborn AM, Jackson BM, Hinnebusch AG (1997) Design of an expression system for detecting folded protein domains and mapping macromolecular interactions by NMR. Protein Sci 6:2359–2364. https://doi.org/10.1002/pro.5560061109

Jiang X, Sun Y, Chen S, Roy K, Price BD (2006) The FATC domains of PIKK proteins are functionally equivalent and participate in the Tip60-dependent activation of DNA-PKcs and ATM. J Biol Chem 281:15741–15746. https://doi.org/10.1074/jbc.M513172200

Johnson BA (2004) Using NMRView to visualize and analyze the NMR spectra of macromolecules. Methods Mol Biol 278:313–352. https://doi.org/10.1385/1-59259-809-9:313

Koenig BW, Rogowski M, Louis JM (2003) A rapid method to attain isotope labeled small soluble peptides for NMR studies. J Biomol NMR 26:193–202

Kong X, Shen Y, Jiang N, Fei X, Mi J (2011) Emerging roles of DNA-PK besides DNA repair. Cell Signal 23:1273–1280. https://doi.org/10.1016/j.cellsig.2011.04.005

Kruger A, Ralser M (2011) ATM is a redox sensor linking genome stability and carbon metabolism. Sci Signal 4:pe17. https://doi.org/10.1126/scisignal.2001959

Lempiäinen H, Halazonetis TD (2009) Emerging common themes in regulation of PIKKs and PI3Ks. EMBO J 28:3067–3073. https://doi.org/10.1038/emboj.2009.281

Lovejoy CA, Cortez D (2009) Common mechanisms of PIKK regulation. DNA Repair 8:1004–1008. https://doi.org/10.1016/j.dnarep.2009.04.006

Luchinat E, Banci L (2016) A unique tool for cellular structural biology: in-cell NMR. J Biol Chem 291:3776–3784. https://doi.org/10.1074/jbc.R115.643247

Lyons BA, Montelione GT (1993) An HCCNH triple-resonance experiment using carbon-13 isotropic mixing for correlating backbone amide and side-chain aliphatic resonances in isotopically enriched proteins. J Magn Reson Ser B 101:206–209. https://doi.org/10.1006/jmrb.1993.1034

Montelione GT, Lyons BA, Emerson SD, Tashiro M (1992) An efficient triple resonance experiment using carbon-13 isotropic mixing for determining sequence-specific resonance assignments of isotopically-enriched proteins. J Am Chem Soc 114:10974–10975. https://doi.org/10.1021/ja00053a051

Mordes DA, Glick GG, Zhao R, Cortez D (2008) TopBP1 activates ATR through ATRIP and a PIKK regulatory domain. Genes Dev 22:1478–1489. https://doi.org/10.1101/gad.1666208

Morita T, Yamashita A, Kashima I, Ogata K, Ishiura S, Ohno S (2007) Distant N- and C-terminal domains are required for intrinsic kinase activity of SMG-1, a critical component of nonsense-mediated mRNA decay. J Biol Chem 282:7799–7808. https://doi.org/10.1074/jbc.M610159200

Neri D, Szyperski T, Otting G, Senn H, Wuethrich K (1989) Stereospecific nuclear magnetic resonance assignments of the methyl groups of valine and leucine in the DNA-binding domain of the 434 repressor by biosynthetically directed fractional carbon-13 labeling. Biochemistry 28:7510–7516. https://doi.org/10.1021/bi00445a003

Olejniczak ET, Xu RX, Fesik SW (1992) A 4D HCCH-TOCSY experiment for assigning the side chain1H and13C resonances of proteins. J Biomol NMR 2:655–659. https://doi.org/10.1007/bf02192854

Perry J, Kleckner N (2003) The ATRs, ATMs, and TORs are giant HEAT repeat proteins. Cell 112:151–155

Selenko P, Serber Z, Gadea B, Ruderman J, Wagner G (2006) Quantitative NMR analysis of the protein G B1 domain in Xenopus laevis egg extracts and intact oocytes. Proc Natl Acad Sci USA 103:11904–11909. https://doi.org/10.1073/pnas.0604667103

Shiloh Y (2003) ATM and related protein kinases: safeguarding genome integrity. Nat Rev Cancer 3:155–168. https://doi.org/10.1038/nrc1011

Shiloh Y, Ziv Y (2013) The ATM protein kinase: regulating the cellular response to genotoxic stress, and more. Nat Rev Mol Cell Biol 14:197–210

Sommer LAM, Dames SA (2014) Characterization of residue-dependent differences in the peripheral membrane association of the FATC domain of the kinase 'target of rapamycin' by NMR and CD spectroscopy. FEBS Lett 588:1755–1766. https://doi.org/10.1016/j.febslet.2014.03.031

Sommer LAM, Meier MA, Dames SA (2012) A fast and simple method for probing the interaction of peptides and proteins with lipids and membrane-mimetics using GB1 fusion proteins and NMR spectroscopy. Protein Sci 21:1566–1570. https://doi.org/10.1002/pro.2127

Sommer LAM, Schaad M, Dames SA (2013) NMR- and circular dichroism-monitored lipid binding studies suggest a general role for the FATC domain as membrane anchor of phosphatidylinositol-3 kinase-related kinases (PIKK). J Biol Chem 288:20046–20063. https://doi.org/10.1074/jbc.M113.467233

Sommer LAM, Janke JJ, Bennett WFD, Bürck J, Ulrich AS, Tieleman DP, Dames SA (2014) Characterization of the immersion properties of the peripheral membrane anchor of the FATC domain of the kinase "target of rapamycin" by NMR, oriented CD spectroscopy, and MD simulations. J Phys Chem B 118:4817–4831. https://doi.org/10.1021/jp501533d

Vuister GW, Bax A (1993) Quantitative J correlation: a new approach for measuring homonuclear three-bond J(HNH.alpha.) coupling constants in 15N-enriched proteins. J Am Chem Soc 115:7772–7777. https://doi.org/10.1021/ja00070a024

Vuister GW, Bax A (1994) Measurement of four-bond HN–Hα J-couplings in staphylococcal nuclease. J Biomol NMR 4:193–200. https://doi.org/10.1007/BF00175247

Walsh JD, Meier K, Ishima R, Gronenborn AM (2010) NMR studies on domain diffusion and alignment in modular GB1 repeats. Biophys J 99:2636–2646

Wullschleger S, Loewith R, Hall MN (2006) TOR signaling in growth and metabolism. Cell 124:471–484. https://doi.org/10.1016/j.cell.2006.01.016

Structural characterization of the membrane-associating FATC domain of ataxia telangiectasia mutated by NMR and MD simulations

Munirah S. Abd Rahim[1], Yevhen K. Cherniavskyi[2], D. Peter Tieleman[2], Sonja A. Dames[1,3$]

From the [1]Chair of Biomolecular NMR Spectroscopy, Department of Chemistry, Technische Universität München, Lichtenbergstr. 4, 85747 Garching, Germany, [2]Department of Biological Sciences and Centre for Molecular Simulation, University of Calgary, Calgary, AB, Canada, [3]Institute of Structural Biology, Helmholtz Zentrum München, Ingolstädter Landstr. 1, 85764 Neuherberg, Germany

Running title: Structure of membrane-associating ATM FATC

[$]To whom correspondence may be addressed: Chair of Biomolecular NMR Spectroscopy, Department of Chemistry, Technische Universität München, Lichtenbergstr. 4, 85747 Garching, Germany, Tel.: +49-89-35831-7103, Fax: +49-89-3229-4002, E-mail: (sonja.dames@tum.de)

Keywords: Ataxia telangiectasia mutated, phosphatidylinositol 3-kinase related kinase, protein membrane interactions, signaling at membranes, NMR, MD simulations

---

ABSTRACT

Ataxia telangiectasia mutated (ATM) plays an important role in the DNA damage response but also in signaling in response to redox signals, the control of metabolic processes and mitochondrial homeostasis. ATM localizes in the nucleus and at the plasma membrane, mitochondria, peroxisomes and other cytoplasmic vesicular structures. It has been shown that the C-terminal FATC domain of human ATM (hATMfatc) can interact with a range of membrane mimetics and thus may act as a membrane anchoring unit. Based on NMR structural data, ^{15}N-relaxation data, NMR data using spin labeled micelles, and MD simulations of micelle-associated hATMfatc, it binds the micelle by a dynamic assembly of three helices with many residues localizing in the head group region. None of the three helices penetrates the micelle deeply or makes significant tertiary contacts to the other helices. NMR monitored interaction studies of mutants in which two conserved aromatic residues were individually and at the same time replaced by alanine show that the double mutation does not abrogate the interaction with micelles and bicelles at the typically used high concentrations, but is sufficient to impair the interaction with small unilamellar vesicles (SUVs), which are usually used at much lower lipid concentration and which are considered a better mimetic for natural membranes. The observed dynamic structure of micelle-associated hATMfatc may enable it to interact with differently composed membranes and/or membrane localized interaction partners and thereby regulate the kinase activity. Moreover, the FATC domain of ATM maybe used as membrane anchoring unit for other biomolecules.

Ataxia telangiectasia mutated (ATM) belongs to the family of phosphatidylinositol 3-kinase related kinases (PIKKs) that phosphorylate Ser/Thr residues of proteins regulating processes such as DNA repair, cell cycle progression, cellular senescence, apoptosis, and metabolic processes (1-4). Recently, it became further aware that PIKKs also play a role in signaling in response to virus infections and during

inflammation (5,6). The function of ATM and of the related mammalian/mechanistic target of rapamycin (mTOR), a central controller of cell growth and metabolism in all eukaryotes that also has links to DNA repair signaling (7,8), has further been related to redox signaling (9-12). Whereas the mTOR pathway negatively controls ATM (13), ATM inactivates mTORC1 in response to reactive oxygen species (ROS) to induce autophagy (12), apparently rather selectively that of peroxisomes (14). ATM also downregulates mTORC1 under hypoxic conditions (11). Other studies support that ATM plays direct roles in modulating mitochondrial homeostasis (15). Activation of ATM by oxidation and other factors has been reviewed (16). Inactivation of ATM leads to Ataxia-Telangiectasia (A-T) disease and more generally plays a role in neuronal development and neurodegeneration (17). Because ATM controls different signaling pathways important for the DNA damage response, cell cycle check points and metabolic processes, it is considered an interesting therapeutic target with respect to cancer (18).

It has been proposed that targeted membrane localization allows spatial separation of individual signaling branches of large signaling networks, thereby potentially improving the reliability of biochemical signaling processes (19). Since PIKKS generally participate in a multitude of signaling pathways in response to ionizing radiation and other stress factors or metabolic signals (2,5,7,16,20,21), their localization may also determine the specific signaling output (22). ATM has not only been found to localize and function in the nucleus but also in the cytoplasm (12). ATM has been localized at microsomes (23) and cytoplasmic vesicles (24), as well as at membrane-associated vesicles (25). More recently, it has been reported that PEX5 peroxisome import receptor binds ATM to localize it to peroxisomes and that ATM can localize to mitochondria (14,15).

Although the total length of PIKK amino acid sequences ranges from about 2500 to 4500 residues, all share a similar domain organization (5,22). Fig. 1A shows human ATM as representative example. The Ser/Thr kinase domain is close to the C-terminus and shows homology to lipid kinases (4). Except for TRRAP, all are catalytically active (1,4). The FRAP-ATM-TRRAP (FAT) domain resides N-terminal of the kinase (22,26). Based on sequence analysis the FAT and the preceding N-terminal region with only low sequence homology between different PIKKs are mostly composed of α-helical repeat motifs that typically form platforms for protein-protein interactions (26-28). The linker region between the kinase and the FAT C-terminal (FATC) domain region varies significantly in length and sequence composition (4,29). It has been referred to as PIKK regulatory domain (PRD) (1,4,29). The highly evolutionary conserved region of the FATC domain is made up by the ~35 C-terminal residues (PFAM domain database entry PF02660) (4,26,30-32). Based on mutagenesis studies and other data, this domain generally plays an important role for the regulation of PIKK function (4,29,31,33-35).

Obtaining high-resolution structural data for PIKKs is challenging due to their large size. For ATM electron microscopy (EM) structural data at lower resolution provided insights in the interaction with DNA (36), the inhibitory effect of dimerization of human ATM (37), and the dimerization properties of the yeast ATM homolog Tel1 (38,39). In 2017, higher resolution EM structures of the closed ATM dimer (PDB-ID 5NP0, 5.7 Å resolution) and the presumably more active open ATM dimer (PDB-ID 5NP1, 5.7 Å resolution for combined data) were published (40).

The FATC domains of all PIKKs are rather hydrophobic and rich in aromatic residues (ATM see Fig. 1B). In line with this, all interact with membrane mimetics, although with somewhat different preferences for membrane features such as surface charge, curvature or packing density,

and thus may all act as membrane anchoring units (32). Like TOR, ATM binds to all tested membrane mimetics including dodecylphosphocholine (DPC) micelles, bicelles composed of dimyristoyl and diheptanoylphosphocholine (DMPC, DihepPC), and small unilamellar vesicles (SUVs) made of DMPC (32). An estimate of the secondary structure content based on secondary chemical shifts suggested that the micelle-immersed human ATM FATC domain contains three helical stretches (32). Here, we present the determined NMR structure and an analysis of the relative orientation on the micelle and its membrane immersion properties and dynamics based on NMR and molecular dynamics (MD) data. We further prepared mutants by replacing conserved aromatic residues that are expected to be important for the membrane affinity and tested their ability to interact with DPC and DihepPC micelles, DMPC/DihepPC bicelles and DMPC SUVs. Overall the data provides a better understanding of the role of the AMT FATC domain in regulating the kinase function as well as the observed localization to specific membrane compartments.

Results

The NMR structure of micelle-immersed hATMfatc consists of three helices with a central flexible linker and a less flexible C-terminal linker

The three-dimensional structure of the human ATM FATC domain (hATMfatc) associated with DPC micelles (PDB-ID 6HKA) was determined by multidimensional heteronuclear NMR spectroscopy in solution. Since cleavage of the GB1tag is not efficient and results in very low yields, all structural restraints were derived from NMR data recorded for the GB1-tagged form (hATMfatc-gb1ent) (32). Previous studies have shown that the GB1tag does not affect the association with DPC micelles and results only in little overlap of NMR signals of the GB1 tag and the FATC domain (41). The structural statistics are given in table 1.

The structure of micelle-associated hATMfatc, residues T68-V100 in hATMgatc-gb1ent corresponding to T3024-V3056 in full-length human ATM, consists of three helical regions (Fig. 1B-D). The structure is overall well-defined with 85.5% of the residues in the well structured region (V72-A83, P86-L92, P94-V100) occupying the most favored region of the Ramachandran plot (table 1). Based on the 20 lowest energy structures the N-terminal longer α-helix (α1) is on average formed by residues G73 to A83 of the 100 residues fusion protein, which corresponds to residues G3029 to 3039 of full-length human ATM. Following a three-residue linker (I84/3040-D85/3041-P86/3042), a second α-helix (α2) is on average formed by residues K87/3043-R91/3047. Following another proline-containing short linker (L92/3048-F93/3041-P94/3049), the C-terminal helix follows.

The central flexible linkage between α1 and α2 results in a high RMSD value of 4.47 Å for residues 70/3026-100/3056 compared to very low ones for the single helical regions (α1: 0.37 Å, α2: 0.22 Å, α3 0.27 Å, table 1) or the region including α2 and α3 (residues 87-99: 1.32 Å). This can be explained by the fact that no interhelical NOE contacts could be observed (table 1). In line with the dynamic linkage between α1 and α2 around D85/3041, it shows a $\{^1H\}$-^{15}N-NOE value of only 0.32 ± 0.10 at 150 mM and 298 K and 0.38 ± 0.11 at 200 mM and 298 K (Fig. 1D). The linkage between α2 and α3 is also not rigid, but the $\{^1H\}$-^{15}N-NOE values in the linker region are not as low (L92/3048: 0.42, F93/3049: 0.48 at 150 mM DPC and 298 K) and of similar size as the ones for K97/3053 (0.43) and W99/3055 (0.48) in the short C-terminal helix. A more detailed description of the ^{15}N-relaxation data is provided in the SI (text and SI Fig. S1-2).

Consistent with the differences in the amino acid sequence to the FATC domain of yeast TOR1 (= y1fatc, Fig. 1 B top), the

overall structural appearance is quite different. y1fatc contains two conserved cysteines that can form a disulfide bond and oxidized y1fatc in the absence of membrane mimetics forms already an α-helix that is followed by a C-terminal disulfide bonded loop (42). In contrast, hATMfatc in buffer is largely unstructured and most backbone amide signals are not visible in the ^{1}H-^{15}N HSQC spectra (32), which hampers its resonance assignment.

Compared to micelle-associated hATMfatc, micelle-associated oxidized y1fatc adopts only a single α-helix that is followed a disulfide bonded loop or bulb (Fig. 1B right side) (43). Even in the reduced micelle-associated state of y1fatc the C-terminus folds back and the whole structure is less dynamic than that of hATMfatc (43). The {^{1}H}-^{15}N-NOE values of oxidized and reduced micelle-associated y1fatc at 298 are more uniform in the well-structured region and do not show residues with significantly lower values in between (43) as observed for micelle associated hATMfatc (Fig. 1D).

The surface of micelle-associated hATMfatc (Fig. 2, top) is largely hydrophobic except for a positively charged surface region formed by K87/3043, R91/3047 and K97/3053 that is in neighborhood to a small negatively charged surface region formed by D85/3041. In contrast that of micelle-immersed y1fatc (Fig. 2 bottom) shows a large acidic region towards the N-terminus and only two small positively charged regions around K2448 and R2456. The C-terminal loop of y1fatc is largely hydrophobic (43).

The helical regions of micelle-associated hATMfatc can move with respect to each other

Additional insights into the dynamics as well as immersion properties (see next section) of micelle-associated hATMfatc were obtained from molecular dynamics simulations. In total 3 runs of MD simulations were performed using as starting structure for each one of the three lowest energy NMR structures (Fig. 3A). The simulation time for each run was 1.3 μs. The first 300 ns were discarded as equilibration time. As illustrated by the pictures of the simulated micelle-associated hATMfatc of each run (Fig. 3B), the relative orientation of the three helices with respect to each other varies in each, due to the dynamic linkages between the helices, especially the one between α1 and α2. Additional information about the conformational freedom are provided based on RMSD and RMSF (global and local) values in the SI (text and SI Fig. S4). Plots of the angle between α1 and α2 as well as between α2 and α3 (Fig. 3C, SI Fig. S5A) as a function of time show that these angles can vary significantly as a function of the simulation time. In summary the ^{15}N-relaxation data and the MD simulations suggest that the reorientation of the helices with respect to each other due to the dynamic central linkage between α1 and α2 and less dynamic linkage between α2 and α3 is the major contribution to their dynamic properties, rather than more local conformational changes.

The hATM FATC domain resides largely in the head group region of DPC micelles

Based on the MD simulations of the three lowest energy NMR structures of micelle-associated hATMfatc in the presence of DPC micelles (Fig. 2C), the three helices immerse mostly into the head group region. To probe this experimentally, we recorded ^{1}H-^{15}N HSQC spectra of hATMfatc-gb1ent in the presence of DPC micelles (50 mM) and increasing amounts of paramagnetic 5- or 16-doxyl stearic acid (5-/16-SASL) (Fig. 3A, SI Fig. S5B). Earlier MD-simulations of DPC micellar systems in the absence and presence of protein showed that 5-/16-SASL can move in the micelle and that 16-SASL can bend such that the doxyl group is close to the head group region and not deep in the interior as commonly assumed (44). The MD data further confirmed that the doxyl group of 5-SASL, as expected (45), resides also near the DPC head groups (44). Residues of hATMfatc that localize close to the head

groups should thus show the strongest spectral changes. The doxyl label of 5- or 16-SASL results in paramagnetic relaxation enhancement (PRE), which reduces the signal intensity of nearby amide groups with an r^{-6} distance dependence (46). In order to better correlate the PRE effects with the average chemical shift changes (SI Fig. S6, S7) as well as with the distance from the micelle center of mass (COM, Fig. 4C) and the surface area that is covered by DPC (Fig. 4D) from the MD simulation, we plotted 1-I(x mM SASL)/I (0 mM SASL), which we refer to a 1-PRE. Thus, the stronger the PRE effect, the closer to 1 is the 1-PRE value (Fig. 3B, SI Fig. S6 and S7). As for the FATC domain of yeast TOR1, the PRE effects with 16-SASL are stronger than with 5-SASL (44). 1 mM 16-SASL results overall in somewhat larger 1-PRE values than 2 mM 5-SASL. Because the nitroxide spin label usually does not induce significant pseudo contacts shifts, the observed chemical shift changes arise from a change in the chemical environment. The plots of the 1-PRE values and average ^{1}H-^{15}N chemical shift changes for the whole fusion protein (Fig. S6, S7) show further that the GB1 tag that does not directly interact with the micelle shows only very small changes. For the hATMfatc part the changes with 5- and 16-SASL show overall a similar trend as a function of the residue sequence position (Fig. 3A, B). Strong PRE effects (1-PRE $\geq$ 0.4) at 2 mM 5-SASL or 1 mM 16-SASL are seen for V72, I84, D85, F93, and G95. In case of 1 mM 16-SASL additionally for G73, L78, L79, Q81, Q82, A83, L92, K97, A98, and W99. Not surprisingly, many of them show also significant chemical shift changes (Fig. 3A, SI Fig. S6, S7). Since the listed residues based on the NMR data should localize near the head groups they should have a distance from the micelle center of mass (COM) that is in a similar range as the phosphorus atom of the DPC head group. Fig. 3C shows the average distance of the COM of each residue of hATMfatc to the micelle COM for run 1. Those for run 2 and 3 are displayed in SI Fig. S8. The profiles as a function of the sequence look very similar for all runs. In line with the 5- and 16-SASL NMR data, residues that show strong PRE effects (Fig. 3B) have mostly distances to the micelle COM that are similar to that of the DPC phosphorus atom (dotted line at 1.914 nm). In contrast, residues that show a small PRE effect, such as T68/3024 at the N-terminus of hATMfatc, show a larger distance to the micelle if they are more solvent accessible or a closer one such as for example L92/3046 if they reside deeper in the micelle. From a plot of the solvent accessible surface (SAS) area covered by DPC that was derived from the three MD runs (Fig. 3D, SI Fig. S9), it can further be estimated which residues immerse deeper and which should still be solvent accessible. As expected, those residues showing a short distance to the micelle COM (Fig. 3C, SI Fig. S8) are 80% or more covered by DPC, for e.g. run1 V72, V76, L79, P86, and L89. Not unexpectedly, these residues are mostly hydrophobic.

In summary, the NMR data using spin labeled micelles and the MD simulations of micelle-associated hATMfatc show that it binds the micelle by a dynamic assembly of three helices with many residues localizing in the head group region. None of the three helices penetrates the micelle very deeply or makes significant tertiary contacts to the other helices.

Mutation of F93/3049 and W96/3052 to alanine abrogates the association of hATMfatc with neutral SUVs but not with micelles and bicelles

Tryptophans but also other aromatic residues are known to play an important role for the affinity between membranes and proteins in general (47,48). For the FATC domain of TOR we have shown previously that replacement of up to 6–7 residues did not result in a significant abrogation of the association with micelles or bicelles. However, replacement of only one tyrosine (Y2463) or one tryptophan (W2466) resulted in an impairment of the interaction with SUVs (49). In order to find out if aromatic

residues of hATMfatc at equivalent positions (F93/3049, W96/3052) have a similar effect, we mutated them individually and at the same time to alanine residues. The free states of the mutant proteins show even less peaks and thus appear to be more dynamic than wild type hATMfatc (SI Fig. S10, left side). This maybe explained with the smaller size of alanine compared to tyrosine or tryptophan. In the presence of 50 mM DPC, they adopt as the wild type a more ordered structure, which reduces the backbone dynamics such that the backbone and side chain amide signals become clearly visible (SI Fig. S10, right side). The interaction with neutral membrane mimetic micelles composed of DPC or the short chain diacyl lipid DihepPC, neutral bicelles composed of DMPC for the planar region and DihepPC for the rim, and small unilamellar vesicles composed of DMPC was further monitored by recording ^{1}H-^{15}N HSQC spectra in the absence and presence of these membrane mimetics (Fig. 5, SI Fig. S11, S12). As indicated by the observed spectral changes neither of these mutations abolished the interaction with micelles or bicelles (table 1). Whereas the single mutants F93/3049A and W96/3052A could still interact with neutral DMPC SUVs (SI Fig. S11, S12), a lack of spectral changes for the double mutant F93/3049A-W96/3052A (Fig. 4, lower right) indicates that it could not.

Discussion

ATM is not only involved in DNA repair but it has also been suggested that ATM plays a role in the oxidative stress response and as a link between genome stability and carbon metabolism (9,10). In line with this, it was recognized that ATM localizes not only in the nucleus but also at cytoplasmic vesicles (24) and more specifically peroxisomes (14) and microsomes (23), the plasma membrane (25), and mitochondria (15). NMR- and CD-monitored interaction studies showed that the ATM FATC domain can interact with all tested membrane mimetics, and thus may besides protein-protein interactions also mediate direct membrane interactions of ATM (32). The presented NMR structure of the micelle-associated state of the FATC domain of human ATM (Fig. 1, 2) and the characterization of its dynamic and immersion properties from MD and further NMR data (Fig. 3, 4) show that membrane association is mediated by three rather flexibly linked helices that immerse largely in the head group region and slightly below and that do not significantly interact with each other. This dynamic assembly may enable specific interactions with other membrane embedded proteins. Recruitment to the plasma membrane involves interactions of the protein CKIP-1 (casein kinase-2 interaction protein-1) that is involved in muscle differentiation and the regulation of the actin cytoskeleton with the ATM C-terminal region, including the catalytic and the FATC domain (50). In addition, interactions with the PEX5 peroxisome import receptor localize ATM to peroxisomes (14).

The plasma membrane (PM) as well as the endo- or lysosomal membranes contain as major components the neutral lipids phosphatidylcholines (PC) and phosphatidylethanolamines (PE), as well as cholesterol. The cytosolic side of the PM contains further a small fraction of the negatively charged lipid phosphatidylserine (PS). Mitochondria and peroxisomes are similarly composed as the ER with PC being the major component, followed by PE and about 10 % phosphosinositol lipids (51). The presence of a C-terminal positively charged surface patch next to a smaller negatively charged one (Fig. 1D), may not only mediate interactions with the positively and negatively charged head group components of PC or PE but additionally enable interactions with negatively charged PS in the PM or phosphorylated PIs (PIPs) at mitochondria (51). The folding-upon-binding to a membrane mimetic, which has for example also been detected for the 30-residue long glucagon-like peptide 1 (GLP-1) (52), and the resulting dynamic helix

assembly of membrane associated hATMfatc may further be helpful to interact with specific receptors or membranes with different packing densities, which depends e.g. on the amount of cholesterol or the ratio of saturated versus unsaturated fatty acids in the lipids (51). Based on the membrane catalysis hypothesis, initial interactions of signaling peptides with the bilayer increase their local concentration and allow them to adopt a structure that is recognized by the target membrane-resident receptors (52). The same maybe true for specific protein domains or segments.

Based on mutagenesis studies the FATC domains of all PIKKs play an important role for their regulation (26,30,31,33-35,53) and share the ability to interact with different membrane mimetics, albeit with varying preferences for specific membrane properties (32,43). The observed evolutionarily conserved sequence differences (e.g. Fig. 1B ATM and TOR) may result in different membrane associated conformations that determine the specific membrane targeting behavior (32). In line with this micelle-associated hATMfatc adopts of a rather dynamic assembly of three helices with a hydrophobic N-terminal region and a more polar C-terminal one, whereas the one of the yeast TOR1 FATC domain consists of a single helix followed by a loop that in the oxidized state contains a disulfide bond and where the N-terminal region is acidic and the C-terminal one largely hydrophobic (Fig. 1C and Fig. 2). Consistent with this, the FATC domain of ATM cannot replace the one of ATR (29) or TOR (33).

The FATC domains of all PIKKs share conserved sequence features (e.g. Fig. 1B ATM and TOR) that maybe important for regulatory function and especially for directly mediating membrane interactions (32). The conserved glycine near the C-terminus of TOR (G2465 of y1fatc (Fig. 1B), G2544 in human TOR) appears to facilitate the back bending of the C-terminal region to the α-helix (Fig. 1C, right side). Except for TRRAP, this glycine is also conserved in all other PIKKS (32) and in case of ATM participates in the flexible linkage between α2 and α3 (Fig. 1C center). The in ATM also evolutionarily completely conserved proline 3042 (= P86), aspartate 3041 (= D85), and alanine 3039 (= A83) form together with I3040 (= I84) in humans but a methionine in other organisms the flexible linker between α1 and α2. The proline and the aspartate are also found in the DNA-PKcs amino acid sequences from most organisms (humans D4113, P4114) and based on $^{13}C^{\alpha}$ secondary shifts also disrupt two helical stretches (32). Interestingly, alanine 3039 of hATMfatc is also in most other PIKKS conserved including TOR, in which the helix of the micelle-associated oxidized and reduced states is distorted around this residue (43).

All PIKK FATC domains contain at least one or more tryptophans and/or one or more tyrosine or phenylalanine and several aliphatic hydrophobic residues (32). Tryptophans are often found at the interface between the apolar interior and the polar aqueous environment (47,48) and many hydrophobic residues show a positive free energy contribution for the transfer of a model peptide from a lipid bilayer to water (54). Replacement of either Y2463 or W2466 (Y2542 and W2545 in human TOR) is already sufficient to abrogate the interaction of y1fatc with DMPC SUVs (49). For hATMfatc, F3049 (= F93) and W3052 (= W96) at equivalent positions have to be replaced simultaneously to achieve the same effect (Fig. 5, SI Fig. S11, S12). However, the respective mutations did not abrogate the interaction with micelles and bicelles (Fig. 5, SI Fig. S11, S12). The different association behavior of FATC mutants with micelles and bicelles compared to SUVs can be explained twofold. First, in case of micelles or bicelles the total concentration of the used detergents or lipids and thus the available membrane mimetic surface area is much higher than for SUVs. The used concentration of DPC and DihepPC was 50 mM and the total lipid concentrations in the DMPC/DihepPC bicelle samples was ~240

mM. However due to the preparation method, the total lipid concentration in the SUV samples is significantly below 50 mM since pure DMPC cannot easily be resuspended at high concentrations and in addition some of the lipid is lost when separating the small from larger uni- and multilamellar vesicles by centrifugation. Whereas 1D ^{1}H NMR spectra can be used to compare the lipid content in samples with micelles and bicelles, this is due to the large size of SUVs and corresponding line broadening not possible. However, besides established methods such as dynamic light scattering, the CD signal may be used to compare different liposome preparations (49,55). A second reason for the different binding behavior of FATC domain to micelles and bicelles versus SUVs may further be a higher affinity for curved membrane surfaces. DPC micelles are rather small, spherical particles that contain ~50-60 DPC molecules, resulting in a molecular weight of ~19 kDa and a radius of gyration of about 17-18 Å (56,57). Bicelles have a rather planar bilayer region that is formed by a long chain phospholipid such as DMPC. However the rim that is formed by a short chain lipid such as DihepPC shows as micelles also a high curvature. The molecular weight of bicelles is usually >~250 kDa and the diameter of the planar region ranges from 21 to 77 Å for q values between 0.2 and 1 (58,59). Even liposomes of the SUV type are much larger than bicelles. Although they are as micelles approximately spherical, they are less curved since the radius is much larger (around 20-100 nm) (60). We suggested already earlier that for proteins with a rather high and broad affinity for different membrane mimetics, SUVs at the usually used lower concentrations are better suited to detect mutants that may also abrogate membrane association in localization studies in cells (49).

The characterization of the membrane association of ATM by NMR and MD simulations was done looking only at the FATC domain (Fig. 1-4). This raises the question on how accessible it is for membrane-interactions in the context of the full-length protein. Based on recent cryo electron microscopy (EM) data, ATM was suggested to be in an equilibrium between a closed, inactive dimer (resolution ~4-6 Å) with restricted access to the substrate binding site and an open, active dimer (resolution ~11.5 Å, if combined data used 5.7 Å) with good access to the substrate binding side (40). Whereas the FATC domain appears not well accessible in the closed, inactive ATM dimer, it appears well accessible for interactions with membranes and regulatory proteins in the open, active state. The conformation of the FATC domain in the provided cryo EM structures is similar to the micelle-associated conformation presented here and also consists to two α-helices and a C-terminal helix or turn-like structure (40). Early studies suggested that DNA damages induce Ser1981 autophosphorylation and that this results in active, monomeric ATM (61), in which the FATC domain is expected to be even better accessible than in the open dimer. Moreover, studies of oxidative activation of ATM indicated that oxidation of Cys2991 which is about 60-80 residues N-terminal of the FATC domain, results in dimerization (62). Thus future membrane-interactions studies may analyze the effect of reactive oxygen species (ROS) or oxidized lipids on C2991. Future localization studies of ATM in cells have to clarify how it varies in response to specific signals and which interactions with specific, especially membrane localized proteins such as the PEX5 peroxisome import receptor (14), as well as membrane regions and specific signaling lipids it involves. Moreover, the oligomerization state under different signaling conditions and the resulting cellular localizations have to be determined. Finally, acetylation of lysine 3016 (53) N-terminal of the highly conserved FATC region of ATM may effect the described localization at the plasma membrane, mitochondria, peroxisomes,

mircrosomes, and other cytosolic vesicles (12,14,15,23-25).

As suggested for the FATC domain of TOR, the one of ATM may also be fused to other proteins or peptides or other substances to tether them to membrane mimetics (63).

Experimental Procedures

Plasmid cloning, protein expression, and purification

The coding sequence for the FAT C-terminal (FATC) domain of human ATM (residues 3024-3056, UniProt-ID 13315) was cloned into GEV2 (64). The resulting fusion protein consisting of GB1 (residues 1-56), a linker region composed of a thrombin (57-62) and an enterokinase (63-67) protease recognition site, and the C-terminal 33 residue of human ATM (68-100) (= hATMfatc-gb1ent) was overexpressed in *Escherichia coli* BL21 at 37 ºC. Since proteolytic removal of the GB1tag is inefficient and the GB1 tag does not disturb the interaction with membrane mimetics and its monitoring, the fusion protein was used for the described NMR studies (32,41). Uniformly ^{15}N-, or ^{15}N-^{13}C –labeled proteins were prepared in M9 minimal medium containing $^{15}NH_4Cl$ and/or ^{13}C-glucose as the sole nitrogen and carbon sources. The expression and the purification by a heating step (65) and IgG affinity chromatography were done as described previously (32,66).

Site-directed mutagenesis

Replacement of one or more aromatic residue in hATMfatc-gb1ent by alanine (Fig. 1B, F93A = F3049A, W96A = W3052A, F93A/W96A = F3049A/W3052A) was achieved by following the QuickChange site-directed mutagenesis protocol (Stratagene). The success of the mutagenesis was verified by DNA sequencing. Cells expressing mutant hATMfatc-gb1ent were lysed by sonication in 50 mM Tris, 150 mM NaCl, 2 mM benzamidine and 0.3 mM EDTA, pH 7.6. Mutant proteins were purified by IgG affinity chromatography as described for the wild type and in the manufacturer's manual (32,66). Fractions containing the target protein were pooled, washed, and concentrated with NMR buffer (50 mM Tris, 100 mM NaCl, pH 7.4 for the single mutants F93A = F3049A, W96A = W3052A or pH 6.5 for the double mutant F93A/W96A = F3049A/W3052A).

Preparation of membrane-mimetics

Dodecylphosphocholine (DPC), 1,2-diheptanoyl-*sn*-glycero-3-phosphocholine (DihepPC), 1,2-dimyristoyl-*sn*-glycero-3-phosphocholine (DMPC), 5-doxyl stearic acid (5-SASL), and 16-doxyl stearic acid (16-SASL) were purchased from Avanti Polar Lipids and/or Sigma-Aldrich. Deuterated DPC (d_{38}-DPC) was obtained from Cambridge Isotopes.

Membrane mimetic DPC micelles were prepared by placing a defined amount of DPC from concentrated stock solution in chloroform (0.5 M) in a glass vial and drying under a stream of nitrogen gas. The resulting DPC film was dissolved in NMR buffer containing the protein of interest. For NMR titration experiments samples containing >30 mM DPC samples were prepared in the same way, whereas those with DPC concentrations < 30 mM were prepared by diluting a 100 mM DPC stock in buffer with a protein stock and buffer. Note that a separate sample was prepared for each DPC concentration to avoid dilution effects and thus to keep the protein concentration constant. DihepPC micelles were prepared by diluting a 0.25 M stock solution in NMR buffer to 50 mM with the respective protein solution and buffer. Micelles form above the critical micelle concentration (CMC), which is 1.1 mM for DPC (67) and 1.4-1.8 mM for DihepPC (68,69).

DMPC/DihepPC bicelles (q= 0.2, [DMPC] = 0.04 M, and [DihepPC] = 0.20 M, cL 15%) were prepared as follows. An appropriate amount of a 0.25 M stock of the long-chain phospholipid (DMPC) in chloroform was placed in a glass vial and the chloroform blown away under a stream

of nitrogen gas. In order to form bicelles, the right amount of the short-chain lipid (DihepPC) in NMR buffer was added and the vial vortexed until a clear solution was obtained. Lastly, the protein solution was added to the concentrated bicelles solution.

Liposomes were prepared by drying an appropriate amount of DMPC in chloroform (0.25 M) under a stream of nitrogen gas. The resulting pellet was dissolved in NMR buffer to obtain a 100 mM solution. To dissolve the pellet, it was exposed to seven cycles of freezing in liquid nitrogen, thawing by incubation in a water bath at 40 °C and thorough vortexing. To induce the formation of small unilamellar vesicles (SUVs) from large uni- and multilamellar vesicles, the DMPC suspension was incubated in an ultra-sonication bath for 30 minutes. A clear supernatant containing only SUVs was obtained after centrifuging the lipid mixture at about 15 krpm in a table-top centrifuge for 5 minutes. The resulting white precipitate at the bottom corresponds to large uni- and multilamellar vesicles. For the preparation of a protein sample in the presence of liposomes, only the clear supernatant containing small unilamellar vesicles was diluted 1:1 with protein solution. Thus, using the 100 mM stock solution the final sample contained < 50 mM DMPC.

NMR sample preparation

For the NMR resonance assignment and structural characterization samples containing ~0.5 mM of ^{15}N or ^{15}N-^{13}C-hATMfatc-gb1ent in 50 mM Tris, 100 mM NaCl, 10 mM TCEP, 0.02% NaN_3 (95% H_2O/5% D_2O), pH 6.5, 150 mM d_{38}-DPC were used. We also prepared samples with 200 mM d_{38}-DPC (180 mM d38-DPC and 20 mM DPC), but the spectral quality was overall lower (broader signals, more noise signals) than for samples with 150 mM DPC (see e.g. SI Fig. S1). The 10 % ^{13}C-labeled hATMfatc-gb1ent sample used for the stereospecific assignment of valine and leucine methyl groups contained 170 mM d_{38}-DPC micelles.

The samples of hATMfatc-gb1ent mutants contained about 0.15 mM ^{15}N-labeled protein in NMR buffer. For the double mutant (F93/W96 = F3049A/W3052A) the pH was 6.5, as for the wild type. The single mutants (F93 = F3049A, W96 = W3052A) were measured at pH 7.4 to improve their solubility and stability.

For NMR experiments with spin labeled DPC micelles, samples containing about 0.1 mM protein and 50 mM undeuterated DPC were prepared. The concentration of 5- and 16-doxyl stearic acid (5-/16-SASL) was increased by stepwise addition of a small amount (1 to at maximum 4 mM) from a 0.25 M stock solution in chloroform.

NMR spectroscopy

NMR spectra were recorded on Bruker Avance 500 MHz, 600 MHz, and 900 MHz spectrometers at a temperature of 298 K. The 500 MHz and 900 MHz spectrometers were equipped with cryogenic probes. Data were processed with NMRPipe (70) and analyzed using NMRView (71). Assignments for the ^{13}C, ^{15}N, and ^{1}H nuclei of micelle-immersed hATMfatc fusion protein were based on 2D ^{1}H-^{15}N and various ^{1}H-^{13}C HSQC spectra, partially without decoupling, 3D HNCA, HNCACB, CCONH-TOCSY, HCCH-TOCSY, HNHA, HNHB and ^{15}N- and ^{13}C-edited NOESY spectra as described (66). The NOESY mixing times were 90 ms for the ^{15}N-edited NOESY, 100 ms for the aromatic and aliphatic ^{13}C-edited NOESY experiments. Information about backbone dynamics was derived from the analysis of ^{15}N relaxation data, including T_1 (spin-lattice longitudinal relaxation rate), T_2 (spin-spin or transverse relaxation rate), and $\{^{1}H\}$-^{15}N NOE.

The immersion depth properties of hATMfatc in DPC micelles were derived by recording ^{1}H-^{15}N HSQC and 1D ^{1}H-NMR spectra of samples containing increasing amounts of paramagnetic 5- or 16-doxyl

stearic acid (5- and 16-SASL). The resulting paramagnetic relaxation enhancement (PRE) effects were derived based on the observed changes in signal intensity. In addition, the average chemical shift changes of the backbone amide nitrogen and proton [$\Delta\delta(N,H)_{av}$] were calculated based on the formula $[(\Delta\delta_{HN})^2 + (\Delta\delta_N/5)^2]^{1/2}$. The interaction of mutant proteins with membrane mimetics was monitored by recording 1D ^1H and 2D ^1H-^{15}N HSQC spectra.

Structure calculation

All structure calculations were performed with XPLOR-NIH (72) using molecular dynamics in torsion angle and Cartesian coordinate space and the standard force field with the parameter files topallhdg_new.pro and parallhdg_new.pro. Distance restraints were generated in NMRView (71) and classified according to NOE-cross peaks intensities. Upper bounds were 2.8 Å, 3.5 Å, 4.5 Å and 5.5 Å. The lower bound was always 1.8 Å. For all NOE restraints r^{-6} sum averaging was used. Backbone dihedral angle restraints for ϕ and ψ as well as hydrogen bond restraints for helical regions were derived based on the determined $^{13}C^{\alpha}$ chemical shifts, observed helix typical NOE restraints and on initial structure calculations.

MD simulations

Molecular dynamics simulations were performed with Gromacs 2016.3 software (73-75). The FATC domain was initially placed randomly near the preequilibrated micelle (50 DPC molecules) and solvated with ~54000 water molecules (box size ~11 nm). Na^+ and Cl^- ions were added to the system to reach 0.1 M salt concentration. The CHARMM36m force field was used for the protein and DPC (76). A 2 fs time step was used. All bonds were constrained with the LINCS algorithm (77) and water bond lengths and angles were kept constant using the SETTLE algorithm (78). Initial velocities were taken from the Maxwell distribution for 303.15 K. A constant temperature of 303.15 K was maintained with the V-rescale thermostat with 0.1 ps coupling constant (79). The DPC micelle with the protein and the water molecules with the ions were coupled to two separate thermostats with the same parameters. Constant pressure of 1 bar was maintained by the isotropic Parrinello-Rahman barostat with 5.0 ps coupling constant and $4.5*10^{-5}$ bar^{-1} compressibility (80). The particle mesh Ewald (PME) algorithm was used for long-range contributions to electrostatic interactions (81,82). Lennard-Jones interactions were cut off at 1.2 nm with a force-switch modifier from 1.0 to 1.2 nm.

Three independent simulations were performed using as starting structures the three lowest energy NMR structures of the micelle-associated FATC domain of human ATM. Each simulation was 1.3 microseconds long. For the analysis of the secondary structure based on DSSP calculations (83), the clustering, the immersion depth, and the fraction of solvent accessible surface area covered by the micelle, the first 300 ns of each simulation were discarded as equilibration time.

RMSD and RMSF calculations were performed on the last 500 ns of each trajectory (800-1300 ns). RMSF analysis with the local fit of the protein structure was performed in addition to the calculations with a whole protein as a reference for the RMSD fit. This was done in order to highlight the fluctuations in particular segments of the protein as if the whole protein is used for RMSD fit, the RMSD/RMSF is dominated by the contributions from a change in relative orientation of the helices and we wanted to highlight local fluctuations in particular regions which aren't the result of the change in helix-helix orientation. RMSF graphs that are marked as ‘local 72-92’ or ‘local 86-98’ (SI Fig. S4) were calculated with the use of a short part of the protein as a reference for the progressive trajectory fitting and subsequent RMSF calculation (residues 72-

92, 86-98; 5 ns windows with the following averaging over all 5 ns intervals). Consequently, the RMSF values will be rather small for the region used for the fit.

The analysis of the angles between the helices in Fig. 3C (SI Fig. S5) starts also from 800 ns, because the relative orientation of the helices changes slowly compared to the local structure of the protein. Thus we let the system equilibrate for a longer period of time to have less bias from the initial structure.

The distance between micelle center of mass (COM) and the whole peptide COM, as well as separate peptide residue COMs, was computed using the simulation period from 300-1300 ns. To analyze peptide stability, the secondary structure of each peptide was computed as a function of time with the gmx do_dssp analysis program, which is part of the Gromacs package. The micelle surface for the images of the micelle associated FATC domain was defined as an iso-surface of averaged DPC density (contour density of 0.250 atoms/A^3). The pictures of the FATC domain alone are representative conformations of the protein as defined by cluster analysis of the protein RMSD performed by the gmx cluster program with the GROMOS clustering algorithm and 0.1 nm cutoff. All three trajectories (excluding the first 300 ns of each run) were combined into a single set of structures and cluster analysis was performed on this combined trajectory. Subsequently, 10 structures, one from each of the first 10 most populated clusters were selected as representative structures of the micelle-associated ATM FATC domain. The central structures of each cluster (in terms of RMSD distance) were selected as a representative for a given cluster. The combined size of the 10 most populated clusters was equal to 69.3% of the complete set of structures sampled. For the picture of a selective structure of micelle-associated hATMfatc for each run, a clustering analysis for reach run was performed. From the most populated cluster a structure with an RMSD corresponding to the average for the whole cluster, thus being in the middle, was selected.

Acknowledgements: We thank Martin Schaad, Lisa A. M. Sommer and Anja Wacker for their previous contributions to the project.

Conflict of interest: The authors declare that they have no conflicts of interest with the contents of this article.

Author contributions: SAD designed the study. MSAR performed the NMR experiments, analyzed the results and calculated the structures supported by SAD. DPT and YKC designed the MD simulations and YKC performed the simulations and analyzed the corresponding results. SAD wrote the paper with MSAR, YKC, and DPT.

References

1. Lovejoy, C. A., and Cortez, D. (2009) Common mechanisms of PIKK regulation. *DNA repair* **8**, 1004-1008
2. Abraham, R. T. (2001) Cell cycle checkpoint signaling through the ATM and ATR kinases. *Genes & development* **15**, 2177-2196
3. Chen, B. P., Li, M., and Asaithamby, A. (2012) New insights into the roles of ATM and DNA-PKcs in the cellular response to oxidative stress. *Cancer letters* **327**, 103-110
4. Lempiainen, H., and Halazonetis, T. D. (2009) Emerging common themes in regulation of PIKKs and PI3Ks. *The EMBO journal* **28**, 3067-3073

5. Quek, H., Lim, Y. C., Lavin, M. F., and Roberts, T. L. (2018) PIKKing a way to regulate inflammation. *Immunology and cell biology* **96**, 8-20
6. Pancholi, N. J., Price, A. M., and Weitzman, M. D. (2017) Take your PIKK: tumour viruses and DNA damage response pathways. *Philosophical transactions of the Royal Society of London. Series B, Biological sciences* **372**
7. Gonzalez, A., and Hall, M. N. (2017) Nutrient sensing and TOR signaling in yeast and mammals. *The EMBO journal* **36**, 397-408
8. Ma, Y., Vassetzky, Y., and Dokudovskaya, S. (2018) mTORC1 pathway in DNA damage response. *Biochimica et biophysica acta* **1865**, 1293-1311
9. Ditch, S., and Paull, T. T. (2012) The ATM protein kinase and cellular redox signaling: beyond the DNA damage response. *Trends in biochemical sciences* **37**, 15-22
10. Kruger, A., and Ralser, M. (2011) ATM is a redox sensor linking genome stability and carbon metabolism. *Science signaling* **4**, pe17
11. Cam, H., Easton, J. B., High, A., and Houghton, P. J. (2010) mTORC1 signaling under hypoxic conditions is controlled by ATM-dependent phosphorylation of HIF-1alpha. *Molecular cell* **40**, 509-520
12. Alexander, A., Cai, S. L., Kim, J., Nanez, A., Sahin, M., MacLean, K. H., Inoki, K., Guan, K. L., Shen, J., Person, M. D., Kusewitt, D., Mills, G. B., Kastan, M. B., and Walker, C. L. (2010) ATM signals to TSC2 in the cytoplasm to regulate mTORC1 in response to ROS. *Proceedings of the National Academy of Sciences of the United States of America* **107**, 4153-4158
13. Shen, C., and Houghton, P. J. (2013) The mTOR pathway negatively controls ATM by up-regulating miRNAs. *Proceedings of the National Academy of Sciences of the United States of America* **110**, 11869-11874
14. Zhang, J., Tripathi, D. N., Jing, J., Alexander, A., Kim, J., Powell, R. T., Dere, R., Tait-Mulder, J., Lee, J. H., Paull, T. T., Pandita, R. K., Charaka, V. K., Pandita, T. K., Kastan, M. B., and Walker, C. L. (2015) ATM functions at the peroxisome to induce pexophagy in response to ROS. *Nature cell biology* **17**, 1259-1269
15. Valentin-Vega, Y. A., Maclean, K. H., Tait-Mulder, J., Milasta, S., Steeves, M., Dorsey, F. C., Cleveland, J. L., Green, D. R., and Kastan, M. B. (2012) Mitochondrial dysfunction in ataxia-telangiectasia. *Blood* **119**, 1490-1500
16. Paull, T. T. (2015) Mechanisms of ATM Activation. *Annual review of biochemistry*
17. Marinoglou, K. (2012) The role of the DNA damage response kinase ataxia telangiectasia mutated in neuroprotection. *The Yale journal of biology and medicine* **85**, 469-480
18. Cremona, C. A., and Behrens, A. (2014) ATM signalling and cancer. *Oncogene* **33**, 3351-3360
19. Mugler, A., Tostevin, F., and Ten Wolde, P. R. (2013) Spatial partitioning improves the reliability of biochemical signaling. *Proceedings of the National Academy of Sciences of the United States of America*
20. Czarny, P., Pawlowska, E., Bialkowska-Warzecha, J., Kaarniranta, K., and Blasiak, J. (2015) Autophagy in DNA damage response. *International journal of molecular sciences* **16**, 2641-2662
21. Shiloh, Y., and Ziv, Y. (2013) The ATM protein kinase: regulating the cellular response to genotoxic stress, and more. *Nat Rev Mol Cell Biol* **14**, 197-210
22. De Cicco, M., Abd Rahim, M. S., and Dames, S. A. (2015) Regulation of the Target of Rapamycin and Other Phosphatidylinositol 3-Kinase-Related Kinases by Membrane Targeting. *Membranes* **5**, 553-575

23. Brown, K. D., Ziv, Y., Sadanandan, S. N., Chessa, L., Collins, F. S., Shiloh, Y., and Tagle, D. A. (1997) The ataxia-telangiectasia gene product, a constitutively expressed nuclear protein that is not up-regulated following genome damage. *Proceedings of the National Academy of Sciences of the United States of America* **94**, 1840-1845
24. Watters, D., Khanna, K. K., Beamish, H., Birrell, G., Spring, K., Kedar, P., Gatei, M., Stenzel, D., Hobson, K., Kozlov, S., Zhang, N., Farrell, A., Ramsay, J., Gatti, R., and Lavin, M. (1997) Cellular localisation of the ataxia-telangiectasia (ATM) gene product and discrimination between mutated and normal forms. *Oncogene* **14**, 1911-1921
25. Yan, J., Khanna, K. K., and Lavin, M. F. (2000) Defective radiation signal transduction in ataxia-telangiectasia cells. *International journal of radiation biology* **76**, 1025-1035
26. Bosotti, R., Isacchi, A., and Sonnhammer, E. L. (2000) FAT: a novel domain in PIK-related kinases. *Trends in biochemical sciences* **25**, 225-227
27. Perry, J., and Kleckner, N. (2003) The ATRs, ATMs, and TORs are giant HEAT repeat proteins. *Cell* **112**, 151-155
28. Knutson, B. A. (2010) Insights into the domain and repeat architecture of target of rapamycin. *Journal of structural biology* **170**, 354-363
29. Mordes, D. A., Glick, G. G., Zhao, R., and Cortez, D. (2008) TopBP1 activates ATR through ATRIP and a PIKK regulatory domain. *Genes & development* **22**, 1478-1489
30. Keith, C. T., and Schreiber, S. L. (1995) PIK-related kinases: DNA repair, recombination, and cell cycle checkpoints. *Science* **270**, 50-51
31. Jiang, X., Sun, Y., Chen, S., Roy, K., and Price, B. D. (2006) The FATC domains of PIKK proteins are functionally equivalent and participate in the Tip60-dependent activation of DNA-PKcs and ATM. *The Journal of biological chemistry* **281**, 15741-15746
32. Sommer, L. A. M., Schaad, M., and Dames, S. A. (2013) NMR- and Circular Dichroism-monitored Lipid Binding Studies Suggest a General Role for the FATC Domain as Membrane Anchor of Phosphatidylinositol 3-Kinase-related Kinases (PIKK). *Journal of Biological Chemistry* **288**, 20046-20063
33. Takahashi, T., Hara, K., Inoue, H., Kawa, Y., Tokunaga, C., Hidayat, S., Yoshino, K., Kuroda, Y., and Yonezawa, K. (2000) Carboxyl-terminal region conserved among phosphoinositide-kinase-related kinases is indispensable for mTOR function in vivo and in vitro. *Genes to cells : devoted to molecular & cellular mechanisms* **5**, 765-775
34. Hoke, S. M., Irina Mutiu, A., Genereaux, J., Kvas, S., Buck, M., Yu, M., Gloor, G. B., and Brandl, C. J. (2010) Mutational analysis of the C-terminal FATC domain of Saccharomyces cerevisiae Tra1. *Current genetics* **56**, 447-465
35. Morita, T., Yamashita, A., Kashima, I., Ogata, K., Ishiura, S., and Ohno, S. (2007) Distant N- and C-terminal domains are required for intrinsic kinase activity of SMG-1, a critical component of nonsense-mediated mRNA decay. *The Journal of biological chemistry* **282**, 7799-7808
36. Llorca, O., Rivera-Calzada, A., Grantham, J., and Willison, K. R. (2003) Electron microscopy and 3D reconstructions reveal that human ATM kinase uses an arm-like domain to clamp around double-stranded DNA. *Oncogene* **22**, 3867-3874
37. Lau, W. C., Li, Y., Liu, Z., Gao, Y., Zhang, Q., and Huen, M. S. (2016) Structure of the human dimeric ATM kinase. *Cell cycle* **15**, 1117-1124
38. Sawicka, M., Wanrooij, P. H., Darbari, V. C., Tannous, E., Hailemariam, S., Bose, D., Makarova, A. V., Burgers, P. M., and Zhang, X. (2016) The Dimeric Architecture of

Checkpoint Kinases Mec1ATR and Tel1ATM Reveal a Common Structural Organization. *The Journal of biological chemistry* **291**, 13436-13447
39. Wang, X., Chu, H., Lv, M., Zhang, Z., Qiu, S., Liu, H., Shen, X., Wang, W., and Cai, G. (2016) Structure of the intact ATM/Tel1 kinase. *Nature communications* **7**, 11655
40. Baretic, D., Pollard, H. K., Fisher, D. I., Johnson, C. M., Santhanam, B., Truman, C. M., Kouba, T., Fersht, A. R., Phillips, C., and Williams, R. L. (2017) Structures of closed and open conformations of dimeric human ATM. *Science advances* **3**, e1700933
41. Sommer, L. A. M., Meier, M. A., and Dames, S. A. (2012) A fast and simple method for probing the interaction of peptides and proteins with lipids and membrane-mimetics using GB1 fusion proteins and NMR spectroscopy. *Protein science : a publication of the Protein Society* **21**, 1566-1570
42. Dames, S. A., Mulet, J. M., Rathgeb-Szabo, K., Hall, M. N., and Grzesiek, S. (2005) The solution structure of the FATC domain of the protein kinase target of rapamycin suggests a role for redox-dependent structural and cellular stability. *The Journal of biological chemistry* **280**, 20558-20564
43. Dames, S. A. (2010) Structural basis for the association of the redox-sensitive target of rapamycin FATC domain with membrane-mimetic micelles. *The Journal of biological chemistry* **285**, 7766-7775
44. Sommer, L. A. M., Janke, J. J., Bennett, W. F. D., Bürck, J., Ulrich, A. S., Tieleman, D. P., and Dames, S. A. (2014) Characterization of the Immersion Properties of the Peripheral Membrane Anchor of the FATC Domain of the Kinase "Target of Rapamycin" by NMR, Oriented CD Spectroscopy, and MD Simulations. *The Journal of Physical Chemistry B* **118**, 4817-4831
45. Koehler, J., and Meiler, J. (2011) Expanding the utility of NMR restraints with paramagnetic compounds: background and practical aspects. *Prog Nucl Magn Reson Spectrosc* **59**, 360-389
46. Yagi, H., Loscha, K. V., Su, X. C., Stanton-Cook, M., Huber, T., and Otting, G. (2010) Tunable paramagnetic relaxation enhancements by [Gd(DPA)(3)] (3-) for protein structure analysis. *Journal of biomolecular NMR* **47**, 143-153
47. Sun, H., Greathouse, D. V., Andersen, O. S., and Koeppe, R. E., 2nd. (2008) The preference of tryptophan for membrane interfaces: insights from N-methylation of tryptophans in gramicidin channels. *The Journal of biological chemistry* **283**, 22233-22243
48. Liu, W., and Caffrey, M. (2006) Interactions of tryptophan, tryptophan peptides, and tryptophan alkyl esters at curved membrane interfaces. *Biochemistry* **45**, 11713-11726
49. Sommer, L. A. M., and Dames, S. A. (2014) Characterization of residue-dependent differences in the peripheral membrane association of the FATC domain of the kinase 'target of rapamycin' by NMR and CD spectroscopy. *FEBS letters* **588**, 1755-1766
50. Zhang, L., Tie, Y., Tian, C., Xing, G., Song, Y., Zhu, Y., Sun, Z., and He, F. (2006) CKIP-1 recruits nuclear ATM partially to the plasma membrane through interaction with ATM. *Cellular signalling* **18**, 1386-1395
51. Sprong, H., van der Sluijs, P., and van Meer, G. (2001) How proteins move lipids and lipids move proteins. *Nat Rev Mol Cell Biol* **2**, 504-513
52. Myers, G. A., Gacek, D. A., Peterson, E. M., Fox, C. B., and Harris, J. M. (2012) Microscopic rates of Peptide-phospholipid bilayer interactions from single-molecule residence times. *Journal of the American Chemical Society* **134**, 19652-19660
53. Sun, Y., Jiang, X., Chen, S., Fernandes, N., and Price, B. D. (2005) A role for the Tip60 histone acetyltransferase in the acetylation and activation of ATM. *Proceedings*

of the National Academy of Sciences of the United States of America **102**, 13182-13187
54. Wimley, W. C., and White, S. H. (1996) Experimentally determined hydrophobicity scale for proteins at membrane interfaces. *Nat Struct Biol* **3**, 842-848
55. Rodriguez Camargo, D. C., Link, N. M., and Dames, S. A. (2012) The FKBP-rapamycin binding domain of human TOR undergoes strong conformational changes in the presence of membrane mimetics with and without the regulator phosphatidic acid. *Biochemistry* **51**, 4909-4921
56. Lazaridis, T., Mallik, B., and Chen, Y. (2005) Implicit solvent simulations of DPC micelle formation. *The journal of physical chemistry. B* **109**, 15098-15106
57. Tieleman, D. P. v. d. S., D.; Berendsen, H.J.C. (2000) Molecular Dynamics Simulations of Dodecylphosphocholine Micelles at Three Different Aggregate Sizes: Micellar Structure and Chain Relaxation. *J. Phys. Chem. B* **104**, 6380-6388
58. Whiles, J. A., Deems, R., Vold, R. R., and Dennis, E. A. (2002) Bicelles in structure-function studies of membrane-associated proteins. *Bioorganic chemistry* **30**, 431-442
59. Luchette, P. A., Vetman, T. N., Prosser, R. S., Hancock, R. E., Nieh, M. P., Glinka, C. J., Krueger, S., and Katsaras, J. (2001) Morphology of fast-tumbling bicelles: a small angle neutron scattering and NMR study. *Biochimica et biophysica acta* **1513**, 83-94
60. Lin, C. M., Li, C. S., Sheng, Y. J., Wu, D. T., and Tsao, H. K. (2012) Size-dependent properties of small unilamellar vesicles formed by model lipids. *Langmuir : the ACS journal of surfaces and colloids* **28**, 689-700
61. Bakkenist, C. J., and Kastan, M. B. (2003) DNA damage activates ATM through intermolecular autophosphorylation and dimer dissociation. *Nature* **421**, 499-506
62. Guo, Z., Kozlov, S., Lavin, M. F., Person, M. D., and Paull, T. T. (2010) ATM activation by oxidative stress. *Science* **330**, 517-521
63. De Cicco, M., Milroy, L. G., and Dames, S. A. (2018) Target of rapamycin FATC domain as a general membrane anchor: The FKBP-12 like domain of FKBP38 as a case study. *Protein science : a publication of the Protein Society* **27**, 546-560
64. Huth, J. R., Bewley, C. A., Jackson, B. M., Hinnebusch, A. G., Clore, G. M., and Gronenborn, A. M. (1997) Design of an expression system for detecting folded protein domains and mapping macromolecular interactions by NMR. *Protein science : a publication of the Protein Society* **6**, 2359-2364
65. Koenig, B. W., Rogowski, M., and Louis, J. M. (2003) A rapid method to attain isotope labeled small soluble peptides for NMR studies. *Journal of biomolecular NMR* **26**, 193-202
66. Abd Rahim, M. S., Sommer, L. A. M., Wacker, A., Schaad, M., and Dames, S. A. (2018) 1H, 15N, and 13C chemical shift assignments of the micelle immersed FAT C-terminal (FATC) domains of the human protein kinases ataxia-telangiectasia mutated (ATM) and DNA-dependent protein kinase catalytic subunit (DNA-PKcs) fused to the B1 domain of streptococcal protein G (GB1). *Biomolecular NMR assignments*
67. Stafford, R. E., Fanni, T., and Dennis, E. A. (1989) Interfacial properties and critical micelle concentration of lysophospholipids. *Biochemistry* **28**, 5113-5120
68. Tausk, R. J., Karmiggelt, J., Oudshoorn, C., and Overbeek, J. T. (1974) Physical chemical studies of short-chain lecithin homologues. I. Influence of the chain length of the fatty acid ester and of electrolytes on the critical micelle concentration. *Biophysical chemistry* **1**, 175-183
69. Weschayanwiwat, P., Scamehorn, J., and Reilly, P. (2005) Surfactant properties of low molecular weight phospholipids. *Journal of Surfactants and Detergents* **8**, 65-72

70. Delaglio, F., Grzesiek, S., Vuister, G. W., Zhu, G., Pfeifer, J., and Bax, A. (1995) NMRPipe: a multidimensional spectral processing system based on UNIX pipes. *Journal of biomolecular NMR* **6**, 277-293
71. Johnson, B. A. (2004) Using NMRView to visualize and analyze the NMR spectra of macromolecules. *Methods in molecular biology* **278**, 313-352
72. Schwieters, C. D., Kuszewski, J. J., Tjandra, N., and Clore, G. M. (2003) The Xplor-NIH NMR molecular structure determination package. *Journal of magnetic resonance* **160**, 65-73
73. Van Der Spoel, D., Lindahl, E., Hess, B., Groenhof, G., Mark, A. E., and Berendsen, H. J. (2005) GROMACS: fast, flexible, and free. *Journal of computational chemistry* **26**, 1701-1718
74. Hess, B., Kutzner, C., van der Spoel, D., and Lindahl, E. (2008) GROMACS 4: Algorithms for Highly Efficient, Load-Balanced, and Scalable Molecular Simulation. *J. Chem. Theory Comput.* **4**, 435-447
75. Abraham, M. J., Murtola, T., Schulz, R., Páll, S., Smith, J. C., Hess, B., and Lindahl, E. (2015) GROMACS: High performance molecular simulations through multi-level parallelism from laptops to supercomputers. *SoftwareX* **1-2**, 19-25
76. Huang, J., Rauscher, S., Nawrocki, G., Ran, T., Feig, M., de Groot, B. L., Grubmuller, H., and MacKerell, A. D., Jr. (2017) CHARMM36m: an improved force field for folded and intrinsically disordered proteins. *Nature methods* **14**, 71-73
77. Hess, B., Bekker, H., Berendsen, H. J. C., and Fraaije, J. G. E. M. (1997) LINCS: A linear constraint solver for molecular simulations. *Journal of computational chemistry* **18**, 1463-1472
78. Miyamoto, S., and Kollman, P. A. (1992) Settle - an Analytical Version of the Shake and Rattle Algorithm for Rigid Water Models. *Journal of computational chemistry* **13**, 952-962
79. Bussi, G., Donadio, D., and Parrinello, M. (2007) Canonical sampling through velocity rescaling. *The Journal of chemical physics* **126**, 014101
80. Parrinello, M., and Rahman, A. (1981) Polymorphic transitions in single crystals: A new molecular dynamics method. *Journal of Applied Physics* **52**, 7182-7190
81. Darden, T., York, D., and Pedersen, L. (1993) Particle Mesh Ewald - an N.Log(N) Method for Ewald Sums in Large Systems. *Journal of Chemical Physics* **98**, 10089-10092
82. Essmann, U., Perera, L., Berkowitz, M. L., Darden, T., Lee, H., and Pedersen, L. G. (1995) A Smooth Particle Mesh Ewald Method. *Journal of Chemical Physics* **103**, 8577-8593
83. Kabsch, W., and Sander, C. (1983) Dictionary of protein secondary structure: pattern recognition of hydrogen-bonded and geometrical features. *Biopolymers* **22**, 2577-2637
84. Laskowski, R. A., Rullmannn, J. A., MacArthur, M. W., Kaptein, R., and Thornton, J. M. (1996) AQUA and PROCHECK-NMR: programs for checking the quality of protein structures solved by NMR. *Journal of biomolecular NMR* **8**, 477-486
85. Koradi, R., Billeter, M., and Wuthrich, K. (1996) MOLMOL: a program for display and analysis of macromolecular structures. *Journal of molecular graphics* **14**, 51-55, 29-32

FOOTNOTES

This work was supported by a grant from the German Research Foundation to S.A.D. (DA 1195/3-2). S.A.D acknowledges further financial support from the Technische Universität München (TUM) diversity and talent management office by a Laura-Bassi award and the Helmholtz portfolio theme 'metabolic dysfunction and common disease' of the Helmholtz Zentrum München. M.S.A.R. is supported by the German Academic Exchange Service (DAAD) by a Ph.D. stipend. Work in DPT's group was supported by the Natural Sciences and Engineering Research Council of Canada. DPT is the Alberta Innovates Technology Futures Strategic Chair in (Bio)Molecular Simulation. Simulations were run on Compute Canada machines, supported by the Canada Foundation for Innovation and partners. This work was undertaken, in part, thanks to funding from the Canada Research Chairs program.

The abbreviations used are: ATM, Ataxia-telangiectasia mutated; ATR, ataxia- and Rad3-related; CMC, critical micelle concentration; DihepPC, 1,2-diheptanoyl-*sn*-glycero-3-phosphocholine; DMPC, 1,2-dimyristoyl-*sn*-glycero-3-phospho-choline; DNA-PKcs, DNA-dependent protein kinase catalytic subunit; DPC, dodecylphosphocholine; FATC, FRAP, ATM, TRRAP C-terminal; GB1, B1 immunoglobulin binding domain of streptococcal protein G (56 residues); hATMfatc-gb1ent, GB1 followed by a thrombin and an enterokinase recognition site (= LVPRGS-DDDDK) and residues 3024-3056 of human ATM; NOE, nuclear Overhauser effect; NOESY, NOE spectroscopy; PIKK, phosphatidylinositol-3 kinase-related kinase; (m)TOR, (mammalian/mechanistic) target or rapamycin; min, minute(s); SI, supplementary information; TOR, target of rapamycin; TRRAP, Transformation/transcription domain-associated protein.

Supporting Information

Superpositions of the spectra with and without $\{^1H\}$-^{15}N NOE of hATMfatc-gb1ent in the presence of 150 and 200 mM DPC and plots of the corresponding data as a function of the residue sequence position including for the 200 mM data also ^{15}N-T_1 and $-T_2$. Plots of the secondary structure content and the angles between helix 1 and 2 and 2 and 3 as a function of the simulation time, plots of global and local RMSF values, of the backbone and side chain RMSD, the distance to the micelle center of mass and the SAS covered by DPC as a function of the residue sequence position, superpositions of the ^1H-^{15}N HSQC spectra of hATMfatc-gb1ent in the presence of 50 mM DPC and 1-4 mM 5- or 16-SASL, plots of 1-PRE values and the average chemical shift changes as a function of the residue sequence position for 1- and 2 mM 5- or 16-SASL data for the whole hATMfatc-gb1ent, superpositions of the ^1H-^{15}N HSQC spectra of hATMfatc-gb1ent-F93/3049A and -W96/3052A in absence and presence of DPC or DihepPC micelles, DMPC/DihepPC bicelles or DMPC SUVs.

Table 1 Statistics for the 20 lowest energy NMR structures of the micelle-associated human ATM FATC domain*	
Experimental restraints	
Distance restraints	All (assigned + ambiguous)
Total	748 (707 + 41)
^{15}N-NOESY	332 (313 + 19)
^{13}C-NOESY aliphatic / aromatic	366 (345 + 21) / 26 (25 + 1)
assigned short/medium/long range[§]	630/61/2
ambiguous short/medium/long range[§]	≤62/≤17/≤3
hydrogen bond	24
ϕ + ψ angle restraints	39
Structural statistics*	
RMSDs from experimental restraints	
Distance (Å)	0.0240±0.0030
Dihedral angle (°)	0.1937±0.1399
RMSDs from idealized geometry	
Bonds (Å)	0.0032±0.0002
Angles (°)	0.3709±0.0177
Improper (°)	0.2409±0.0145
Lennard-Jones energy (kcal mol^{-1})[$]	-141±31
Procheck (84) Statistics[#]	
Residues in most favored regions (%)	85.5
Residues in additional allowed regions (%)	14.5
Residues in generously allowed regions (%)	0.0
Residues in disallowed regions (%)	0.0
Average RMSD to mean structure	
Residues 70/3026-100/3056 (backbone/heavy) (Å)	4.47/5.26
Residues 73/3029-83/3039 (backbone/heavy) (Å)	0.37 / 0.89
Residues 87/3043-99/3055 (backbone/heavy) (Å)	1.32 / 2.33
Residues 87/3043-91/3047 (backbone/heavy) (Å)	0.22 / 1.35
Residues 95/3051-99/3055 (backbone/heavy) (Å)	0.27 / 1.72

*None of the structures had distance restraints violations > 0.5 Å or dihedral angle violations > 5°, RMSD = root mean square deviation, PDB-ID 6HKA; [§] short: i, i or i±1, medium: i, i±2 or 3 or 4, long range: here only i, i±5, note for ambiguous restraints two options were taken into account, thus the ≤ before the given numbers; [$]Calculated for the full 100 residue protein hATMfatc-gb1ent, but residues 1-67 had not been restrained and thus should not contribute significantly to the calculation; [#]For the well structured regions 72-83, 86-92, 94-100.

Table 2 Summary of the NMR-monitored interaction analysis of mutant hATMfatc-gb1ent proteins with different neutral membrane mimetics

Mutation	DPC micelles (50 mM)	DihepPC micelles (50 mM)	DMPC/DihepPC bicelles, (q = 0.2, [DMPC] = 0.04 M, and [DihepPC] = 0.20 M, cL 15%)	DMPC SUVs (< 50 mM DMPC)
F93/3049A	+	+	+	+
W96/3052A	+	+	+	+
F93/3049A-W96/3052A	+	+	+	-

+ = strong spectral changes indicating an interaction with the respective membrane mimetic, - = no significant spectral changes/interaction.

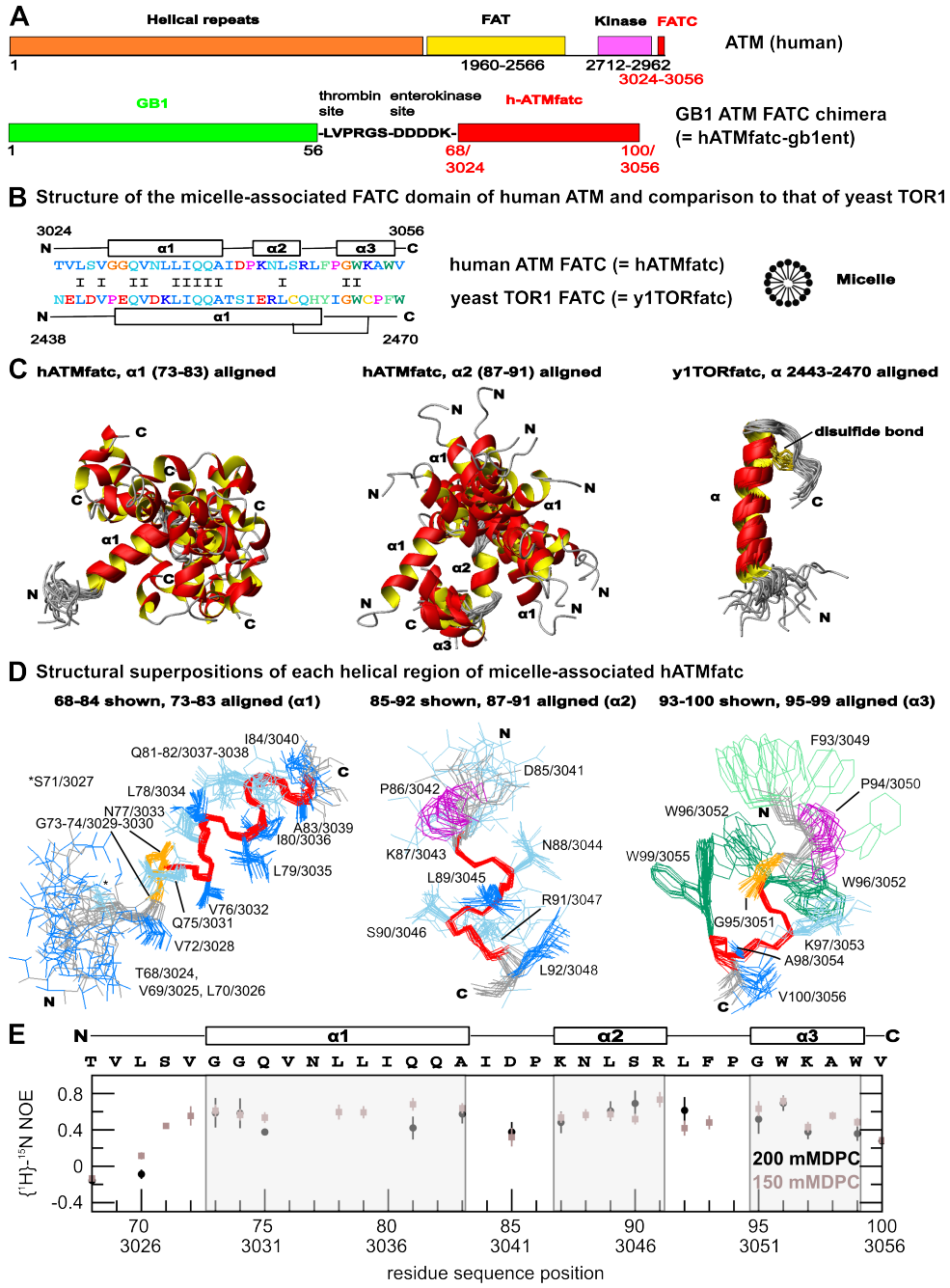

Fig. 1: NMR structure of the micelle-associated FATC domain of human ATM and comparison to that of yeast TOR1. (A) Human ATM (hATM) consists of a long N-terminal region and a FAT domain, which are both made up of helical repeats, the catalytic Ser/Thr kinase domain, and the FATC domain (26). To structurally characterize the C-terminal FATC domain (residues 3024-3056, Uniprot-ID Q13315) it has been fused to the B1 domain of streptococcal protein G (GB1, 56 residues, =hATMfatc). B) Superposition of the amino acid sequences of the FATC domains of hATM and yeast TOR1 and schematic representation of the secondary structure content in micelles (schematic representation to the right). Aromatic residues are shown in light (F, H, Y) and dark (W) green, hydrophilic one in light blue, except K and R in blue and D and E in red, and those containing methyl groups in dark blue. Prolines are colored purple and glycines (G2465) in orange. (C) The NMR structure of hATMfatc in the presence of micelles (150 mM DPC) consists of three helices with a central dynamic linker (table 1, PDB-ID 6HKA, BMRB-ID 27167 (66)) and is overall different to that

earlier determined of the micelle-immersed oxidized yeast TOR FATC domain (y1fatc, PDB-ID 2KIO) (43). For the ribbon representations the 20 lowest energy structures have been superimposed for the indicated regions. (D) Each helical stretch of micelle-associated hATMfatc is shown in line mode. The backbone of the helical stretches is depicted in red. The color coding of the side chains is the same as in (B) except that charged side chains are also colored light blue. All structure pictures were made with the program MolMol (85). (E) Information about the backbone dynamics from a plot of the $\{^1H\}$-^{15}N NOE values of hATMfatc with 150 or 200 mM DPC as a function of the residue sequence position. No data can be obtained for prolines (86, 94) or peaks that overlap with other peaks or noise signals (SI Fig. S1). Values around 0.5-0.8 are typical for structured proteins. Lower NOE values indicate increased backbone flexibility. SI Fig. S1 shows the 2D $\{^1H\}$-^{15}N NOE and reference spectra and S2 additionally the ^{15}N-T_1 and -T_2 relaxation times at 200 mM DPC as well as a plot of the ^{15}N-relaxation data for the full hATMfatc-gb1ent fusion protein.

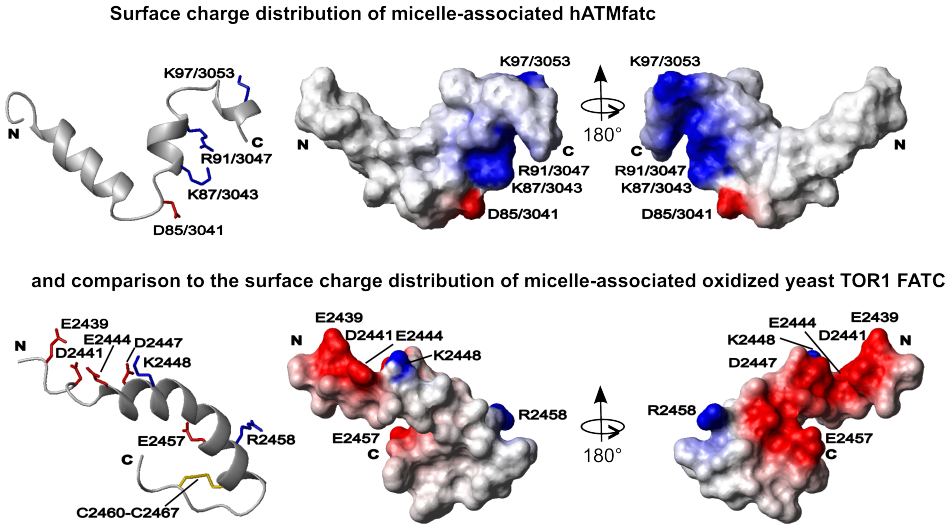

Fig. 2: The surface charge distribution of micelle-associated hATMfatc differs from that earlier determined for oxidized y1fatc (see also Fig. 1B-C) (43). Visualization of the surface charge distribution. Positively charged areas and side chains in the stick mode in the ribbon representation are colored blue and negatively charged ones red. All structure pictures were made with the program MolMol (85). See also Fig. 1.

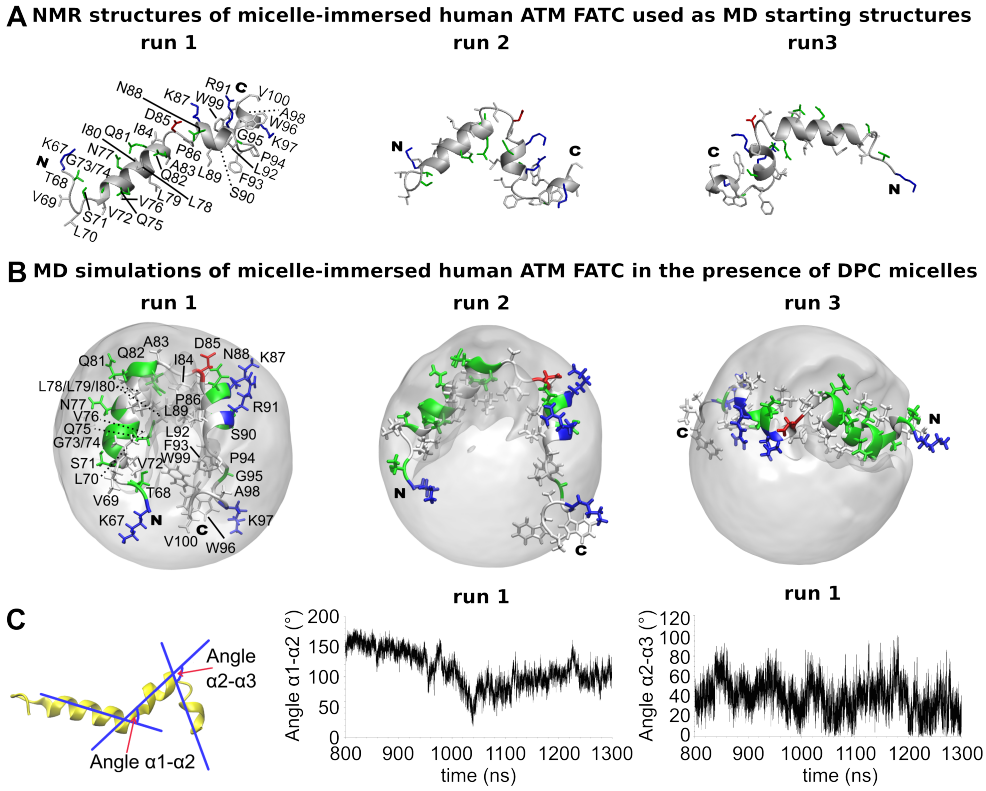

Fig. 3: Characterization of the dynamic properties of the micelle-associated FATC domain of human ATM (hATMfatc) from MD simulations. (A) Ribbon representations of the three lowest energy structures that were used as starting structures for three independent MD simulation runs. (C) Representative structure pictures of the MD simulations of hATMfatc in the presence of DPC micelles. The structures shown are the conformations of hATMfatc, which are the closest to the middle of the most populated cluster of structures for a given simulation run. The DPC micelle is shown as a transparent averaged density iso-surface. The peptide is shown in a ribbon representation. In both, (B) and (C), negatively charged side chains or residues are shown in red, positively charged ones in blue, polar ones in green and aliphatic ones in grey. For simplicity only the residue numbering as used in the pdb entry (PDB-ID 6HKA) is given. The N- and C-termini are indicated by the letters N and C. (D) Information about the movement of the 3 helices with respect to each other from an analysis of the variation of the angle between helix 1 and 2 as well as the one between helix 2 and 3 for run 1. Analogous plots for runs 2 and 3 are shown in SI Fig. S5A. Plots of the secondary structure content as a function of the simulation time are shown in SI Fig. S3. Plots the root mean square fluctuations (RMSF, global and local) and the backbone and side chain RMSD values as a function of the residues sequence position as well as a superposition of the top 10 cluster structures are shown in SI Fig. S4.

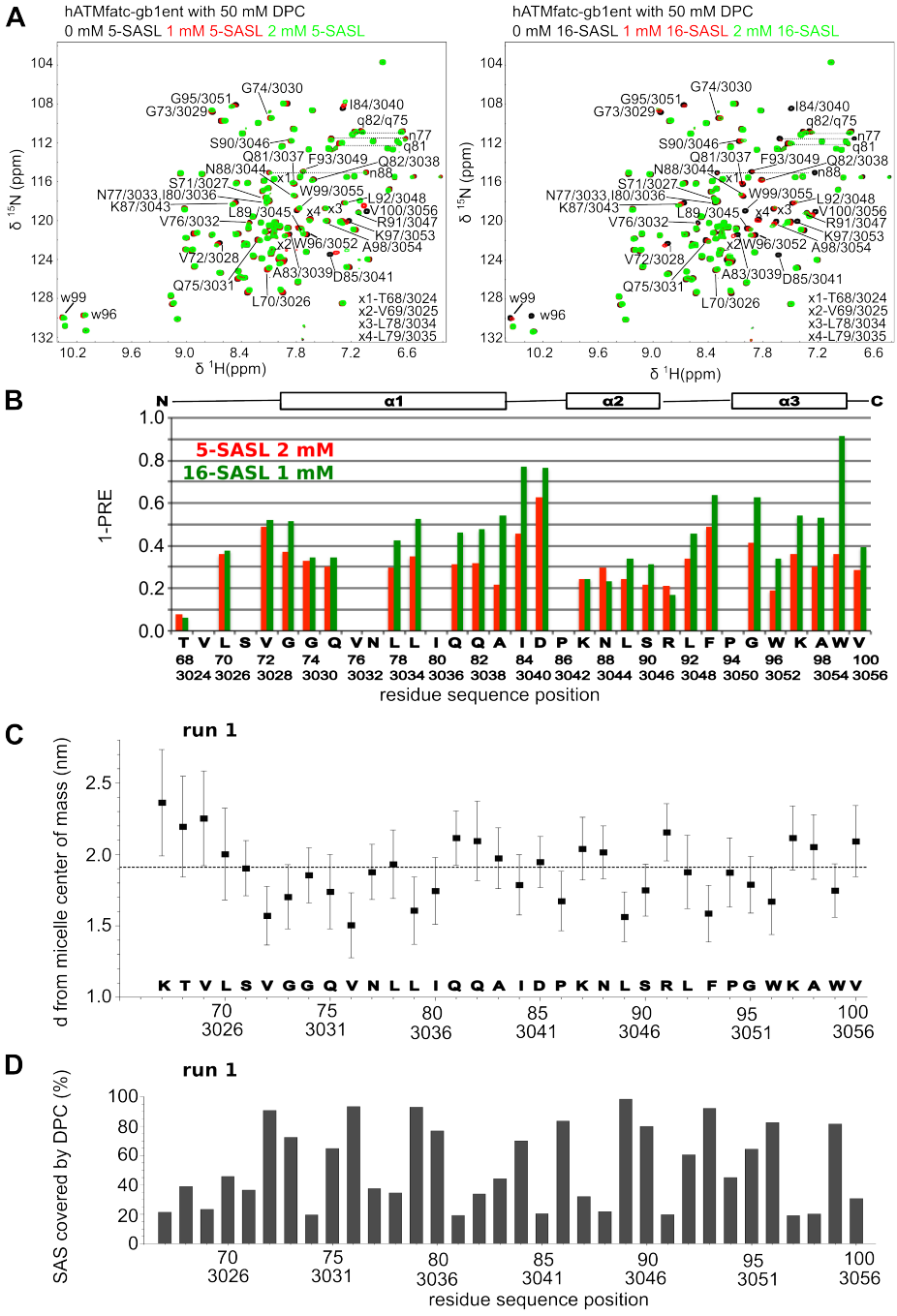

Fig. 4: Analysis of the membrane immersion properties of hATMfatc by NMR and MD simulations. (A) Superpositions of the ^{1}H-^{15}N HSQC spectra of hATMfatc-gb1ent in the presence of DPC micelles and 1 or 2 mM of paramagnetically tagged 5- (left) or 16- (right) doxyl stearic acid (5-/16-SASL). Superpositions including also the spectra in the presence of 3 and 4 mM 5- or 16-SASL are shown in SI. Fig. S5B. The hATMfatc signals are labeled by the residue sequence position in hATMfatc-gb1ent/human ATM and the one letter amino acid code. The color coding is indicated at the top. (B) Diagrams of the paramagnetic relaxation enhancement (PRE) effects due to the presence of 1 mM 5- or 16-SASL as a function of the residue sequence position. Since the spectral changes with 5-SASL were overall smaller compared to 16-SASL, 1-PRE values for 2 mM were analyzed for 5-SASL and for 1 mM for 16-SASL. To better compare the PRE effects to the average chemical shift changes (SI Fig. S6, S7), 1-PRE (= 1- I(x mM SASL)/I (0 mM SASL)) was plotted. Accordingly, the larger the

PRE effect, the higher the 1-PRE value. The sequence is given at the bottom and a schematic representation of the location of the helices at the top. Since both, 5- and 16-SASL reside near the DPC head groups, amide groups also residing in the head group region should show the strongest changes. (C) Diagram of the average distance of the center of mass (COM) of each residue of hATMfatc to that of the DPC micelle from the MD run 1. The averaging was performed over the last microsecond of the run. The dotted line corresponds to the average distance of the phosphor atom of the DPC head group to the micelle COM (1.914 nm). The respective plots for runs 2 and 3 are shown in SI Fig. S8. (D) Diagram of the percentage of the solvent accessible surface area (SAS) of each residue of hATMfatc covered by DPC from the MD simulations. Residues with shorter distances to the micelle COM in (C) show usually a higher percentage in (D). The respective plots for runs 2 and 3 are shown in SI Fig. S9.

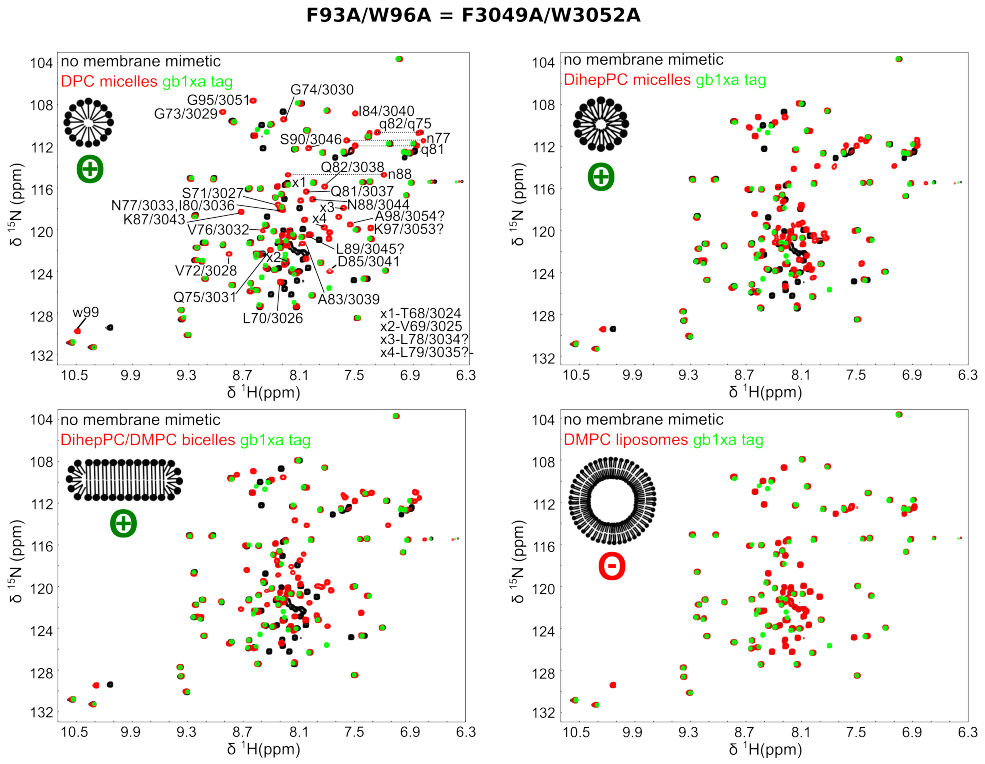

Fig. 5: Characterization of the role of conserved aromatic residues for the membrane affinity of hATMfatc. The pictures show superpositions of the ^{1}H-^{15}N HSQC spectra of the double mutant hATMfatc-gb1ent-F93/3049A-W96/3052A in the absence and presence of DPC micelles (50 mM DPC, upper left), DihepPC micelles (50 mM DihepPC, upper right), DMPC/DihepPC bicelles (q = 0.2, [DMPC] = 0.04 M, and [DihepPC] = 0.20 M, cL 15%, lower left) or DMPC liposomes (< 50 mM DMPC, lower right). A green plus below a schematic representation of the used membrane mimetic indicates strong spectral changes and thus interactions and a red plus no significant changes and thus no significant interactions. The spectrum of the free form is always shown in black and the one with the respective membrane mimetic in red. To better identify the signals of the ATM FATC part, the spectrum of the GB1 tag followed by a thrombin and factor Xa site (= GB1xa) is additionally shown in green on top. Accordingly all peaks with a green peak on top belong to the GB1 tag. Since the GB1 tag does not interact with membrane mimetics it signals do not significantly shift (41). In the picture of the spectra in the absence and presence of DPC, hATMfatc signals in the presence of DPC (red) are labeled by the 1-letter amino acid code and the sequence position based on similarity to the respective wild type spectrum. Small letters indicate side chain signals. A question mark behind the label indicates tentative assignments. Note that some red peaks that appear at new positions could not be assigned in this way and those have no label. Superpositions of the ^{1}H-^{15}N HSQC spectrum of the

wild type protein with that of each mutant are given in SI Fig. S10. The superposition of the ^{1}H-^{15}N-HSQC spectra of hATMfatc-gb1ent-F93/3049A-W96/3052A in the presence of stepwise increasing concentrations of DPC is displayed in SI Fig. S11A. Analogous plots for the single mutants F93/3049A and W96/3052A are shown in SI Fig. S11B and S12A, respectively. Superpositions of the spectra of each single mutant (F93/3049A, W96/3052) in the absence and presence of different membrane mimetics are shown in SI Fig. S11C and S12B, respectively.

Structural characterization of the membrane-associating FATC domain of ataxia telangiectasia mutated by NMR and MD simulations

Munirah S. Abd Rahim[1], Yevhen K. Cherniavskyi[2], D. Peter Tieleman[2], Sonja A. Dames[1,3$]

From the [1]Chair of Biomolecular NMR Spectroscopy, Department of Chemistry, Technische Universität München, Lichtenbergstr. 4, 85747 Garching, Germany, [2]Department of Biological Sciences and Centre for Molecular Simulation, University of Calgary, Calgary, AB, Canada, [3]Institute of Structural Biology, Helmholtz Zentrum München, Ingolstädter Landstr. 1, 85764 Neuherberg, Germany

[$]To whom correspondence may be addressed: Chair of Biomolecular NMR Spectroscopy, Department of Chemistry, Technische Universität München, Lichtenbergstr. 4, 85747 Garching, Germany, Tel.: +49-89-35831-7103, Fax: +49-89-3229-4002, E-mail: (sonja.dames@tum.de)

Running title: structure of membrane-associating ATM FATC

Supplementary results

Structure of micelle-associated hATMfatc

In 11 of the 20 lowest energy structures the C-terminal region forms an α-helix that includes residues G95/3051-W99/3055, in 7 of the 20 a 3^{10} helix is formed by residues P94/3050-A98/3054, and in 2 of the 20 only a turn-like structure is formed.

Backbone dynamics of micelle-associated hATMfatc

The association of the FATC domain of human ATM fused to GB1 (hATMfatc-gb1ent) with the significantly larger DPC micelles should modulate the dynamic properties. Fig. 1E and SI Fig. S2A shows the $\{^1H\}$-^{15}N-NOE data for the hATMfatc part (residues 68-100) in the presence of 150 mM and 200 mM DPC at 298 K. The respective spectra are shown in SI Fig. S1. Consistent with the transition from a rather unstructured, dynamic state in the free from to a more ordered one associated with micelles (1) the $\{^1H\}$-^{15}N-NOE values at both DPC concentrations are generally in the range typical for a mostly folded protein (≈ 0.6-0.8). At 150 mM DPC, the conditions used to derive structural restraints, the average value for residues L70/3026 to W99/3055 is 0.53 ± 0.02. The values for the helical regions are slightly higher: 0.60 ± 0.01 for G73/3029-A83/3039, 0.58 ± 0.01 for K87/3043-R91/3047, and 0.56 ± 0.02 for G95/3051-W99/3055. For comparison, the average value for the well-structured GB1 tag (residues 2-56) is 0.64 ± 0.01 (SI Fig. S2B). Since at higher DPC concentrations the

binding equilibrium is expected to be shifted more towards the bound state, we also recorded ^{15}N-relaxation and structural data at 200 mM DPC. However, the spectral quality was overall lower due to stronger line broadening, which in SI Fig. S1 is illustrated by spectra superpositions for the {^{1}H}-^{15}N-NOE data for samples with 150 and 200 mM DPC. Thus, the micelle-associated hATMfatc structure was calculated using the structural data from the 150 mM DPC samples recorded at 298 K. The {^{1}H}-^{15}N-NOE values at 200 mM at 298 K are very similar to that at 150 mM (Fig. 1E and SI Fig. S2A). The average ^{15}N-T_1 and -T_2 values of the GB1 tag (SI Fig. S2B, 517.6 ± 0.4 ms and 60.1 ± 0.1 ms at 200 mM DPC at 298 K) that does not interact with DPC micelles are in a range typical for an about 6 kDa protein flexibly linked to another object and similar to those observed for the GB1tag fused to the micelle-associated FATC domain of the kinase DNA-PKcs (1,2). The association of the hATMFatc part (~4 kDa) with the ~20 kDa DPC micelle results in average values for the residue range L70/3026 to W99/3055 of 767.6 ± 8.6 ms for ^{15}N-T_1 and 26.5 ± 0.8 ms for ^{15}N-T_2 (SI Fig. S2A, B) at 200 mM DPC and 298 K. The ^{15}N-T_2 values are lower than those of the micelle-associated DNA-PKcs FATC domain (average value ~40 ms (1)). This can be explained by an exchange contribution from the relative movement of the helices with respect to each other due to the dynamic linkages (Fig. 1C). The low {^{1}H}-^{15}N-NOE values for residues in these linkers also indicate these regions are dynamic. D85/3041 in the linker between α1 and α2 shows a value of 0.32 ± 0.10 and L92 in the linker between α2 and α3 of 0.42 ± 0.08 (all at 150 mM DPC, 298 K, Fig. 1E, SI Fig. S2).

Dynamic information from the MD simulations of micelle-associated hATMfatc

The top left panel of SI Fig. S4A shows the RMSF values for run 1 calculated by fitting to the starting structure. These global RMSF values for run1 are overall high and vary significantly as a function of the residue sequence position. The latter is however not observed for runs 2 and 3 (SI Fig. S4A, middle and bottom left panels). If the contribution of the relative movement of the helices with respect to each other is reduced by fitting only to the residue range 72 to 92 or 86 to 98 and to multiple structures that were obtained as average from 5 ns intervals, local RMSF values are obtained, which are overall much smaller for all runs (SI Fig. S4A middle and right column). That the relative orientation of the helices with respect to each other varies in all runs, mainly due to the dynamic linkage between the helices 1 and 2, is also illustrated by a superposition of representative structures of the top 10 clusters, which correspond to 69.3 % of the total population, from a clustering analysis based

on the relative RMSD (SI Fig. S4B). Superimposing α1, the other two helices do not superimpose as well. The backbone and side chain RMSD values as a function of the sequence are plotted in SI Fig. S4C. Due to the mentioned dynamic properties, these are also overall high.

Supplementary figure legends

Fig. S1: Analysis of changes in the backbone dynamics of hATMfatc-gb1ent upon interaction with DPC micelles ((A) 150 mM, (B) 200 mM) based on $\{^1H\}$-^{15}N-NOE data. Positive peaks are colored black and red, negative peaks in blue and yellow. Each plot shows a superposition of the spectrum without (reference spectrum) and with NOE-effect (NOE spectrum). The plots to the right are the same as the ones to left but show additionally the spectrum of the GB1 tag followed by a thrombin and factor Xa site (= GB1xa) in green on top to facilitate the identification of the peaks corresponding to the FATC part (no green peaks on top). The unassigned data for the free form and a partially assigned version of the one at 150 mM have been published (1).

Fig. S2: Backbone dynamics of hATMfatc-gb1ent based on ^{15}N-relaxation data. For 200 mM DPC ^{15}N-T_1 (top panel), ^{15}N -T_2 (middle panel) and $\{^1H\}$-^{15}N NOE values (bottom panel) have been plotted. For 150 mM DPC only $\{^1H\}$-^{15}N NOE values (bottom panel) have been plotted. (A) shows the data for the hATMfatc part alone. The secondary structure content and the sequence are displayed at the top. In addition sequence stretches adopting a helical structure have been shaded grey. (B) shows the data for the full 100-residue long hATMfatc-gb1ent fusion protein. Indicated by the negative $\{^1H\}$-^{15}N NOE values and high ^{15}N-T_2 values, the linker region between GB1 and hATMfatc shows strongly increased backbone dynamics and thus flexibly links the FATC to the GB1 part.

Fig. S3: Secondary structure content of micelle-immersed hATMfatc as a function of the simulation time for the three independent MD runs starting each from one of the three lowest energy NMR structures. The color coding is given to the lower right.

Fig. S4: (A) Plots of the root mean square fluctuations (RMSF) as a function of the residue sequence positions. The left plot shows the RMSF fluctuations calculated by fitting the whole hATMfatc domain to the respective starting structure. For the right two plots the contribution from movements of the helices with respect to each other has been reduced by calculating the RMSF for two sections of the protein (residues 72-92 or 86-98) and using multiple structures for the progressive fit that were obtained by splitting the last 500 ns of the simulation into 5 ns intervals, calculating average RMSF values for each interval with the reference structure taken as the structure at the beginning of each interval. (B) Ribbon representation in the same color coding as in Fig. 3 showing a superposition of 10 structures taken from the middle of each of the top 10 best clusters from a clustering analysis based on the relative RMSD of all three trajectories combined. (C) Plots of the backbone and side chain RMSD values as a function of the residue sequence position that were calculated by fitting the whole hATMfatc domain to the respective starting structure.

Fig. S5: (A) Information about the movement of the 3 helices with respect to each other from an analysis of the variation of the angle between helix 1 and 2 as well as the one between helix 2 and 3 for all three runs. The analysis of the angles between the helices starts from 800

ns, and not 300 ns because the relative orientation of the helices changes slowly compared to the local structure of the protein. Thus we let the system equilibrate for a longer period of time to have less bias from the initial structure. (B) Superpositions of the ^{1}H-^{15}N HSQC spectra of hATMfatc-gb1xa in the presence of DPC micelles and 1 to 4 mM paramagnetically tagged 5- (left) or 16- (right) doxyl stearic acid (5-/16-SASL). The hATMfatc signals are labeled by the residue sequence position in hATMfatc-gb1ent/human ATM and the one letter amino acid code. The color coding is indicated at the top.

Fig. S6: Diagrams of the paramagnetic relaxation enhancement (PRE) effects due to the presence of 1 or 2 mM 5-SASL as a function of the residue sequence position for the full hATMfatc-gb1ent. To better compare the PRE effects to the average chemical shift changes in the second plot, 1-PRE (= 1- I(x mM SASL)/I (0 mM SASL)) was plotted. Accordingly, the larger the PRE effect, the higher the 1-PRE value. As expected the GB1 tag that does not directly interact with DPC micelles shows only minor PRE effects or chemical shift changes.

Fig. S7: Diagrams of the paramagnetic relaxation enhancement (PRE) effects due to the presence of 1 or 2 mM 16-SASL as a function of the residue sequence position for the full hATMfatc-gb1ent. To better compare the PRE effects to the average chemical shift changes in the second plot, 1-PRE (= 1- I(x mM SASL)/I (0 mM SASL)) was plotted. Accordingly, the larger the PRE effect, the higher the 1-PRE value. As expected the GB1 tag that does not directly interact with DPC micelles shows only minor PRE effects or chemical shift changes.

Fig. S8: Diagrams of the average distance of the center of mass (COM) of each residue of hATMfatc to that of the DPC micelle for all three MD runs. The averaging is performed over the last microsecond of the run. The dotted line corresponds to the average distance of the phosphor atom of the DPC head group to the micelle COM (1.914 nm).

Fig. S9: Diagrams of the percentage of the solvent accessible surface area (SAS) of each residue of hATMfatc covered by DPC from the MD simulations for all three independent runs. Residues with shorter distances to the micelle COM in SI Fig. S8 show usually a higher percentage in the corresponding diagrams here.

Fig. S10: Superposition of the ^{1}H-^{15}N HSQC spectra of the wild type, the mutant, and the GB1 tag followed by a thrombin and factor Xa site (= GB1xa) for each mutant. Peaks with a green peak on top belong to the GB1 tag. Since the GB1 tag does not interact with membrane mimetics its signals do not significantly shift (3). The peaks of the wild type spectrum are labeled by the 1-letter amino acid code and the sequence position based. Small letter indicate side chain signals. The left side shows the spectra superpositions in the absence of DPC, the right side in the presence of DPC.

Fig. S11: (A)-(B) Superpositions of the ^{1}H-^{15}N HSQC spectra of hATMfatc-gb1ent-F93/3049A-W96/3052 and F93/3049A in the presence of stepwise increasing concentrations of DPC. (B) The pictures show superposition of the ^{1}H-^{15}N HSQC spectra of the single mutant hATMfatc-gb1ent-F93/3049A in the absence and presence of DPC micelles (50 mM DPC, upper left), Dihep-PC micelles (50 mM DihepPC, upper right), DMPC/Dihep-PC bicelles (q = 0.2, [DMPC] = 0.04 M, and [Dihep-PC] = 0.20 M, cL 15%, lower left) or DMPC liposomes (< 50 mM DMPC, lower right). The spectrum of the free form is always shown in black and the one with the respective membrane mimetic in red. A green plus in the upper left of each plot indicates strong spectral changes and thus interactions and a red plus

no significant changes and thus no significant interactions. To better identify the signals of the ATM FATC part, the spectrum of the GB1 tag followed by a thrombin and factor Xa site (= GB1xa) is additionally shown in green on top. Accordingly peaks with a green peak on top belong to the GB1 tag. Since the GB1 tag does not interact with membrane mimetics its signals do not significantly shift (3). In the picture of the spectra in the absence and presence of DPC, hATMfatc signals in the presence of DPC (red) are labeled by the 1-letter amino acid code and the sequence position in hATMfatc-gb1ent/human ATM based on similarity to the wild type spectrum. Small letters indicate side chain signals. A question mark behind the label indicates tentative assignments. Note that some red peaks that appear at new positions could not be assigned in this way. Note that free hATMfatc was not assigned since the signals of many backbone amide groups were not detectable.

Fig. S12: (A) Superpositions of the ^{1}H-^{15}N HSQC spectra of hATMfatc-gb1ent-W96/3052A in the presence of stepwise increasing concentrations of DPC. (B) The pictures show superposition of the ^{1}H-^{15}N HSQC spectra of the single mutant hATMfatc-gb1ent-W96/3052A in the absence and presence of DPC micelles (50 mM DPC, upper left), Dihep-PC micelles (50 mM DihepPC, upper right), DMPC/Dihep-PC bicelles (q = 0.2, [DMPC] = 0.04 M, and [Dihep-PC] = 0.20 M, cL 15%, lower left) or DMPC liposomes (< 50 mM DMPC, lower right). The spectrum of the free form is always shown in black and the one with the respective membrane mimetic in red. A green plus in the upper left of each plot indicates strong spectral changes and thus interactions and a red plus no significant changes and thus no significant interactions. To better identify the signals of the ATM FATC part, the spectrum of the GB1 tag followed by a thrombin and factor Xa site (= GB1xa) is additionally shown in green on top. Accordingly peaks with a green peak on top belong to the GB1 tag. Since the GB1 tag does not interact with membrane mimetics its signals do not significantly shift (3). In the picture of the spectra in the absence and presence of DPC, hATMfatc signals are labeled by the 1-letter amino acid code and the sequence position based on similarity to the wild type spectrum. Small letters indicate side chain signals. A question mark behind the label indicates tentative assignments. Note that some red peaks that appear at new positions could not be assigned in this way.

Supplementary References

1. Sommer, L. A. M., Schaad, M., and Dames, S. A. (2013) NMR- and Circular Dichroism-monitored Lipid Binding Studies Suggest a General Role for the FATC Domain as Membrane Anchor of Phosphatidylinositol 3-Kinase-related Kinases (PIKK). *Journal of Biological Chemistry* **288**, 20046-20063
2. Walsh, J. D., Meier, K., Ishima, R., and Gronenborn, A. M. (2010) NMR studies on domain diffusion and alignment in modular GB1 repeats. *Biophysical journal* **99**, 2636-2646
3. Sommer, L. A. M., Meier, M. A., and Dames, S. A. (2012) A fast and simple method for probing the interaction of peptides and proteins with lipids and membrane-mimetics using GB1 fusion proteins and NMR spectroscopy. *Protein science : a publication of the Protein Society* **21**, 1566-1570

Abd Rahim et al.
SI Fig. S1

A hATMfatc-gb1ent with 150 mM DPC

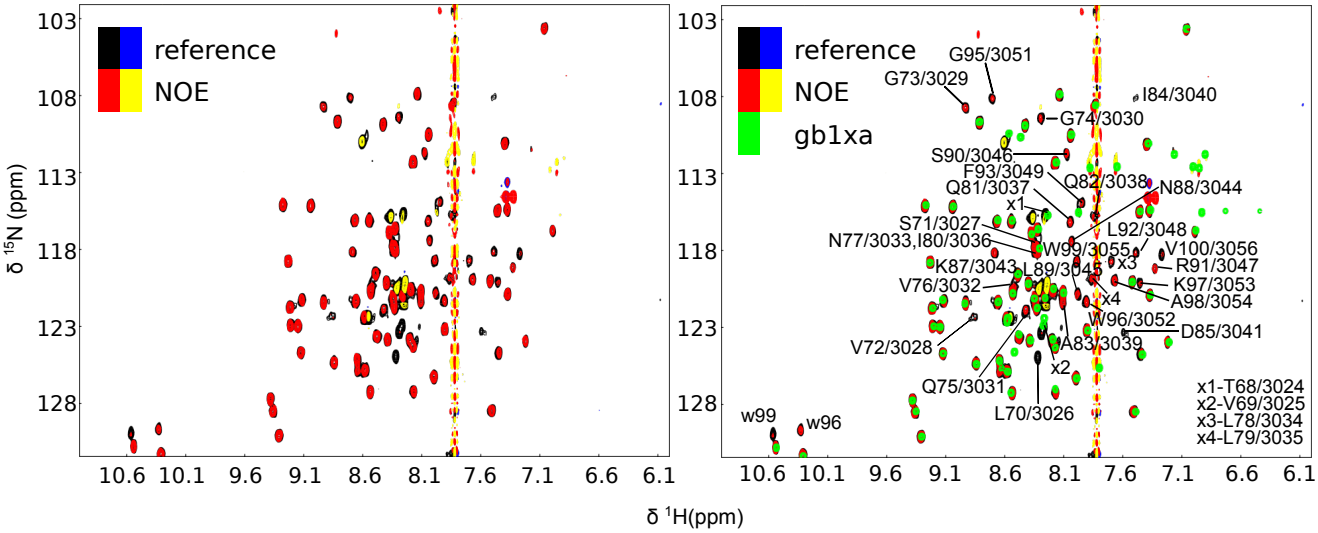

B hATMfatc-gb1ent with 200 mM DPC

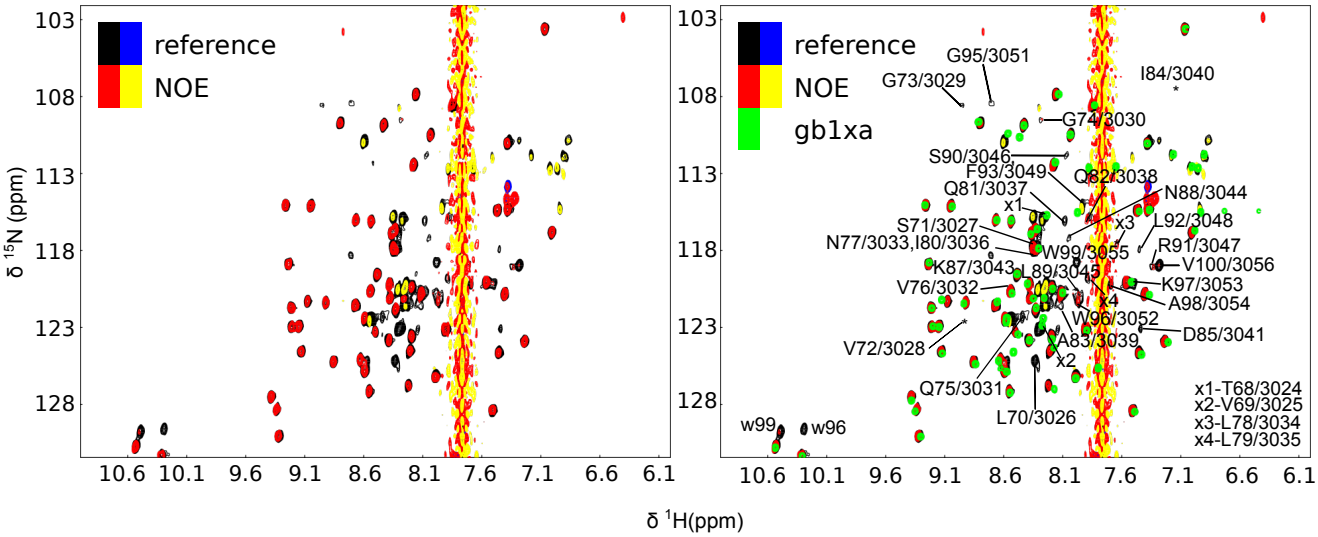

Abd Rahim et al.
SI Fig. S2

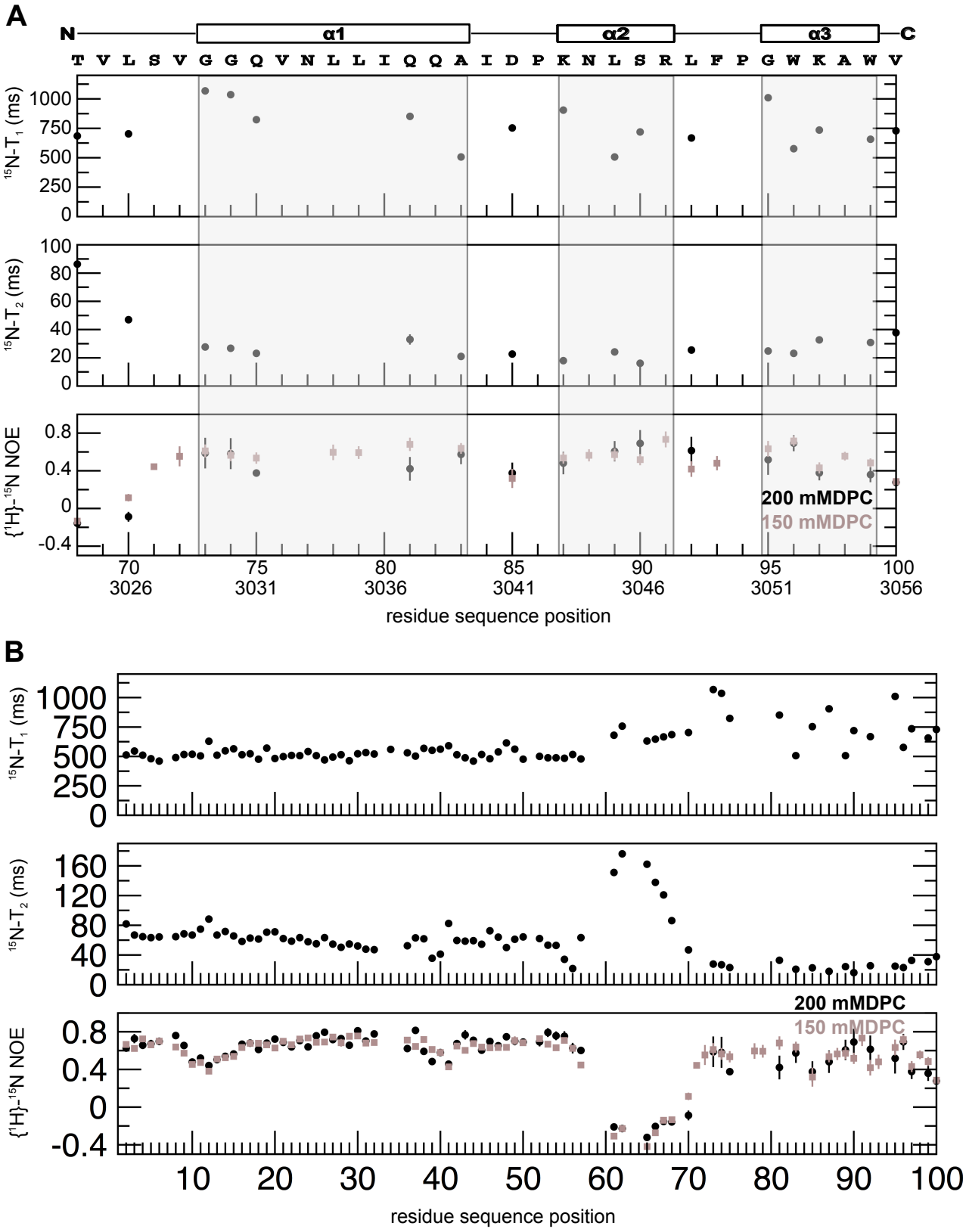

Abd Rahim et al.
SI Fig. S3

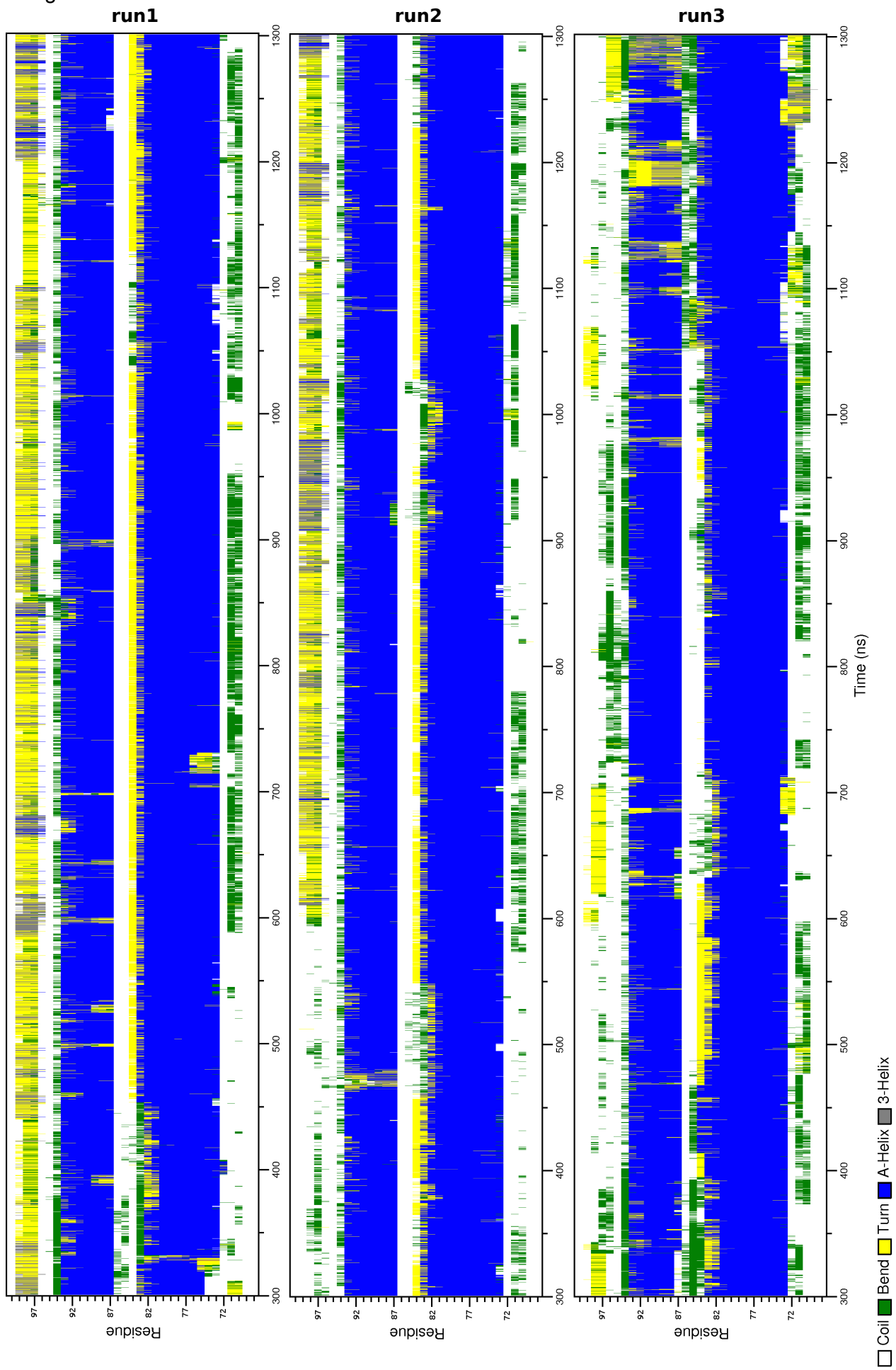

Abd Rahim et al.
SI Fig. S4

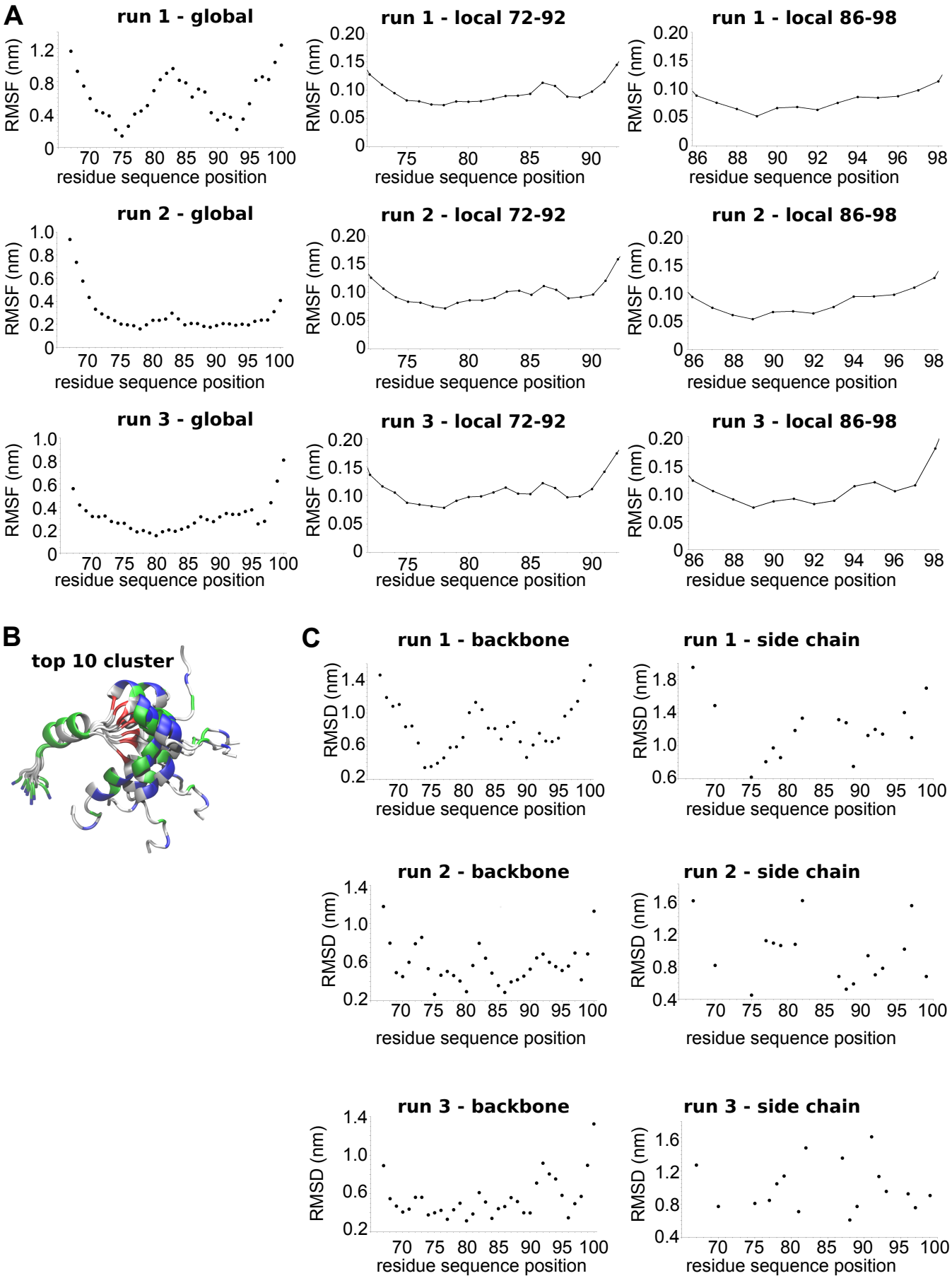

Abd Rahim et al.
SI Fig. S5

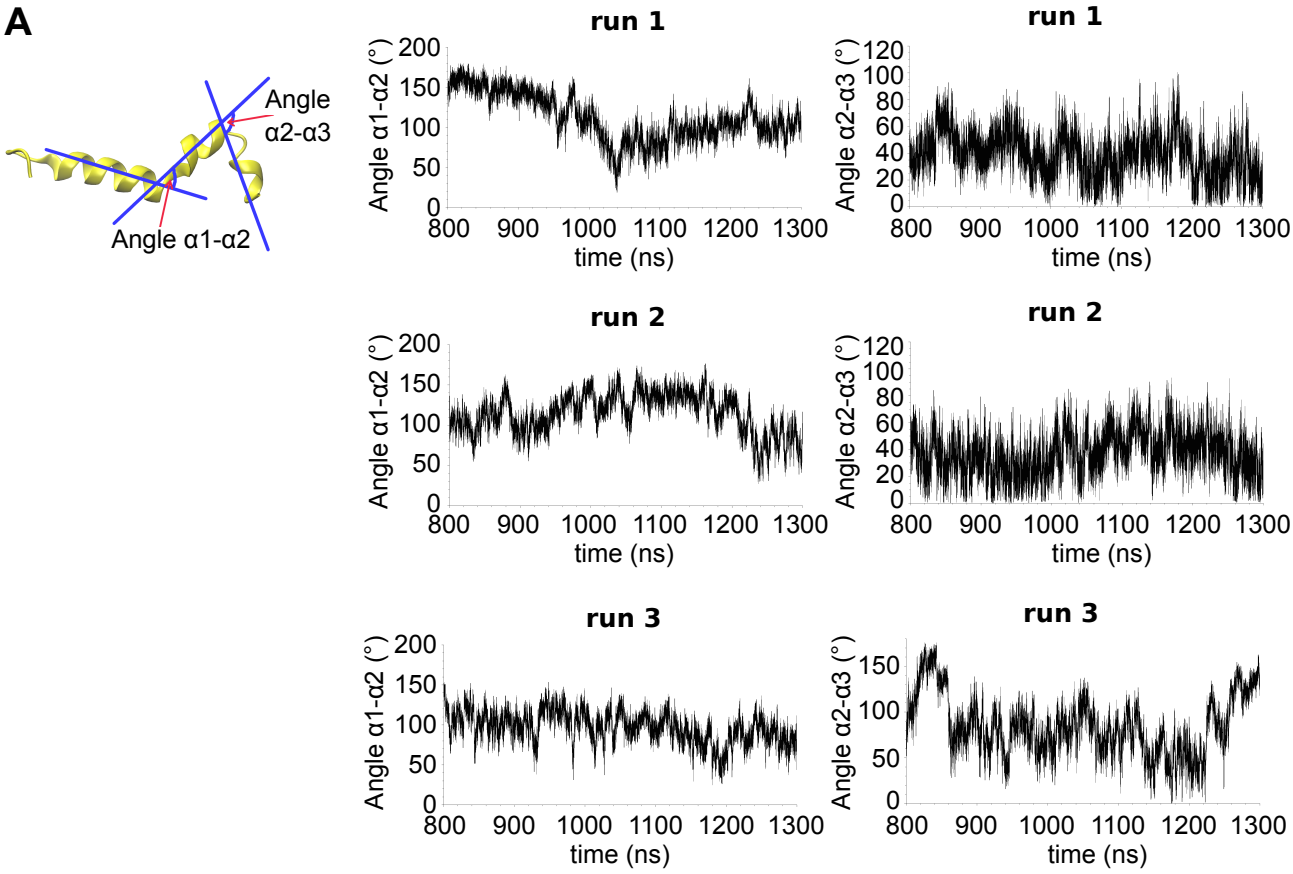

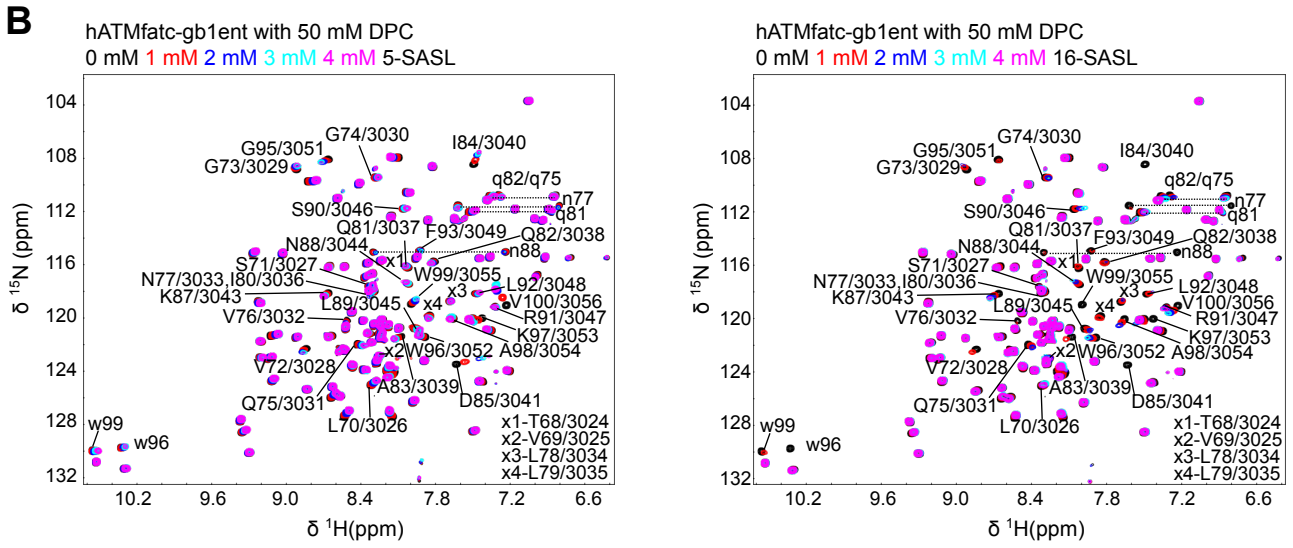

Abd Rahim et al.
SI Fig. S6

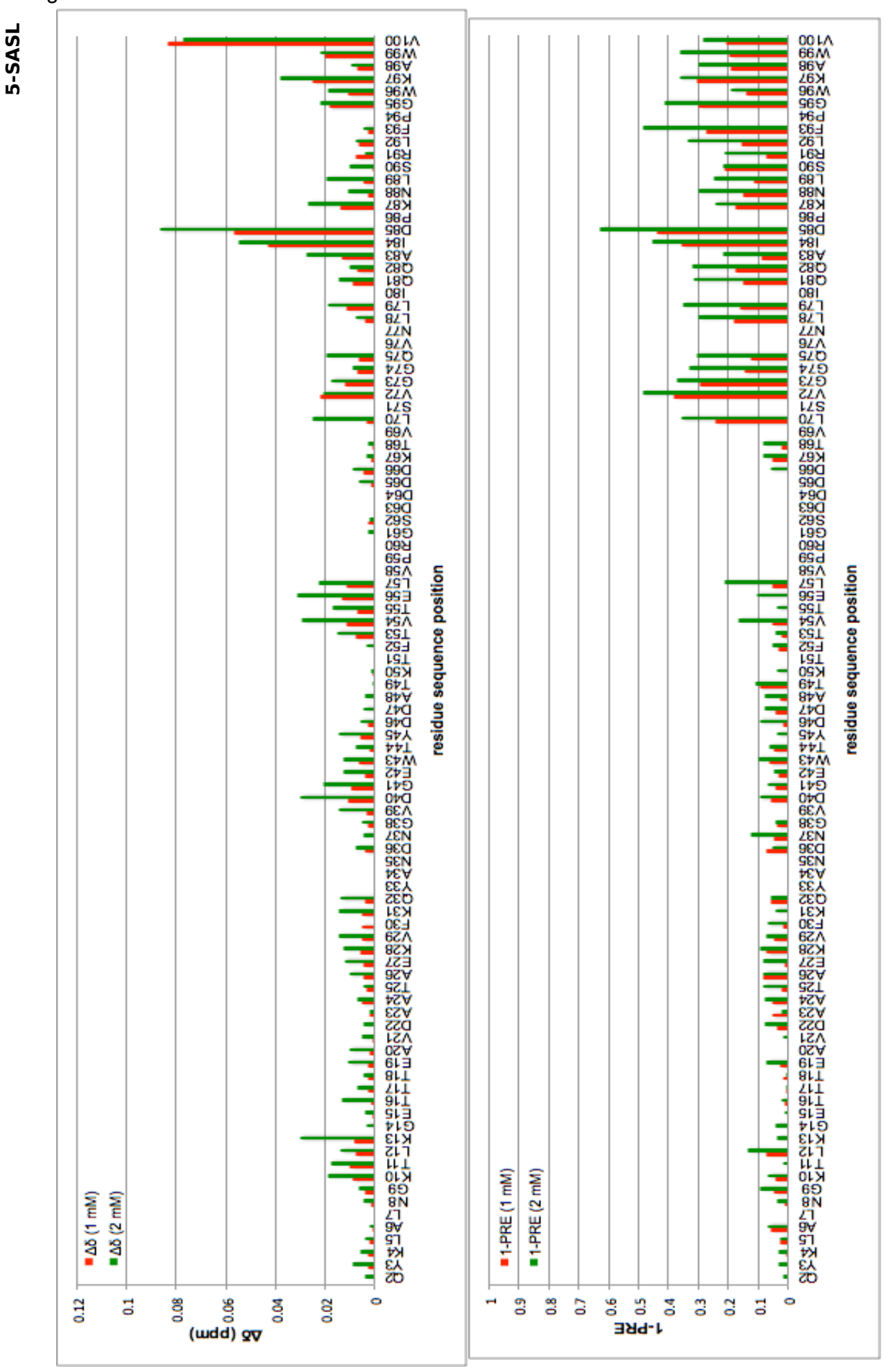

Abd Rahim et al.
SI Fig. S7

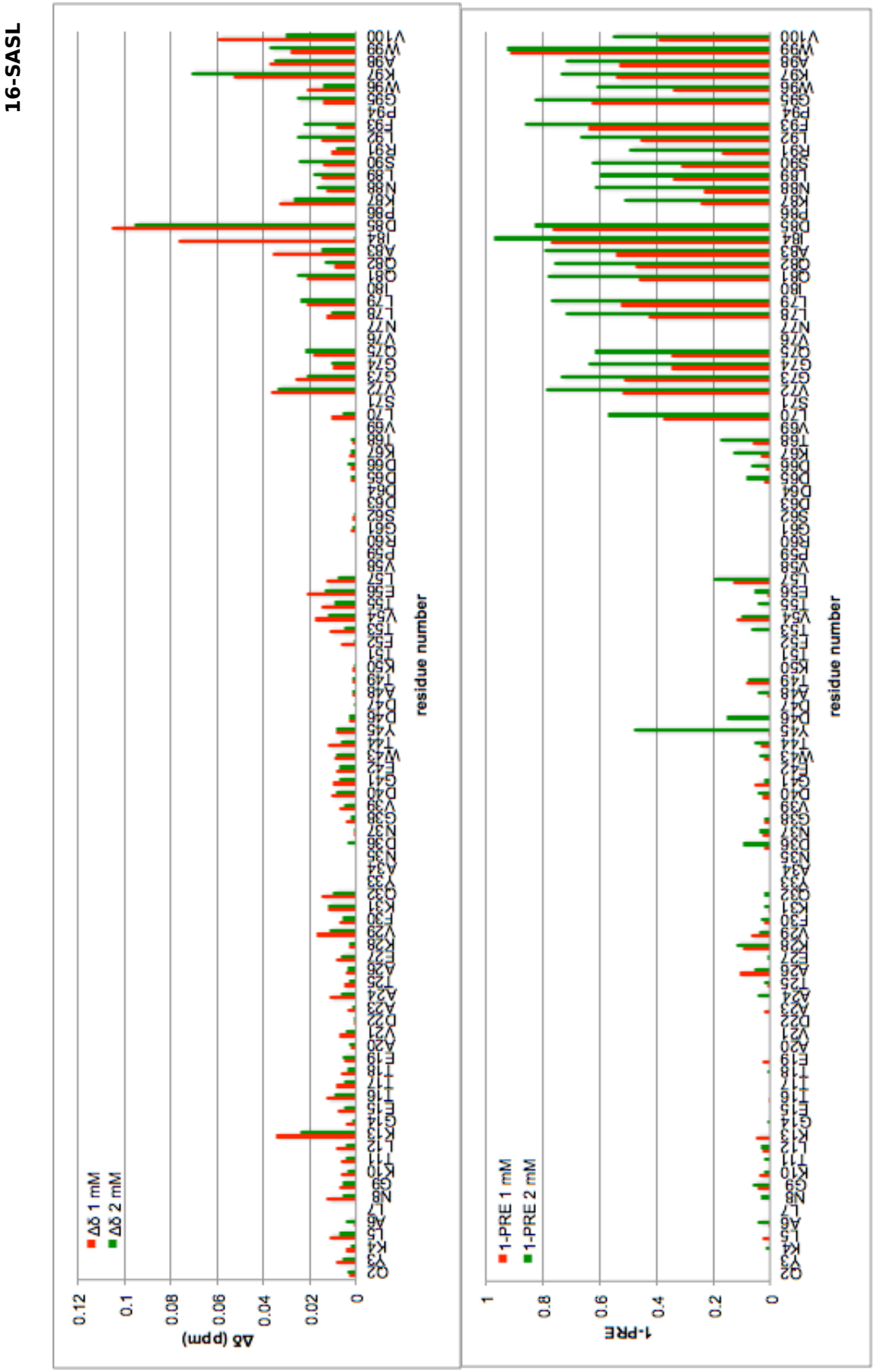

Abd Rahim et al.
SI Fig. S8

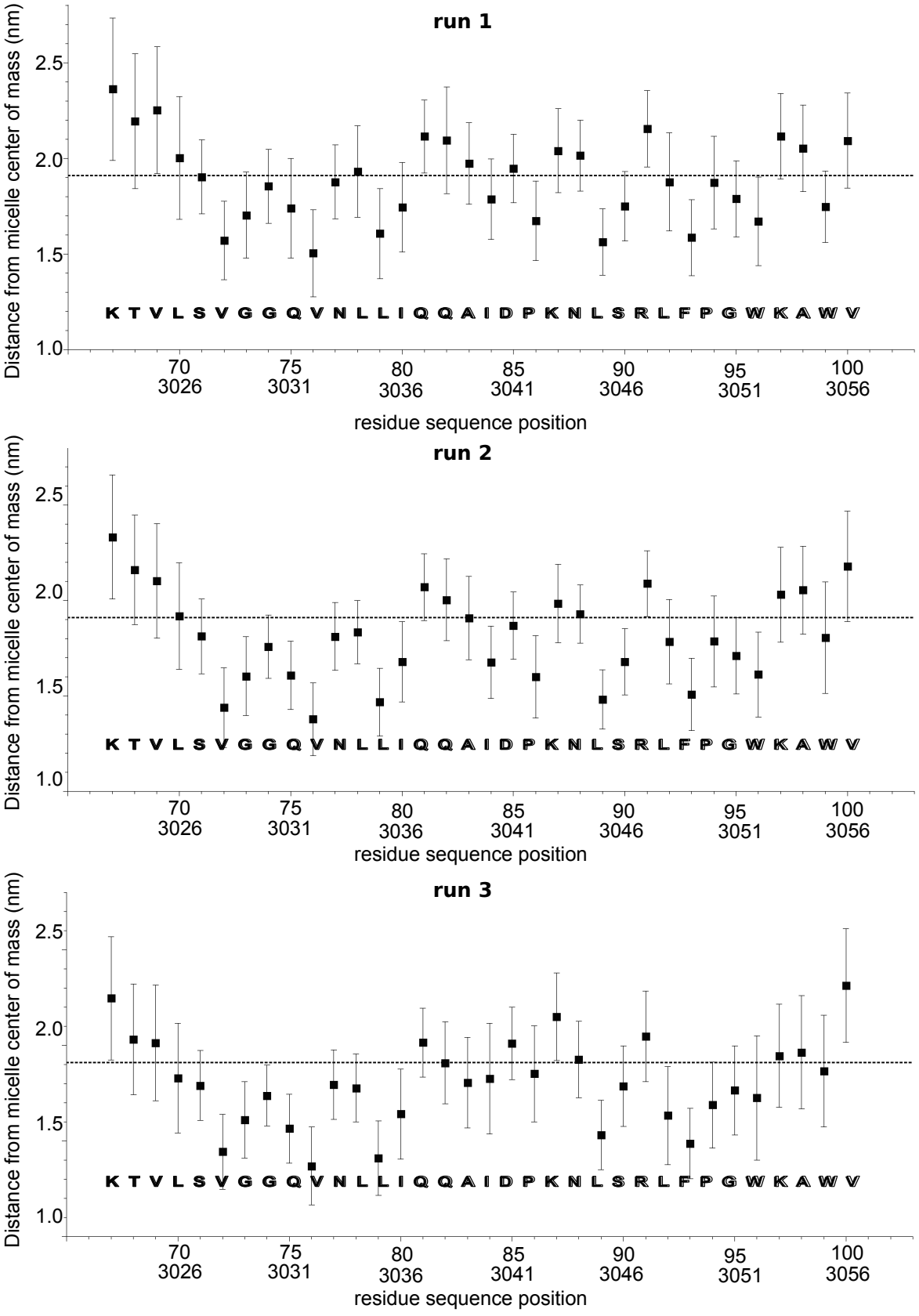

Abd Rahim et al.
SI Fig. S9

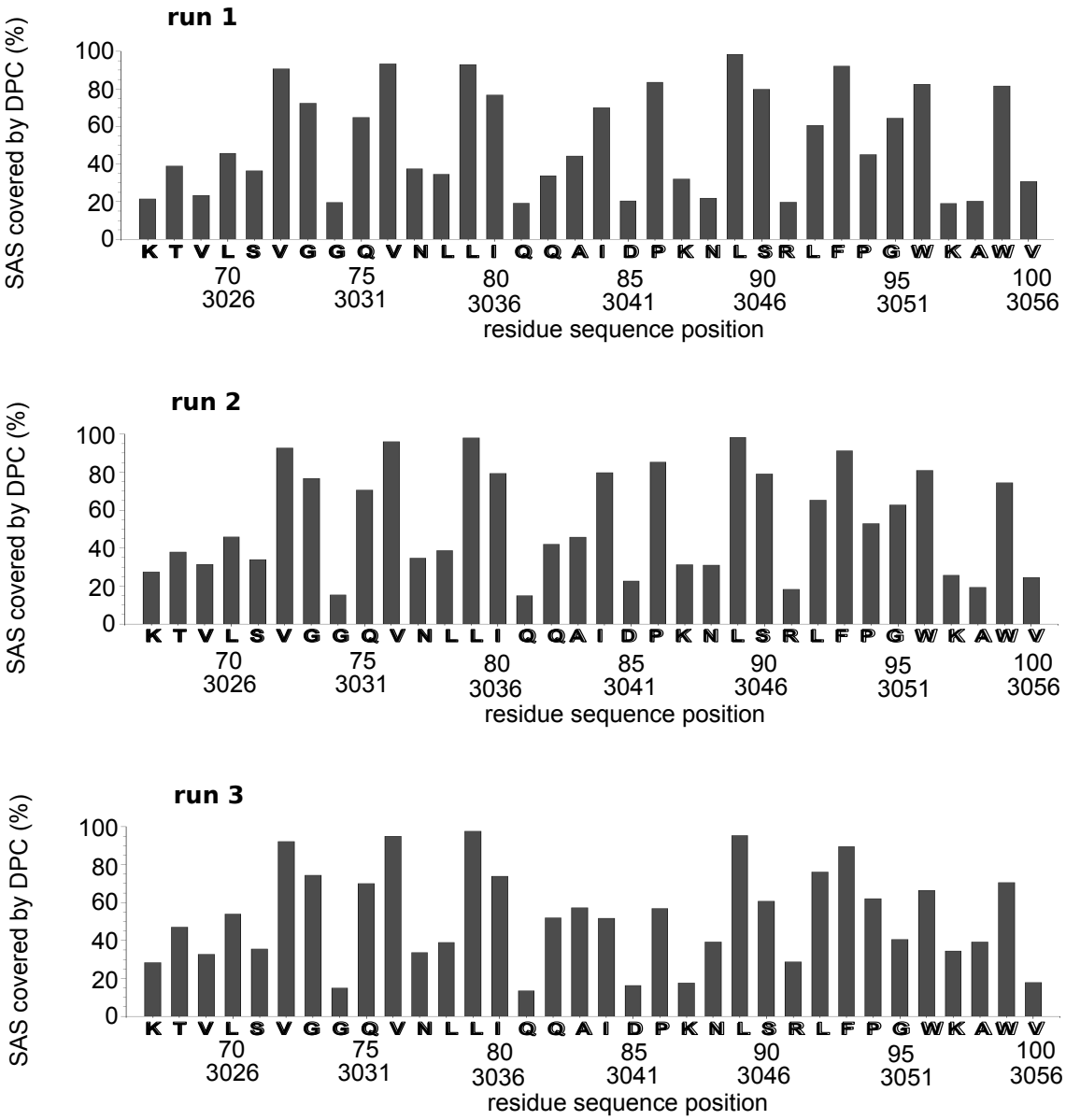

Abd Rahim et al.
SI Fig. S10

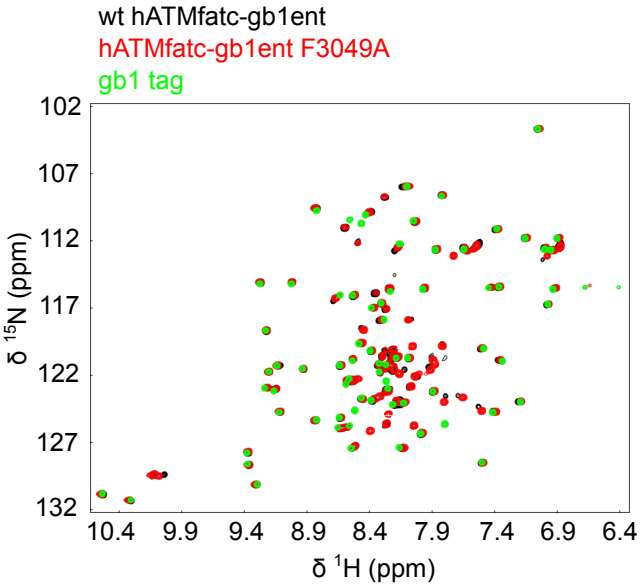

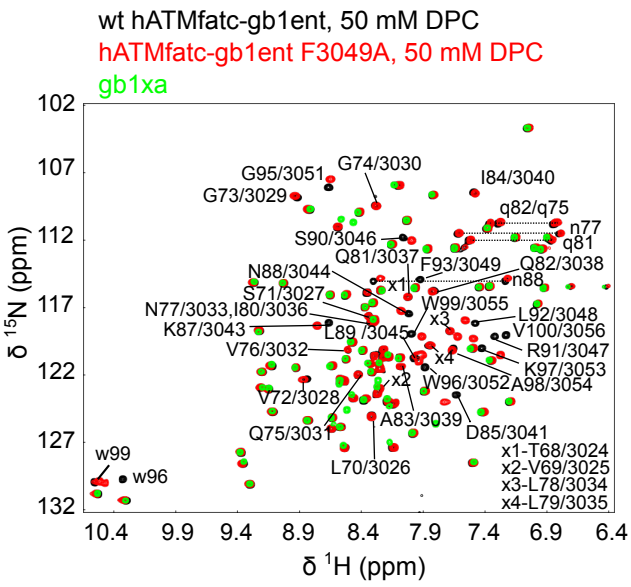

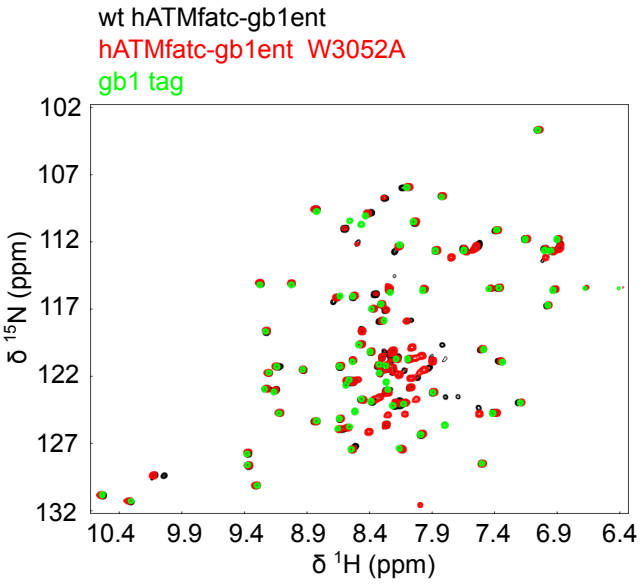

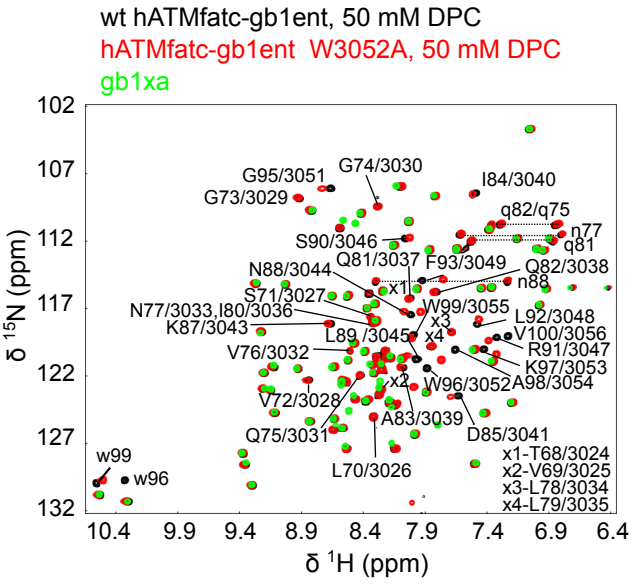

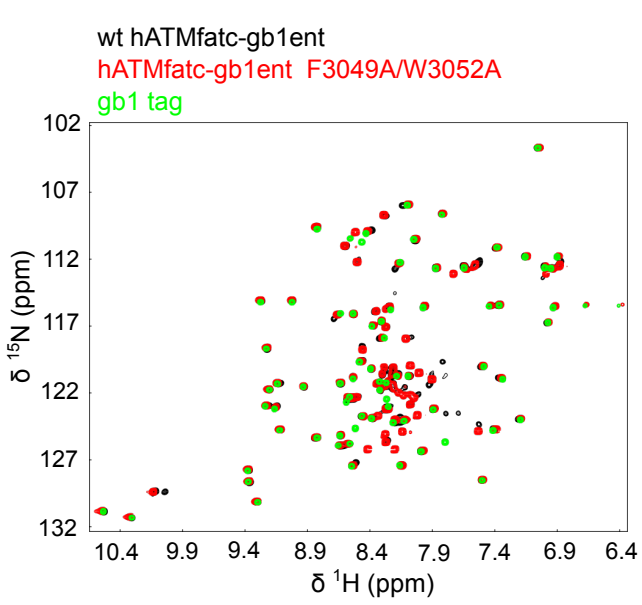

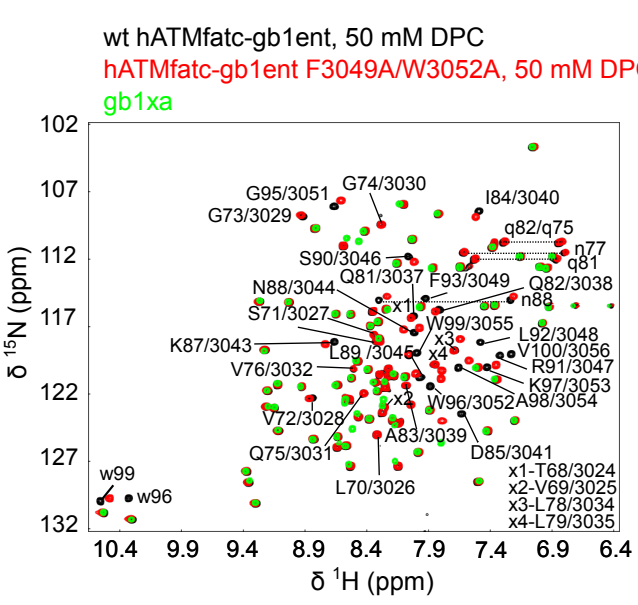

Abd Rahim et al.
SI Fig. S11

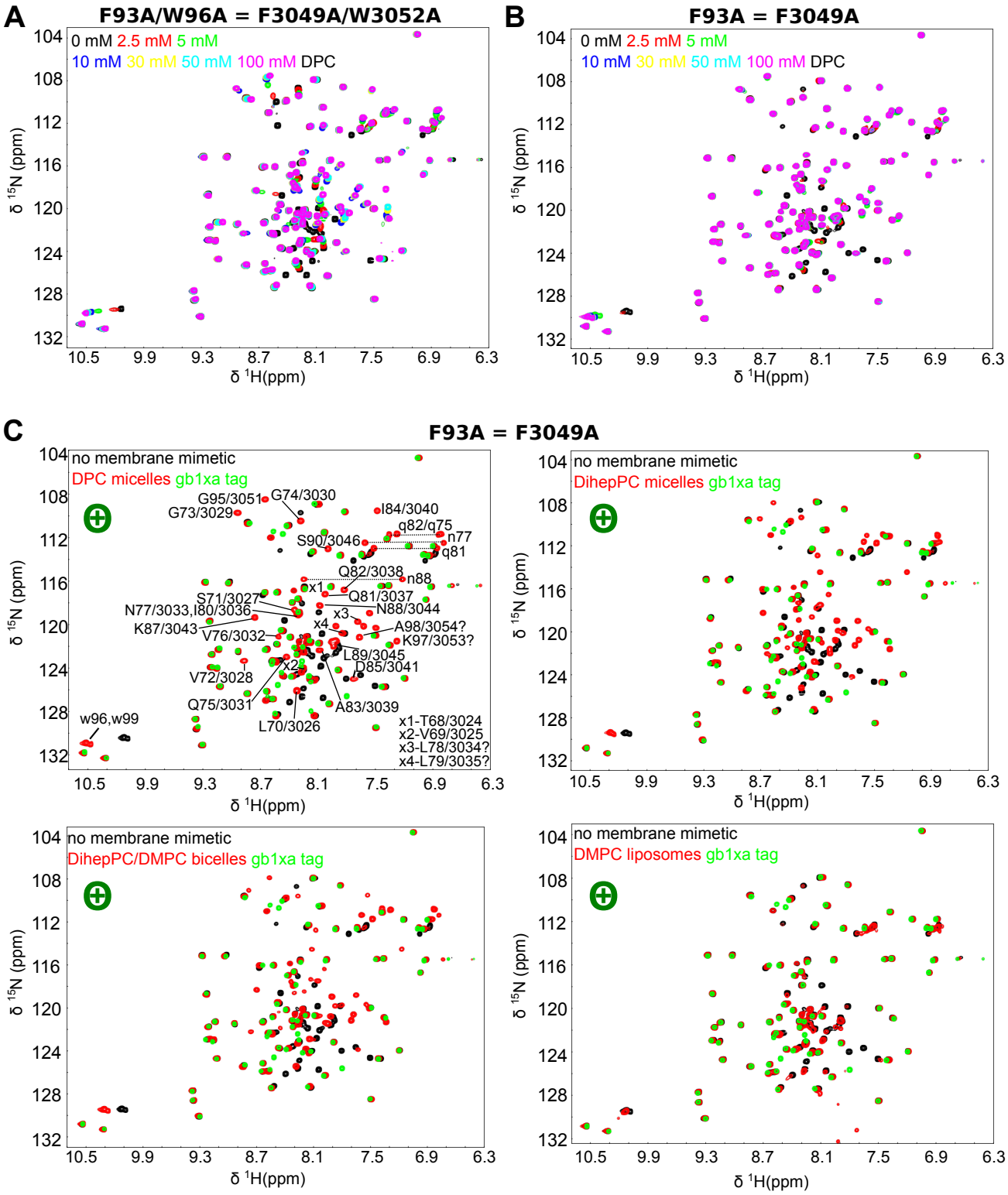

Abd Rahim et al.
SI Fig. S12